

**UNCLASSIFIED**

UCRL-2043(Del.)

1 - 2

**UNIVERSITY OF CALIFORNIA**

**Radiation Laboratory**

**Contract No. W-7405-eng-48**

Photostat Price \$ 22.80

Microfilm Price \$ 7.20

Available from the  
Office of Technical Services  
Department of Commerce  
Washington 25, D. C.

**MTA QUARTERLY PROGRESS REPORT**

**June, July, August, 1952**

**December 8, 1952**

**LEGAL NOTICE**

This report was prepared as an account of Government sponsored work. Neither the United States, nor the Commission, nor any person acting on behalf of the Commission:

A. Makes any warranty or representation, express or implied, with respect to the accuracy, completeness, or usefulness of the information contained in this report, or that the use of any information, apparatus, method, or process disclosed in this report may not infringe privately owned rights; or

B. Assumes any liabilities with respect to the use of, or for damages resulting from the use of any information, apparatus, method, or process disclosed in this report.

As used in the above, "person acting on behalf of the Commission" includes any employee or contractor of the Commission to the extent that such employee or contractor prepares, handles or distributes, or provides access to, any information pursuant to his employment or contract with the Commission.

**Berkeley, California**

**SECRET**

**UNCLASSIFIED**

2043-1

# SECRET

-3-

UCRL-2043

## TABLE OF CONTENTS

	Page No.
1. CAVITY DESIGN	4
2. 200 MC SPARKING AND X-RAYS IN A MERCURY PUMPED VACUUM SYSTEM	7
3. HIGH VOLTAGE BREAKDOWN FOR OUTGASSED METALS	8
4. SPARK DAMAGE AND HIGH VOLTAGE BREAKDOWN OF METALS AT 14 MEGACYCLES	14
5. ION PUMP DEVELOPMENT	15
6. MARK I HIGH FREQUENCY PROGRAM	16
7. DYNAMIC BEHAVIOR OF MARK I	17
8. M. T. A. MECHANICAL DESIGN	18
9. MARK I TARGET	21
10. A-12 TARGET AND LATTICE PHYSICS PROGRAM	25
Introduction	25
Experiments with UCRL Water Lattice	25
Inelastic Cross Sections for Deuterons and Protons	27
High Energy Nuclear Processes	33
Extrapolation of Total Neutron Yields to High Deuteron Energies	34
11. A-12 TARGET THEORETICAL AND ENGINEERING PHYSICS	57
Primary and Secondary Targets	57
Lattice Studies	60
Study of Two Group Neutron Flux Calculations in Water Using a First Collision Source	69
12. NUCLEAR CHEMISTRY	102
Fission and Capture in A-12 Targets	102
Isotopic Composition in Primary and Secondary Targets	104
Fission Product Distribution at High Energies for Uranium and Thorium	105
Absolute Beta-Counting	105
Separation of Tantalum and Niobium by Solvent Extraction	106
Instrumentation	107
Corrosion Studies	108
Zirconium Spallation Products	115
13. TARGET DEVELOPMENT	127
Target Analysis	127
Design Development	128
Target Design	133
Experimental Engineering	134
14. MATERIALS RESEARCH	136
Physical Metallurgy	136
Chemical Metallurgy	137
Irradiation Experiments	137
15. A-12 CHEMICAL PROCESS STUDIES	139
Process Research	139
Process Development	141
Process Design	144
16. ELECTRON MODEL CLOVERLEAF CYCLOTRON STUDIES	146
Electron Model II	144
Electron Model III	146

# SECRET

2043-2

# SECRET

-4-

UCRL-2043

## 1. CAVITY DESIGN

S. W. Kitchen  
UCRL

As reported in the previous quarterly report (UCRL-1903) a final drift tube table for A-12 was prepared. (UCRL-1859.) This table contained the geometry specifications for a tenth-scale model with the exception of the first twenty drift tubes. Since then each half cell of this group has been individually modeled for resonance. In Fig. 1, the diameter of the drift tube in each cell obtained in this way is plotted as a function of the tenth-scale axial position of the electrical center line of the drift tube. The diameters chosen for the model are those on the smooth curve. It will be noted from Fig. 2 that the diameters of drift tubes 14 - 20, when gap splitters are inserted in gaps 13 - 20, are well below the average A-12 drift tube diameter of 100 inches. The reason this happens is that the additional capacity introduced by the gap splitters required compensation through reduction in area of the face of the drift tubes.

In view of the uncertainties introduced by half-cell modeling, it was considered advisable to check the overall characteristics of this group of drift tubes in a small model ( $\sim 1/30$  scale), where indicated corrections to the dimensions could readily be made. This model has been designed and is in the process of construction.

The basis on which the decision to change the majority of the A-12 drift tubes from thick cylinders to thin cylinders was the gain in shunt impedance at the high  $\beta$  end. This gain was determined from measurements in the vicinity of the design parameters. In order to provide data for more comprehensive calculations, extensive shunt impedance measurements over more parameters have been made on the thin cylinder geometry. The data thus far indicates that, in addition to significantly higher shunt impedance at high  $\beta$ 's, in this region the shunt impedance of the thin cylinders is almost independent of  $D/d$ . This behavior contrasts with that of the thick cylinders where the shunt impedance falls off badly with  $D/d$ .

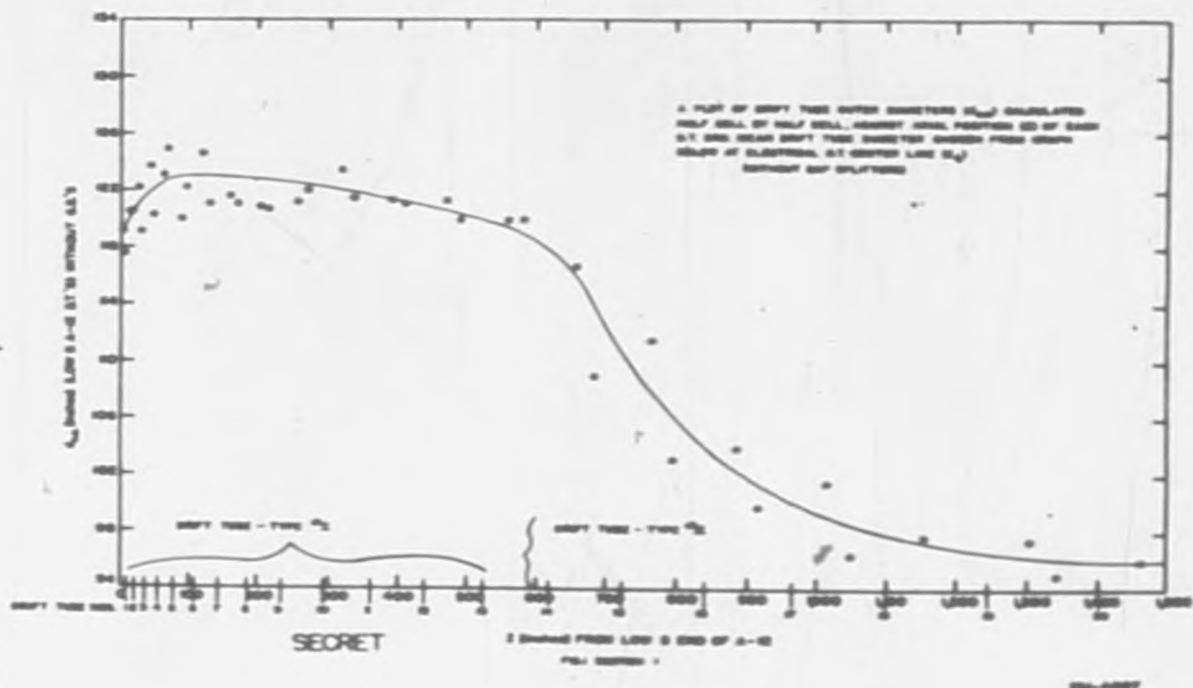
The theoretical investigations of the A-12 beam behavior previously described became the full responsibility of CRDC early in this period, and will no longer be reported here.

The group during this period consisted of S. A. Colgate, M. L. Good, B. V. Hill, S. W. Kitchen, and A. D. Schelberg.

# SECRET

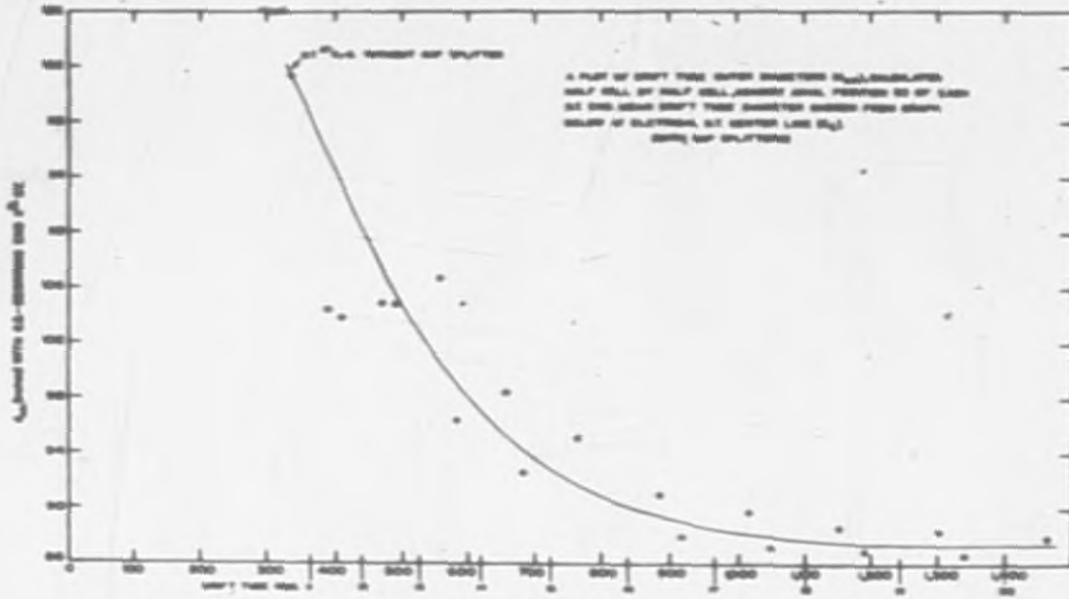
DECLASSIFIED

2043-3



CONFIDENTIAL

2043-4



SECRET

DERIVED FROM LOW SPEED A-C  
FILE NUMBER 1

50-4000

2043-5

## 2. 200 MC SPARKING AND X-RAYS IN A MERCURY PUMPED VACUUM SYSTEM

W. D. Kilpatrick  
UCRL

The following table is an addition to the list of characteristics concerning the sparking of different metal electrodes at 200 Mc as reported in the previous M. T. A. Quarterly Report UCRL-1903.

<u>Material</u>	<u><math>E_0</math></u>	<u>Inherent Sparks</u>	<u>Initial spark Rate</u>	<u>Initial X-ray Intensity</u>
Rh	0.35	300	135	0.05
oil-on-RH	0.17	---	27,000*	1.0
Pt	0.24	30,000	2,000	2.5

The data listed are for 2.3 Mv across a gap of 3.3 in., except for the case of oil-on-Rh which is for 1.0 Mv\* because of the high sparking rate which apparently could not be diminished because of the presence of oil. The Rh sample was Rh plate 0.8 mil thick, as compared with previously reported 0.1 mil thickness. The Pt sample was made with the use of a hydrogen furnace, and hydrogen impregnation probably accounts for the poor results. Previous experience with hydrogen furnace technique on copper shows a similar effect.

The conclusions drawn from the experiments are:

- 1) The Rh sample of 0.8 mil Rh plate gave the same results as 0.1 mil plate previously reported.
- 2) The oil-on-Rh experiment was a satisfactory test for distinguishing the oil effect. The threshold gradient for oil is low (170 kv/cm); and if sparking cleanup exists with oil present, the clean-up is extremely slow with a large number of sparks.
- 3) Pt is probably as good as Rh, but the presence of hydrogen induces sparking and excludes any definite conclusions concerning the sparking characteristics of the base metal.

On August 1, 1952, the test cavity in which these experiments were made was disassembled for shipment to CRD in Livermore, California. The transfer was completed August 14, 1952, and the equipment is now in the custody of W. Salisbury and T. Karuth.

RECORDED

2043-60

### 3. HIGH VOLTAGE BREAKDOWN FOR UNOUTGASSED METALS

H. G. Heard and E. J. Lauer,  
UCRL

#### Breakdown Voltage Coefficient

During this quarter measurements of the breakdown voltage coefficient were extended to those metals which have pre-spark drains in excess of that which can normally be supplied by the existing 100 kv power supply. The new data are shown in relation to other materials in Table 1.

To get sparking voltage data for these metals a 0.5  $\mu$ fd. condenser charged to 100 kv was connected to the gap as shown in Fig. 1. Each discharge of the 0.5  $\mu$ fd condenser would charge the 0.015  $\mu$ fd condenser up to the vacuum gap sparking voltage ten times or so. The gap voltage would rise according to a  $1/e$  voltage in 0.038 second between sparks and fall very rapidly when a spark occurred. The gap voltage vs. time was displayed on an oscilloscope and recorded photographically. The sparking voltage distributions were taken from the photographs.

This technique was compared to the method formerly<sup>1</sup> used by measuring the most probable sparking voltage by both methods for a given sample. The test with Hastalloy B showed that for a given spacing the most probable sparking voltage was 50 kv as compared to 60 kv obtained by the former method.

The observed reduction in breakdown voltage is accounted to the rate at which sparking occurs. With the technique discussed above 10 or more sparks can occur per second whereas the former method only allowed approximately 10 to 20 per minute. It was generally observed that the first spark in the series occurred at a higher voltage. One may infer from these data that breakdown voltage is a decreasing function of increasing sparking rate.

#### Test of Cranberg Hypothesis of Spark Initiation

Knowing that much experimental data on vacuum sparking fits the relation

$$V \sim d^{1/2} \quad \text{where: } V = \text{electrode voltage} \quad (1)$$

d = electrode spacing

Cranberg has proposed<sup>2</sup> that particles removed from the surface of the electrodes by the electric field will initiate a vacuum spark if they deliver a critical energy per unit area to the target electrode. That is the voltage-gradient product is a constant of the electrode material which for parallel-plane geometry can be derived from (1). If all the hypothetical particles with binding energies less than or equal to a value corresponding to the gradient predicted by  $V \sim d^{1/2}$  can be removed without a spark then no sparks should occur until the field exceeds this value.

<sup>1</sup> H. Heard and E. Lauer, UCRL-1774, (1952).  
<sup>2</sup> L. Cranberg, J. A. P., Vol. 23, p-518, (1952).

2043-7

A test has been performed in which the electrodes have been conditioned as mentioned above by the following technique:

- (1) At a distance  $d_1$  apply a voltage  $V_1$  at least once without getting a spark.  $V_1$  is the most probable sparking voltage for the electrode spacing  $d_1$ . This procedure removes all particles whose binding energy corresponds to the field  $V_1/d_1$ .
- (2) Turn off the voltage and enlarge the gap to the maximum value available. Turn on the full supply voltage.
- (3) Turn off the voltage and reduce the spacing to  $d_2 = nd_1$ .
- (4) Turn on the voltage and raise it until the first spark occurs.

According to Cranberg's hypothesis a spark will not occur until the gradient reaches a value corresponding to or exceeding the value applied in the special conditioning of the electrodes. That is  $E_2$  must be equal to or greater than  $E_1$  which specifies that

$$\frac{V_2}{d_2} = \frac{V_2}{nd_1} = \frac{V_1}{d_1} \quad \text{or } V_2 = n V_1$$

If however the spark mechanism depends upon the relation  $V \sim d^{1/2}$  a spark will occur at

$$\frac{V_1^2}{d_1} = \frac{V_2^2}{d_2} = \frac{V_1^2}{nd_1} \quad \text{or } V_2 = \sqrt{n} V_1$$

Since in four trials with carbon electrodes the data agree better with a ratio of root  $n$  rather than between  $V_2$  and  $V_1$ ; results of the experiment are regarded as evidence against Cranberg's theory. If the first spark had occurred at  $V_2 = nV_1$  and further sparks had occurred at  $V_2 = \sqrt{n} V_1$  the test could be regarded as extremely strong evidence for the theory. The fact that the observed data do not substantiate Cranberg's theory cannot be regarded as absolute proof that the theory is incorrect since particles could conceivably get onto the electrodes between steps (1) and (3).

#### Initiation of Vacuum Sparks

**Mechanical.** For some time now it has been postulated without proof that dust particles can cause high vacuum sparks. It has been found that vacuum sparks can be initiated over a wide range of d-c voltages gap spacings and electrode geometries if particles which are presumed to be dust are dislodged from the inner surface of the vacuum system by a mechanical blow.

UNCLASSIFIED

2043-8



To show that sparks were initiated by particles rather than a mechanical shock causing gap variations, the vacuum system was equipped with a long vertical pipe having a door near the base. An oscilloscope sweep was triggered when the pipe was struck a hammer-blow near the top. The time after the mechanical shock until the first spark was measured by the sweep length which occurred up to the spark signal. The statistics for sparks initiated with the door open and closed reveal a peak in time for sparks initiated by particles with a free fall time of  $1/2 gt^2$ . The results of this experiment indicate that at least some sparks can be initiated by particles removed from a surface inside the high-vacuum casing. It suggests that all vacuum sparks may be caused by particles which are similar in nature to those derived from mechanical shocks.

Electrical. High voltage breakdown between electrodes has been initiated by applying a very fast pulse to electrodes which are biased by a fixed d-c voltage. The step function pulse, which rises to approximately 10 kv in  $2.5 \times 10^{-9}$  sec., was generated by shorting a charged coaxial line. To eliminate stray capacity effects the transmission line was made an integral part of the support of the high voltage electrode.

A delay exists between application of the pulse and initiation of breakdown. This delay, which is a function of gap spacing and total d-c voltage, varies from 5 to  $50 \times 10^{-9}$  sec. for the range investigated.

Breakdown could not be initiated unless the ratio of pulse to d-c gap voltage was large. For a given applied voltage the fast pulse would not initiate breakdown until the gap was narrowed to a critical value. This is interpreted as specifying that particles which initiate breakdown must come from the electrodes and not from dust particles removed from the vacuum liner, etc.

Each of the triggered sparks was followed by a flurry of sparks which appear as a secondary event. Sparks were triggered during the quiescent period following those flurries. A bake-in effect was noted for the triggered sparks in the larger gaps.

Since this work was still in early stages at this writing descriptions and conclusions will be deferred to a later report.

**TABLE I**  
**BREAKDOWN COEFFICIENTS FOR SPARK CONDITIONED**  
**METALS IN MERCURY PUMPED SYSTEM AT LOW PRESSURE**

$v = Ad^{1/2}$

<u>METALS</u>	<u>BREAKDOWN COEFFICIENT</u> KILOVOLTS/(mm) <sup>1/2</sup>	<u>NUMBER OF SPARKS</u> <u>AT WHICH DATA</u> <u>WAS TAKEN</u>	<u>ALLOY COMPOSITION</u>
Invar	197	25,000	63.8% Fe, 36% Ni, 0.2% C
Stainless Steel (non-magnetic)	179	56,000	71.8% Fe, 8% Ni, 18% Cr, 2% Mn, 0.2% C
Manganese Steel	172	27,000	86% Fe, 13% Mn, 1% C
GP 720	161	19,000	60% Cu, 20% Ni, 20% Mn
Hardened Steel R <sub>c</sub> = 60-65	159	12,500	Pack-carburized 8 hrs. @ 1700° F. water quench from 1450° F. temper. @ 350° F.
Chrome Plated Copper (outgassed at red heat in vacuum)	143	5,000	-----
Inconel	134	12,000	73% Ni, 17.5% Co, 6.5% Fe, 2.5% Ti, 0.2% Mn
Hastalloy B	126	25,000	-----
Nickel	89.5	13,000	-----
0.01 inch Chrome Plated on Copper (unoutgassed)	89.4	40,000	-----

2043-10

TABLE I (cont.)

<u>METALS</u>	<u>BREAKDOWN COEFFICIENT KILOVOLTS/(mm)<sup>1/2</sup></u>	<u>NUMBER OF SPARKS AT WHICH DATA WAS TAKEN</u>	<u>ALLOY COMPOSITION</u>
Hot-rolled Steel	89	62,400	99% Fe, 1% C
E. T. P. Copper <sup>3</sup>	74	22,500	-----
Cupalloy <sup>3</sup>	71	11,000	-----
Tantalum <sup>3</sup>	71	20,000	-----
Aluminum <sup>2</sup>	57	8,700	-----
Lead	54	12,500	-----
Vacuum Fused Copper <sup>3</sup>	54	24,000	-----
C-15 Anodic Carbon	36	10,000	-----
Spectrographic Carbon <sup>4</sup>	36	14,000	-----
Silver	27	14,000	-----

1 Data extrapolated from value at 0.2 mm.

2 Data extrapolated from value at 0.5 mm.

3 Current supplied by discharging 0.5  $\mu$ fd condenser charged to 100 kv.

4 National Carbon Company, Lot No. 542, Sample 2

Traces of impurities detected spectrographically are: relative intensity 3-copper

2-magnesium

1-iron

barely visible: boron, silver, sodium

absent: aluminum, calcium, lead, manganese,  
potassium, silicon, tin, titanium,  
vanadium.

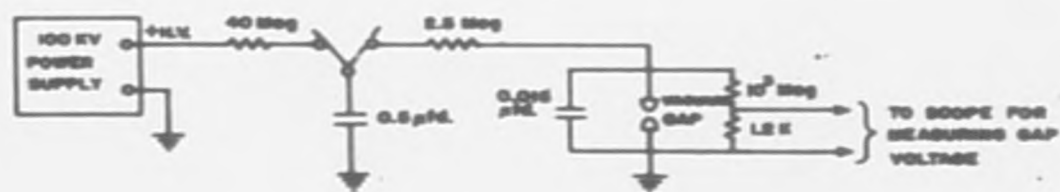


FIG. 1 SECTION 3

MU-4889

SECRET

2043-12

**4. SPARK DAMAGE AND HIGH VOLTAGE  
BREAKDOWN OF METALS AT 14 MEGACYCLES**

W. W. Chupp and H. G. Heard  
UCRL

A detailed research report on this subject was written and issued during the quarter under the number UCRL-1962. An abstract of this report follows.

Spark damage and breakdown voltage measurements have been made on Inconel, E. T. P. copper, D. H. P. copper, tantalum, molybdenum, nickel, C-18 carbon, K-Monel, stainless steel and satin chrome-plated copper. These tests were conducted in the oil pumped XC-cyclotron cavity. Measurements were extended to approximately 1000 kv and a peak energy storage of approximately 10 joules. Breakdown voltages are quoted for tests made in the presence of a 15,000 gauss magnetic field.

2043-13

## 5. ION PUMP DEVELOPMENT

E. J. Lofgren  
UCRL

The work during the quarter is covered by two research reports abstracts of which are given below.

### A HIGH VACUUM HIGH SPEED ION PUMP

John S. Foster Jr., E. O. Lawrence and E. J. Lofgren

A vacuum pump based on the properties of a magnetically collimated electric discharge is described. It has a speed in the range 3000 to 7000 liters a second and a base pressure in the order of  $10^{-6}$  mm.

This is an abstract of UCRL-1930.

### DESIGN OF RADIATION HEATED CATHODES FOR ION PUMPS

William E. Bush

The ion pump requires cathodes of unusual durability to withstand the positive ion bombardment associated with the high intensity arcs. Design and operation of radiantly heated tungsten and tantalum cathodes is discussed.

This is an abstract of UCRL-1929.

## 6. MARK I HIGH FREQUENCY PROGRAM

William R. Baker  
UCRL

Per plan, the responsibility for the oscillator system has been gradually shifted from UCRL to CRDC personnel. It is now believed that little, if any, further help will be needed and that the CRDC organization is fully capable in the operation and maintenance of the equipment. However, until such time as the L-2 test facility has been completed, the B-1 system at Berkeley must be relied upon for tube testing and related work.

In line with this, tests were made recently on four new tubes of the 2332 variety. These included one of the longer of the molybdenum powder coated grid idea that had been offered as a possible solution to the thermal grid emission problem. Unfortunately, these tubes did not perform any better than the earlier models and this grid problem continues to be the limiting feature of the tubes. RCA is continuing research on this, and there is an optimistic feeling that an answer will be found soon.

2043-15

## 7. DYNAMIC BEHAVIOR OF MARK I

John F. Waddell  
UCRL

The experimental work on this problem has been completed, save for final data to be taken on the Mark I system itself. A complete technical report is in process of preparation, and will be published within a few weeks.

Engineering work on the application of the research done by this group to the rf regulator system for Mark I is nearly complete. The amplifier units will be re-installed shortly at Livermore.

Experiments have shown that with a proper combination of phase-lead and phase-lag correction in the system, stability may be achieved with system response-time of approximately  $2 \times 10^{-3}$  seconds, i. e., the system can be made to have nearly as great a speed with time-quantization (sampling) as it could have were there no quantization of time. Moreover, there are indications that a substantial increase in loop gain can be made permitting closer regulation of rf level in the cavity than the minimum required. The reader is referred to report UCRL-1774 for discussion of the factors involved.

On the night of 5-6 June 1952 an experiment was conducted upon Mark I itself. Data taken at this time showed conclusively the similarity between the Mark I machine, the laboratory-scale model (using the wine vat cavity), and the equivalent network model based upon the early research of this group into the dynamic behavior of a self-excited oscillator with resonant load. (1)

The research originally contemplated on the Mark II project will not be undertaken by this group, hence completion of the Mark I will terminate this problem.

The group participating in this work includes, in addition to the writer, Harold D. Morris, Walter H. Nelson, and Margaret Mendenhall.

(1) Preliminary Considerations Regarding Stability of Mark I as a Closed-loop system, UCRL-1597, Nov. 1, 1951. A more detailed account of this work will be included in the pending final report.



## 8. M. T. A. MECHANICAL DESIGN

W. M. Brobeck  
UCRL

### Distribution of Activities

During this period approximately 20 members, compared to 37 in the last quarter, of the Mechanical Engineering and Drafting section were employed on the MTA project. Their effort was distributed as follows: 9 persons on the Mark I program; 7 persons on A-12; 4 persons on J-16.

### Mark I Accelerator Program (Livermore Linac)

Design. Tests by other groups have indicated that inconel will probably be a satisfactory refractory facing for drift tube surfaces to reduce sparking damage in the 0-1 gap. As a result, the following equipment was designed:

1. Inconel facings to be installed over the existing drift tube\* surfaces at each end of the 0-1 gap. These facings consist of 12 pie-shaped sectors per drift tube of 1/16 inconel sheet formed to the drift tube contour and extending from inside the bore to a 6 foot diameter. The surfaces between the inconel and the existing copper shell will be chemically blackened to increase the transfer of heat from the inconel.
2. A new No. 1 drift tube with a protrudent nose, adjacent to the bore, and a thinner shell to concentrate the region of high field. This drift tube will have an outside diameter of 58 inches compared to 115 inches for the existing drift tube, an inconel shell, a new magnet designed for the proton voltage gradient, and will be connected to the existing stem. A new manifold will be used at the top of the stem.
3. A recontoured No. 0 drift tube with a nose protruding from a concave shell. The nose will be made of inconel sheet and the rest of the shell will be made of copper sheet.

Item 1 is intended to be installed if the run now in progress is not successful in holding proton gradient. Items 2 and 3 are intended to be used together if 1 is not a sufficient improvement.

Design was also completed on an improved centering adjustment for the cavity discharge probe.

---

\* The end face of the liner is referred to as the zero drift tube.

Fabrication (W. C. Twitchell). The only major work in progress during this quarter is the fabrication of a replacement drift tube No. 1 for Mark I. This new drift tube is smaller in diameter (50" approx.) and is made from 4 Inconel spinings (2 shells and 2 bore tubes). The neck of the drift tube is a shaped copper piece. A new magnet is being constructed to fit the smaller outline.

The job was started in July and by the end of August, 1952, most of the critical material was on hand and the fabrication orders had been placed for the major components. The use of Inconel with copper has presented some unique fabrication problems.

This drift tube is scheduled for completion in October, 1952.

XC Magnet. This magnet is being used by research groups for sparking tests. Design of test electrodes and their attachments has been done for the experimental group in connection with sparking tests for Mark I. Design work has also been done on means for converting XC to a mercury pumped oil free system to more nearly approximate Mark I operating conditions.

#### A-12 Program (Full Scale Linac)

Mechanical design was completed on the following items.

1. A mass spectrograph for analyzing the constituents of the arc of Ion Pump 5B.
2. A 1/2-wave transmission line (8-1/4 in. O. D. x 40 ft. long) which will be connected to the B-1 cavity.
3. The 0.03 scale rf model of the low energy end (first 20 drift tubes) of the A-12 Accelerator to check the dimensions arrived at by calculation.

Construction was completed on item 1 and is in progress on items 2 and 3.

Target. The joint UCRL-CRDC design group, initiated on October 1, 1951, was reorganized into a CRDC target design and development group on July 1, 1952. UCRL engineers and draftsmen were assigned other duties. Participation by UCRL mechanical design personnel in MTA target development is now limited to consultation.

#### J-16 Program (Cloverleaf Cyclotron)

Electron Model No. 2 (300 Mev model). No mechanical design was required in this quarter. This machine has been disassembled and the parts will be used for other purposes.

Electron Model No. 3 (350 Mev model). Magnetic field mapping has been completed, and final assembly of this machine is proceeding. Very little engineering work was required in this quarter.

20-inch Cyclotron. No mechanical design was required in this quarter. This machine has been rebuilt and is being used for other than MTA research work.

DECLASSIFIED

2043-19

### 9. MARK I TARGET

G. S. Windle, G. B. Rosenblatt, Jr., G. M. Kibler,  
O. J. Elgert, D. E. Lord, and L. W. Roberts  
CRDC



#### Solid Target Fabrication

A visit was made to Bohn's Adrian, Michigan plant to witness and test target backing plate extrusions. Initial extrusions were not successful because of failure of the die while in the press. It was later determined that the failure resulted from faulty heat treatment of the outer die. A second die failure subsequently occurred and Bohn is now fabricating a die of radically altered construction in their own shops. However, three samples of extruded target backing sections have been received and, although they do not meet tolerances, may be satisfactory for anticipated immersed pilot casting experiments.

While at Adrian, completed extrusions sixteen inches wide were observed, and Bohn has been asked to quote on a sixteen inch extrusion in addition to the present eight inch section which they have contracted to fabricate. The use of sixteen inch wide extrusions would simplify target fabrication and handling procedures at Livermore and also reduce target costs slightly.

A laboratory scale immersed casting unit was designed and constructed. It will not be used however, due to the cessation of the project.

Approval has been received, however, to complete the pilot immersed casting experiment on at least one section, for which equipment had already been delivered. Installation was therefore carried out on the preheat oven, hydraulic press assembly, press frame, melting tank, pressure and cover backing plates and electrical controls and panels. Equipment already fabricated prior to August 15, and installed shortly thereafter include quench tank, brush drive speed reducer and the complete crane assembly including truss supports.

#### Welding of Solid Target Cover Plate

Alcoa Laboratories at New Kensington, Pennsylvania, were visited to discuss possible cover plate welding procedures. In addition to a cold-welded method which was demonstrated by Alcoa personnel, it was confirmed that welding problems would not be difficult to overcome. Further investigation, however, has been abandoned.

DECLASSIFIED

2043-20

A laboratory scale target section was fabricated, using the Mullard ultrasonic soldering iron. A sample was shown by ultrasonic testing to be quite satisfactory. Had full scale target fabrication continued, this method of bonding bismuth to aluminum would have received more intensive investigation, since commercial size transducers are now available.

#### Ultrasonic Inspection

Accuracy of ultrasonic inspection improved during the quarter. Ultrasonic prediction of flaw locations in several specimens were later proven accurate by metallographic examination. Included among the tests was the radiant heat target specimen discussed below.

Preliminary inspections of zirconium clad uranium and copper clad stainless steel were also made.

A scanner-recorder electronic unit was placed in operation as accessory equipment. However, some modification and development work will be necessary at such time as ultrasonic inspection is applied to other than the Mark I Target Program. CRD-T1-129 (LWS-24513) entitled "Mark I Solid Target Inspection by Ultrasonics" was issued containing information obtained during development work on Mark I Solid Target.

#### Mechanical Stress Cycling

The vibrating of bismuth-coated aluminum bars was continued during the quarter. In addition to uncovered bars, an equal number of bars with aluminum cover plates were vibrated. The tests included ultrasonic inspection prior to and following the vibrating tests. No serious changes in bond flaws nor bismuth cracks were observed in covered and uncovered bars.

#### Thermal Cycling by Radiant Heating

Metallographic examination of the sectioned mockup target plate together with ultrasonic inspection before and after thermal cycling failed to indicate any cause for concern regarding target failure through  $10^5$  thermal cycles simulating spark-down conditions in the accelerator.

#### Corrosion Studies in System Steel Bismuth

Measurement of corrosion depth of Sicromo-5S steel test strip using hydrogen as a reducing agent showed a rate below 1,000 mils per year which represents no significant reduction below that for 5 percent chrome steel. Confirming data on the use of additives (Ti and Mg) are being obtained to substantiate previous indications on the effectiveness of these materials. A report on the entire subject has been prepared (CRD-T1-74) and will be presented at the Liquid Metals Conference in Schenectady, October 8 and 9.

2043-21

### Deuteron Fate

A 1180 microamp hour deuteron bombardment was completed on the "fate" sample in the cyclotron at Berkeley. Following sufficient decay time for safe handling, the sample was analysed ultrasonically, after which it was sectioned for metallographic examination. The results of this second bombardment appear to confirm those obtained on a previous sample, both ultrasonically and from visual inspection in that the micro structure of the aluminum is definitely altered in the vicinity of the range end. A report will be issued as soon as metallographic examination is completed.

### Induced Gamma Activities in the Solid Target

Radiation of an actual target section was equivalently repeated by R. E. Batsel on the UCRL "Linac" for approximately 1.5 microamp hours at 30 Mev. The data so obtained were reported in detail in CRD-TI-116 issued September 23, 1952. Results of this experiment indicate that handling of an irradiated solid target, both at Livermore and at the processing plant, would be entirely practical from the health hazard viewpoint.

### Revisions to Target Design

Using the procedure developed by R. L. McKisson target design calculations for spiral sweeping have been made for a peak to average beam intensity of 10 to 1. With a beam diameter of 2.5 feet at the last drift tube and using spiral sweeping, the minimum setback is 44 feet and the minimum target diameter is 17 feet for a peak heat flux of 416,000 Btu/hr/ft<sup>2</sup>. This is only a small reduction from the 33 to 1 case which has a setback of 44 feet and a target diameter of 18 feet with spiral sweeping. However, any further reduction in peak to average beam intensity should reduce the target size to a greater degree.

In order to maintain the cyclic  $\Delta T$  at the back bond to less than 40° F with spiral sweeping, a faster precession rate must be used than can be obtained with the present magnet. The minimum precession rate for the 10 to 1 case is 93 r.p.s. and 127 r.p.s. for the 33 to 1 case. An economic study would be required to determine the desirability of using spiral sweeping versus using the present magnet with a minimum setback possible with circular precession.

### Metallography

In order to improve polishing and etching procedures investigation has shown that electro-polishing and etching in an electrolytic solution of sulphuric acid, orthophosphoric acid and dextrose, combined with careful mechanical polishing, produced an improved surface on samples, revealing flaws previously shown by ultrasonic inspection. The correlation between the two methods of inspection has therefore been considerably improved.

General

[REDACTED] termination of  
the Mark I Target Research Project is being expedited in order to provide  
essential data for reports now in preparation. Remaining activities are being  
confined to those items which are substantially complete and merely await  
final experimentation for equipment operability and/or confirmative data.  
A comprehensive report of this termination was outlined in LWS-24517, dated  
August 8, 1952, which was paraphrased in a letter from Mr. Fred Powell to  
Mr. J. A. Derry (LWS-12595) dated September 3, 1952.

*elite*

2043-23

## 10. A-12 TARGET AND LATTICE PHYSICS PROGRAM

### Introduction

C. M. Van Atta  
UCRL

During the period covered by this report the trend of the MTA target and lattice research program has been increasingly toward fundamental problems as contrasted with specific design questions. In line with this policy the detailed measurement of flux distributions in the small scale water lattice was concluded, and the results obtained to date are reported below.

The inelastic cross sections for deuterons up to 190 Mev and protons up to 340 Mev in a variety of target materials have been determined. These results together with other cross sections previously measured mostly at UCRL and of importance in MTA target processes are compiled and discussed in this report.

The high energy processes of the target have been studied theoretically in some detail. By a Monte Carlo method the spectrum of neutrons expected at 50 and 100 Mev nuclear excitation for the uranium nucleus has been calculated. Also a detailed theory of the high energy cascade processes of the target has been set up and the neutron yield calculated at several energies for both protons and deuterons. The computed results are compared with experimental values, and neutron yields to be expected for deuterons up to 700 Mev are given.

The effort of the experimental group is now being concentrated on the use of stripped deuterons from 510 Mev  $\text{He}^3$  particles from the 184-inch cyclotron. A continuous-flow, closed purification system has been constructed which permits recirculation of the  $\text{He}^3$  sample repeated through the cyclotron. In preliminary tests with a two liter sample of helium operation of the cyclotron for a period of 12 hours resulted in no detectable loss of helium. It is expected that in the next few weeks a beam of about 320 Mev deuterons of sufficient intensity to measure neutron yields will be available.

### Experiments with UCRL Water Lattice

John Ise  
UCRL

With the recent change in emphasis of the MTA target program from data immediately necessary for engineering design to more fundamental research, the UCRL water lattice was retired from active use, at least for the near future. Prior to this cessation of water lattice runs, however, several experiments were performed on the effect of thin water blankets between the beam

2043-24



hole wall and the surrounding lattice, on the effect of graphite reflectors, and on the flux smoothing produced by separating the primary and secondary target.

In Figs. 1 and 2 are shown a series of flux distributions (measured with bare gold foils, and therefore responding primarily to thermal neutrons) in the horizontal plane of the beam, at various depths laterally into the side wing of the water tank, and along a line parallel to the beam. The curves are labelled according to the depth into the side tank in inches. The curves in Fig. 1 were obtained with a collimating tunnel of graphite, acting as a neutron reflector, 24 in. long, 8 ft. by 8 ft. cross section and with 12 in. thick walls, placed just in front of the tank, and the position of the uranium primary and secondary is blocked in at the top of the page. Fig. 2 shows the same distributions without the graphite. The effect of the graphite in raising the flux near the entrance end of the tank is obvious from Fig. 1. A similar, smaller, effect is noticeable in Fig. 2, this being presumably due to reflection by the concrete shielding blocks in the cyclotron cave.

An experiment was also carried out to determine the effect of placing the Be primary at various distances from the uranium secondary, with regard to smoothing the total flux and perhaps maximizing production. To this end, three runs were made using a 12 in. x 12 in. x 9 in. uranium secondary placed with the front face 28 in. from the front face of the tank and an axially symmetric 8 in. x 8 in. x 4 in. beryllium primary placed in three different positions -- in immediate contact with the secondary, separated from the secondary by 12 in., and separated by 22 in. In Fig. 3 are shown the beam hole traverses (just inside the water tank side wing) parallel to the beam in each of these cases, along with the corresponding distribution for the solid uranium primary and secondary. In addition to the smoothing effect there is a considerable decrease in total flux which increases with separation of the beryllium and uranium targets. This is reasonable in view of the angular spread of stripped neutrons from the beryllium primary, the lack of complete lateral coverage of the beam hole by the beryllium, and the fact that for complete reflection (albedo of 1.00) beryllium thicknesses of about 9 in. (instead of 4 in. available with the present supply of beryllium) are necessary. It may perhaps be desirable to repeat these experiments at some later date, when larger amounts of beryllium are available.

#### Effect of Water Blanket

The studies of production throughout the lattice as a function of the initial water blanket thickness have been continued, and in Figs. 4 and 5 the production is low for blanket thicknesses of  $1/8$  in. and  $1-1/8$  in. The predicted loss in production (integrated over the lattice) is about 25 percent when the blanket thickness is increased from  $1/8$  in. to  $1-1/8$  in. Comparison of Figs. 4 and 5 does not show this loss very conclusively, although the Q-metal foil activities are so low that the uncertainties in the experimental points really preclude a very accurate determination of the difference between these two curves. Gold foil activities were also obtained throughout the lattice and inside the uranium bars, and are being presently compared with the Q-metal

foil curves in an attempt to determine the production loss, if any, more accurately.

Inelastic Cross Sections for Deuterons and Protons

W. E. Crandall and G. P. Millburn  
UCRL  
A. V. Shelton  
CRDC

Neutrons are produced in a target bombarded by energetic particles by transferring the kinetic energy of the particle to nuclear excitation leading to spallation, evaporation, fission and stripped neutrons. In competition with the primary processes of transferring kinetic energy to the nucleus is the loss of energy, through electromagnetic interaction, to the sea of electrons in the target. Analytically we can express the yield as an integral

$$Y(T_b) = \int_0^{T_b} \frac{\sigma_i(T)}{\frac{dT}{dx}(T)} \eta(T) dT \quad (1)$$

where

$Y(T_b)$  = average number of neutrons produced in a thick target by a bombarding particle of kinetic energy  $T_b$ .

$\sigma_i(T)$  = inelastic cross section for a particle of kinetic energy  $T$ .

$\frac{dT}{dx}(T)$  = atomic stopping power of target for a particle of kinetic energy  $T$ .

$\eta(T)$  = average number of neutrons resulting from the interaction of a particle of kinetic energy  $T$  with nucleus.

The energy dependence of  $\eta(T)$  is complicated since it involves not only the neutrons resulting from the primary excitation of the nucleus by the bombarding particle but also the neutrons resulting from secondary interactions. Ultimately we would hope to determine this dependence through a knowledge of the energy dependence of all the other parameters in our integral expression.

The atomic stopping of various targets is well known and therefore need not be investigated. The inelastic cross sections are in most cases only roughly known as a function of energy and, therefore, a series of experiments is now in progress to obtain better values of the pertinent cross sections which, in conjunction with neutron yield measurements, make it possible to understand better the events transpiring in the target.

The simplest method of measuring the inelastic cross section consists in measuring the transmission of the bombarding particles through an attenuator composed of the desired target nuclei. In such an experiment it is important to differentiate between the bombarding particles that are elastically scattered, charged particles emitted from excited nuclei, and in the case of deuterons the protons resulting from deuteron stripping. The elastically scattered particles are measured by having the detector subtend a sufficiently large solid angle behind the attenuator. The secondary particles as well as the stripped protons are more troublesome and will be considered separately in the section on the analysis of the data.

#### Experimental Setup and Procedure

The high energy beam of particles from the cyclotron pass through an ionization chamber A (Fig. 6) which serves as a beam monitor. These particles then impinge on an attenuator B, of thickness  $N$ , placed at a distance  $L$  from a faraday cup C, which measures the number of charges particles transmitted by the attenuator.

The current  $I_0$  from the ionization chamber is amplified by an electrometer D, whose output current through a bleeder resistor E is proportional to the ionization chamber current. Similarly the current  $I$  from the faraday cup produces an output current in a bleeder resistor F proportional to  $I$ . The ratio of the current,  $R = I/I_0$ , is measured by a null method with a Leed's and Northrup recorder G.

The experimental procedure consists in measuring  $R(N, L)$  for various thicknesses  $N$  and for several positions  $L$ . Figs. 7 and 8 are a plot of the experimental data for proton bombardment of beryllium and uranium, while Figs. 9 and 10 are the corresponding curves for deuteron bombardment. The extrapolation of  $R$  to  $L = 0$  measures the attenuation due to inelastic events and Figs. 11 through 14 show these extrapolated curves.

In addition to the complete attenuation curves, the ratio of the attenuation for Be, Al, Cu, Mo, Ta, and U for thicknesses equal to one-quarter of the range of 190 Mev deuterons, backed in every case by uranium equal to one-half the range, were measured, and also the corresponding ratios for proton bombardment. By this technique the ratio of the inelastic cross sections, free from secondary contamination can be measured as explained in the next section.

#### Analysis of the Data

The experimental transmission ratio  $R$  is related to the attenuator thickness by

$$R = \frac{I}{I_0} = e^{-\sigma_i N} + \Sigma_N \quad (2)$$

UNCLASSIFIED

2043.27

where

$\bar{\sigma}_i$  = average inelastic cross section

$L_N$  = fraction of current due to secondary charged particles.

The number of secondary charged particles escaping from the target is extremely sensitive to the fraction of the bombarding energy transmitted to the secondary. For example if we are measuring the transmission through an attenuator whose thickness,  $N$ , is 90 percent of the range of the incident particle,  $N_R$ , and if we assume that the range is related to the kinetic energy of the particle,  $T$ , by

$$R \approx KT^2 \quad (3)$$

then, if a particle has an inelastic event at the point  $x$  in the attenuator, only secondary particles carrying off the following fraction of the bombarding energy,

$$\frac{T_{sec}}{T_{incid}} = \sqrt{\frac{N-x}{N_R-x}} \quad (4)$$

will escape from the attenuator (Fig. 15).

Since at high energies, multiple emission of particles predominates it is extremely unlikely that the contributions from secondaries in the case of attenuator approaching a range in thickness can be very large. In particular, for uranium attenuators, the coulomb barrier will suppress the emission of charged particles near the end of the range, while the size of the nucleus in relation to the mean free path of nucleons in nuclear matter will tend to lead to multiple emission of particles in the case of inelastic events at higher energies and therefore the measured attenuation should be almost entirely due to inelastic events with very little secondary contribution.

For lighter elements, particularly beryllium, the contribution from knock-on events should be much more serious. If we now use attenuators of thickness  $N_x$ , backed by uranium of thickness  $N_2$  then the measured current ratio will be

$$R_x = \frac{I}{I_0} = e^{-\sigma_x N_x} (1 + L_{N_x}) e^{-\sigma_2 N_2} (1 + L_{N_2}) \quad (5)$$

where

$L_{N_x}$  = fraction of secondaries, arising from  $N_x$ , transmitted to faraday cup

$L_{N_2}$  = fraction of secondaries, arising from  $N_2$ , transmitted to faraday cup.

DECLASSIFIED

2043-21

In every case  $N_x$  is adjusted to give the same increment of energy reduction of the bombarding particle, while the thickness of uranium is held constant and sufficient to make the total attenuation almost equal to the range of the bombarding particle. Under these conditions the ratio of the attenuation due to any two attenuators will be

$$\frac{R_x}{R_y} = \frac{e^{-\sigma_x N_x (1 + \Sigma_{N_x})}}{e^{-\sigma_y N_y (1 + \Sigma_{N_y})}} \quad (6)$$

and is independent of the effect of the uranium backing,  $N_2$ .

$\Sigma_{N_x}$  and  $\Sigma_{N_y}$  should be extremely small since only secondary particles receiving the fraction of bombarding energy

$$\frac{T_{esc}}{T_{bomb}} = \sqrt{\frac{N_2'}{N_2}} \quad (7)$$

where

$N_2$  = thickness of uranium backing used, and

$N_2'$  = thickness of uranium backing to end of range of bombarding particle would contribute to the measured current. The ratios of the inelastic cross section  $\sigma_x$  for energy increments defined by the thickness  $N_x$ , where the criterion for an inelastic event is governed by the relation (7), can easily be calculated. Since the absolute cross section is most easily obtained for heavy elements, this technique is a simple and accurate means of measuring the cross section of lighter elements.

For the case of deuteron bombardment the secondary particles are primarily stripped protons. The current measured by the faraday cup is then

$$I = I_0 e^{-\sigma_1 N} + \int_{N-n}^N I_0 e^{-\sigma_1 x} \sigma_2 (1 - e^{-\sigma_3 (N-x)}) dx \quad (8)$$

where

$I_0$  = incident deuteron beam

$\sigma_1$  = average inelastic cross section for deuterons

$\sigma_2$  = effective stripping cross section for deuterons

$\sigma_3$  = average inelastic cross section for protons

$N$  = attenuator thickness

$n$  = maximum depth in target from which stripped particles can escape.

2043.25

If we say that the stripped protons have on the average half the deuteron energy at the point of stripping, then

$$n = N \quad \text{for} \quad 0 < N < \frac{N_R}{2}$$

$$n = N_R - N \quad \text{for} \quad \frac{N_R}{2} < N < N_R$$

where

$N_R$  = total range of incident deuterons.

The expression for the transmitted current can easily be integrated and by least squares fitting the values of  $\sigma_1$ ,  $\sigma_2$ , and  $\sigma_3$  determined. In particular  $\sigma_1$  is determined directly by the initial current and the attenuated current at the end of the range, since the integral in our expression approaches zero at both these limits.

Summary

A summary of the cross sections is given in Table I where we have also included related cross sections by other experimenters. Fig. 16 shows the inelastic cross sections plotted against the mass number A, while Fig. 17 shows the inelastic cross sections for protons and neutrons plotted against the kinetic energy of bombarding particle.

UNCLASSIFIED

2043-30

Table I  
Cross Sections

Element	Energy in Mev	Deuterons		Protons				Neutrons	
		Inelastic Stripping		Inelastic				Inelastic	
		(1) 190-	(1) 190-0	(2) 150-200	(2) 200-270	(2) 270-340	(3) 310-340	(4) 90	(5) 270
Be		0.45	0.40	0.173	0.169	0.152	0.131	0.19	0.12
C				0.205	0.203	0.187		0.24	0.145
Al		0.96		0.408	0.383	0.345	0.312	0.45	0.28
Cu		1.59		0.732	0.660	0.606	0.605	0.83	0.60
Mo		2.20					0.830		
Ta		3.10							
Pb				1.51	1.56	1.44		1.77	1.45
U		3.45	1.0-1.4	1.91	1.76	1.60	1.56	1.95	1.58

- (1) Present paper.  
 (2) Kirshbaum (to be published) -- Inelastic event defined as one in which primary particle lost 10 percent or more of its initial energy.  
 (3) Present paper -- Inelastic event defined as one in which primary particle lost 40 percent or more of its initial energy  
 (4) DeJuren and Knable (Phys. Rev. 77, 606-14 (1950)) -- measured total and lower limit of inelastic/total  
 Cook, McMillan, Sewell and Peterson (Phys. Rev. 72, 1264-5 (1947)) -- measured total  
 (5) DeJuren (Phys. Rev. 80, 27-30 (1950)) -- measured total and lower limit of inelastic/total

REPRODUCED

2043-31

High Energy Nuclear Processes

Warren Heckrotte  
UCRL

1. Energy Spectrum of Particles Boiled off from the Uranium Nucleus with a Given Excitation Energy

The energy spectrum of particles boiled off from an excited nucleus can be determined by a Monte Carlo type calculation. For excitation energies up to about 100 Mev, it is possible to neglect the charged particle emission, which greatly simplifies the problem. The energy spectrum and associated data has been determined for excitation energies of 50 to 100 Mev. The energy spectrum for 50 and 100 Mev is given in Fig. 18. The mean neutron energy and the number of evaporated particles is given below.

	E = 50	E = 100
mean neutron energy	2.05	3.04
number of evaporation neutrons	5.7 ± 0.5	10.6 ± 0.7

The role played by fission has not been considered in the above. Fission will have the effect of modifying the distributions as given for neutron energies to the left of the energy of the peak. For higher neutron energies the distribution should not be materially affected.

For higher nuclear excitation energies it is necessary to take account of the charged particle emission. The principal stumbling block here is the determination of nuclear binding energies for nuclei which are far from the region of stability. The best one can do here is make more or less intelligent extrapolations from the known binding energies; this is being done.

2. Theory of High Energy Nucleon Reactions with Nuclei

The theory of the interaction of a high energy nucleon with a nucleus has been studied. It is expected that one can obtain theoretically the energy and angular distribution of high energy particles which are knocked out of the nucleus by the incident particle. The theory itself has been worked out by various authors and several applications have been made. There has been, however, no clear cut agreement with experiment except in several limited cases. It has been hoped that some idea of the validity of the theory could be obtained beyond that already realized before embarking on extended applications of the theory. At this time this has not been accomplished, since such questions seem to be as involved as carrying through the actual calculations and checking against experimental data.

3043-32



### 3. Stripping Cross Section for Deuterons

Experimental results on the stripping cross section of deuterons yield a value several times larger than that given theoretically. This can be understood qualitatively on the basis of the transparent nuclear model. That is, even if both nucleons of the deuteron strike within the nuclear area there is a finite probability that they emerge without having interacted directly with any nucleon in the nucleus. Rough estimates indicate that this effect will account for the large stripping cross section as measured. However, the theoretical calculation of the effect, while simple in principle, has proved to be rather formidable, and has not as yet been carried through.

#### Extrapolation of Total Neutron Yields to High Deuteron Energies

F. L. Adelman, F. N. Holmquist and J. F. Lepore  
UCRL

In order to estimate total neutron yields at higher energies, we have attempted to set up as detailed a model of the interaction of high energy deuterons with uranium as can be readily calculated. In carrying out the computation, experimental data is incorporated wherever possible.

The model used will be discussed and preliminary results will be presented here. However, a more detailed report will be made in the future.

Fig. 19 is a diagrammatic representation of the model. When a deuteron strikes a nucleus, one or more of the following events will take place:

(a) Either the proton (S. P. in Fig. 19) or the neutron (S. N.) may be separated from its partner without colliding with any of the nucleons of the nucleus. For the purpose of simplifying the computation, all such stripped particles are assumed to have half the energy of the interacting deuteron. This assumption is consistent with the spectrum observed by Hadley and York, and corresponds, in fact, to taking the average energy of the stripped particle:

(b) One of the incident nucleons may collide with a nucleon in the nucleus, causing one or more nucleon to be ejected from the nucleus at high velocity. The relative numbers of such knocked-on protons (K. P.) or neutrons (K. N.) are taken as the relative numbers of protons and neutrons in the uranium nucleus (5:8); for simplicity, the energy of a knocked-on nucleon is taken to be half the energy of the incident nucleon or  $E_D/4$ . This assumption is consistent with the results of collision of free nucleons.

(c) Due to the various interactions, the residual nucleus may be excited, and low energy neutrons (n) and protons will be evaporated. The protons die by ionization, but the neutrons are emitted with a mean energy above the fission threshold of  $U^{238}$ .

The high energy neutrons and protons from (a) and (b) continue on and collide with other uranium nuclei, causing additional processes (b) and (c). Once again, the particles from (b) and subsequent collisions, now of energy  $E_D/8$  or less, will continue to interact, as in Fig. 19, until the energy of the particles ejected becomes so low as to be indistinguishable from the tail of the evaporation spectrum. A numerical integration over the range energy curve is required in order to arrive at the numbers of evaporation neutrons produced. Partly in order to avoid a double numerical integration, experimental data is used to evaluate the number of evaporation neutrons produced by fast protons, as indicated by the diagram. All the evaporation neutrons produced in these various processes are then permitted to multiply as in the ordinary fast effect in uranium.

Some of the numbers included require some examination. Thus,

(a) An effective stripping cross section has been assumed. Two points (190 Mev and 700 Mev) were computed using experimental data on nuclear transparency and calculated data for Serber and electric stripping. The curve used in these preliminary calculations is not the only reasonable relationship, and, in fact, a more realistic curve through these points will lead to lower numbers at low energies and higher predictions at higher energies.

(b) The number of evaporation neutrons was estimated from experimental data, making allowances for those neutrons produced from fission. There is some reason to believe that the data is too low at low energies, but this will be investigated.

(c) The number of knock-out nucleons was calculated by energy conservation.

(d) The use of a mean energy  $E_D/2$  for the stripped particles appears to be fairly satisfactory, although the correct distribution may later be taken into account. However, the choice of  $E_{inc}/2$  for the mean energy of the knocked-out nucleons is less satisfactory. For example, at low energies, the emission of low energy nucleons is probably somewhat inhibited. On the other hand, the effect of multiple collisions inside the uranium nucleus will be to give a larger number of lower energy particles.

(e) The ratio 5:8 of knocked-out protons to neutrons will be modified at all energies by the possibility of multiple collisions and charge exchange. Furthermore, at low energies, proton emission will be reduced by the coulomb barrier.

(f) The assumed fast effect will be modified by more recent measurements on the  $U^{238}$  fission cross section and on the energy spectrum of the evaporation neutrons.

Preliminary results of the calculation are shown in Fig. 20, along with the experimental data. The agreement with the measured values is excellent. An

RECEIVED

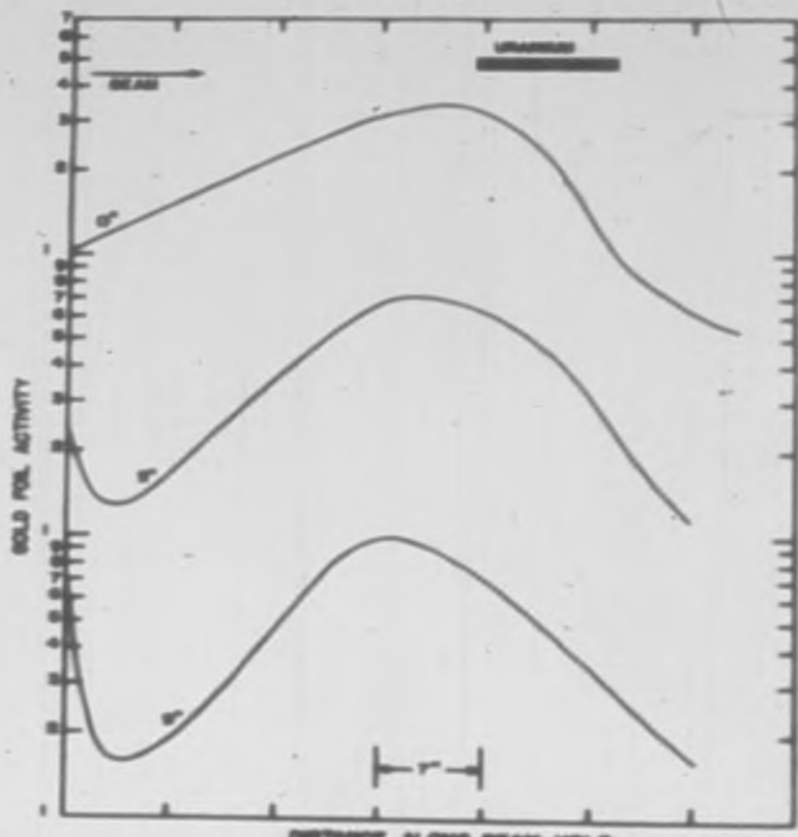
2043-34

additional check is provided by a similar calculation for 350 Mev protons. In this case the experimental value is 12.8; the calculated is 12.4.

Previous attempts to extrapolate the internal yields have been discussed in UCRL-951 and UCRL-1389, and a suggestion for extrapolating the total yield appeared as CRD-T4A-126 (LWS-24442). In none of these, however, were all the processes which take place included. It should be noted that the preliminary extrapolated neutron yields reported here are significantly lower than those of CRD-T4A-126.

DECLASSIFIED

2043-35



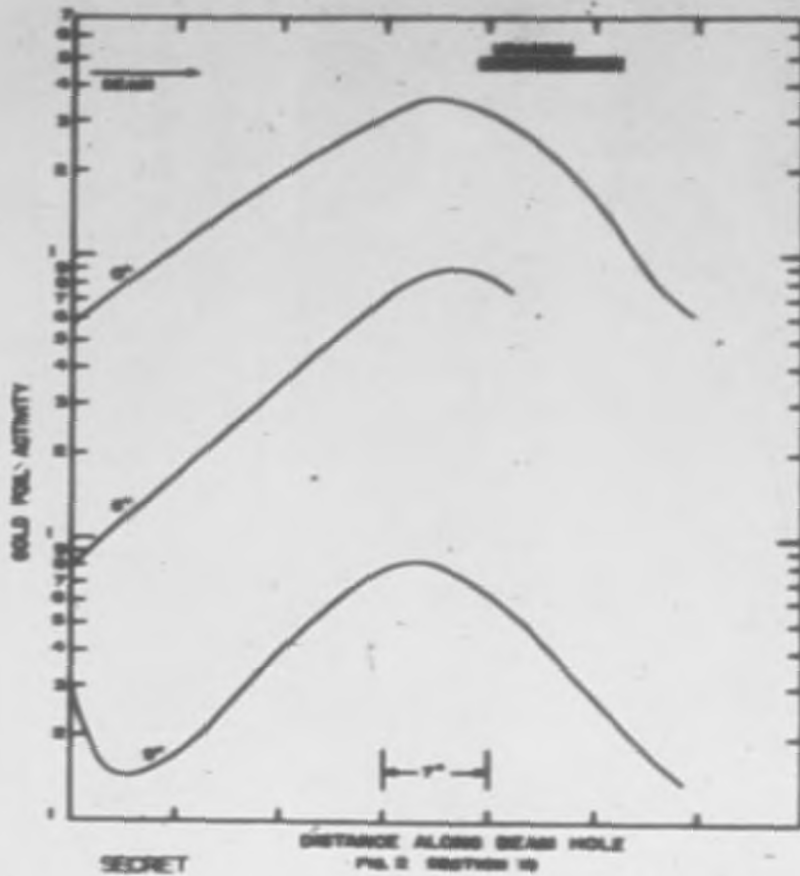
SECRET

DISTANCE ALONG BEAM HOLE  
FIG. 1 SECTION 10

ML-3000

DECLASSIFIED

2043-36



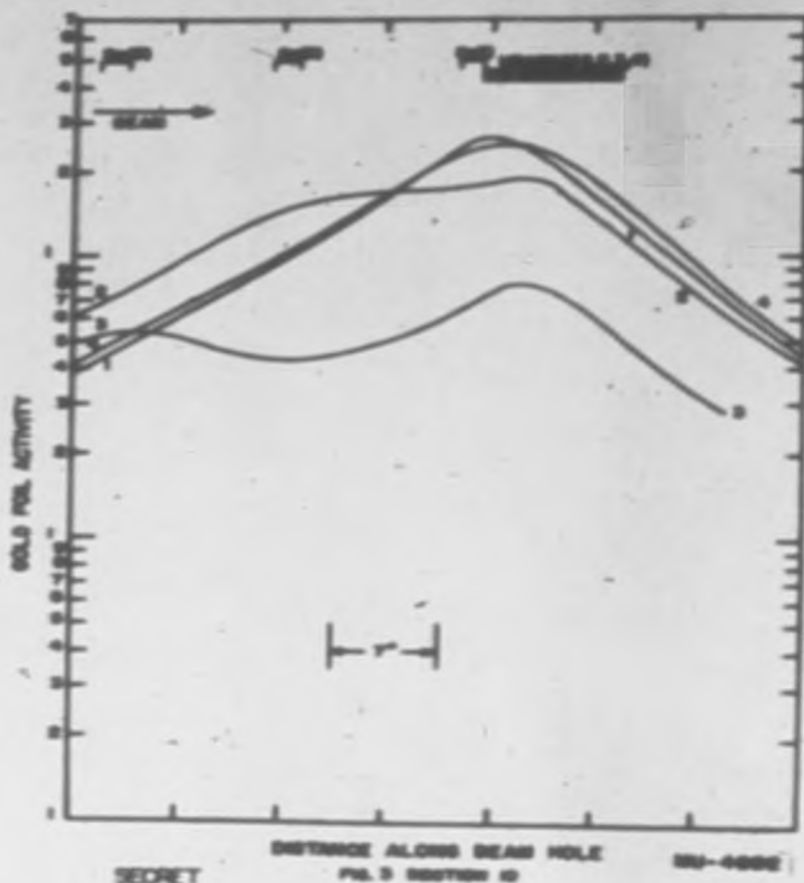
SECRET

DISTANCE ALONG BEAMS HOLE  
FIG. 2 SECTION 10

NU-5001

UNCLASSIFIED

2043-37

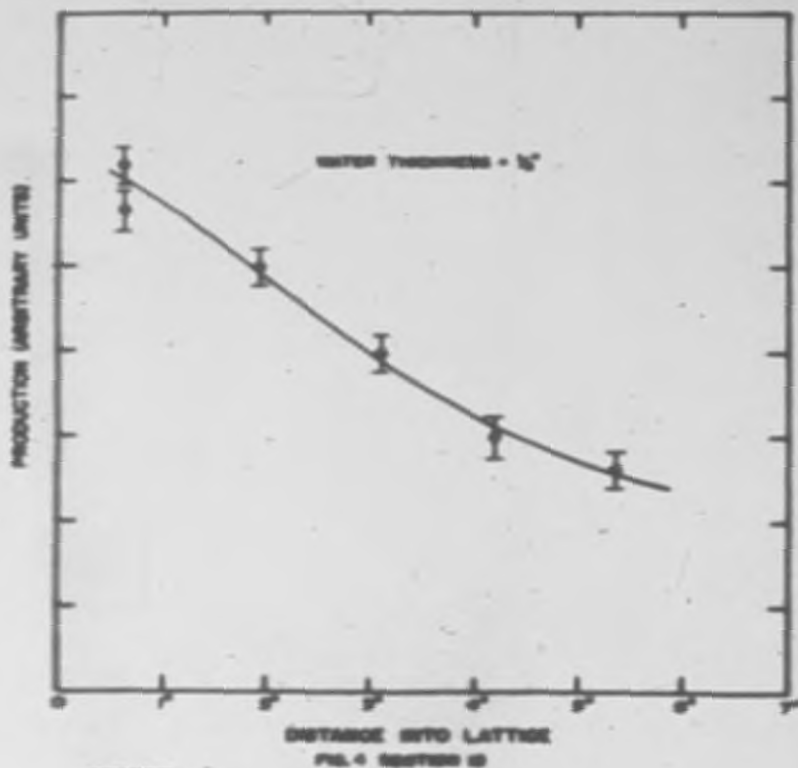


SECRET

UCAL-2043

UNCLASSIFIED

2043-38

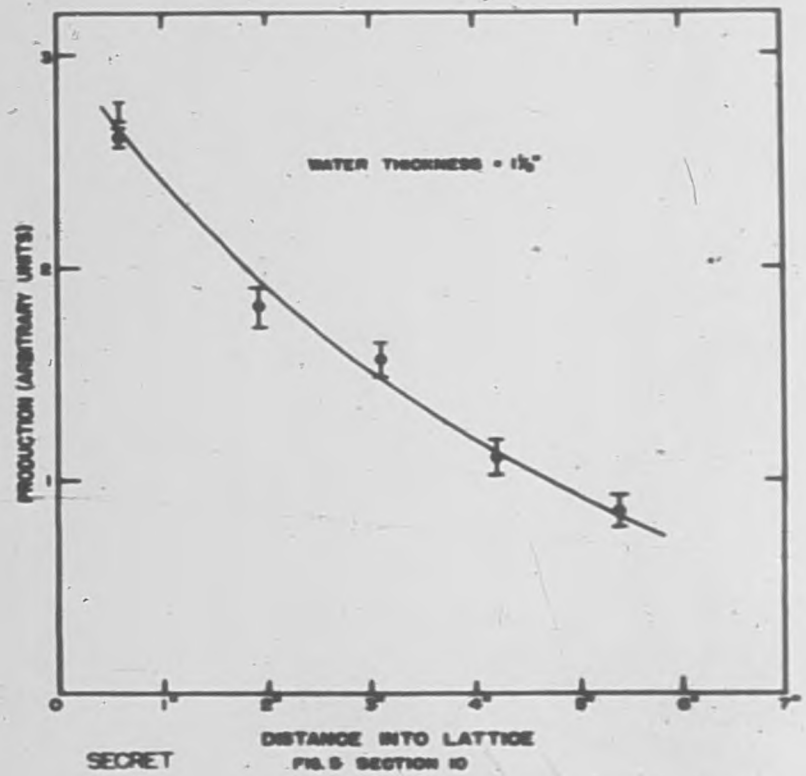


SECRET

NU-6000

DECLASSIFIED

2043-39



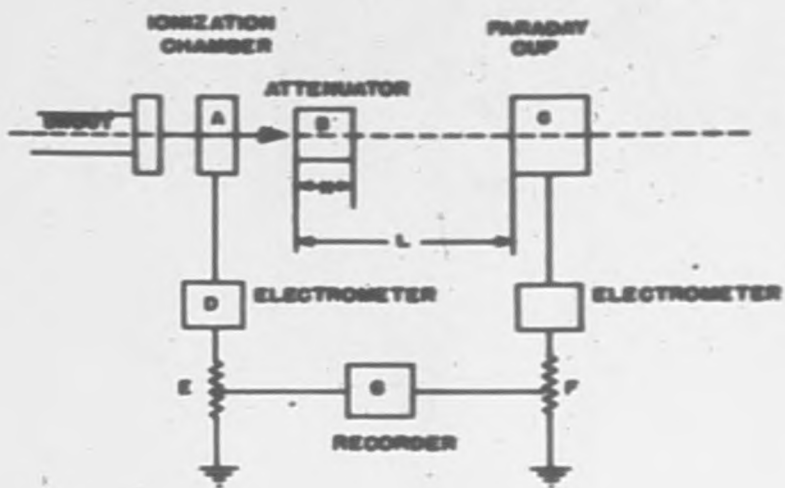
SECRET

FIG. 5 SECTION 10

NU-4894

2043-40





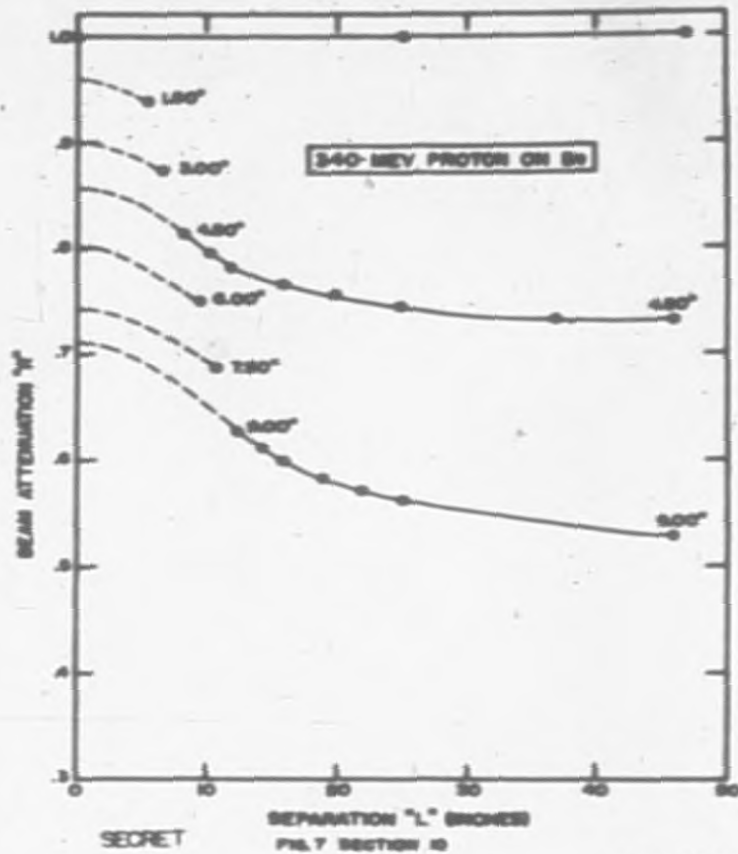
BLOCK DIAGRAM OF EXPERIMENTAL SETUP

FIG. 6 SECTION 10

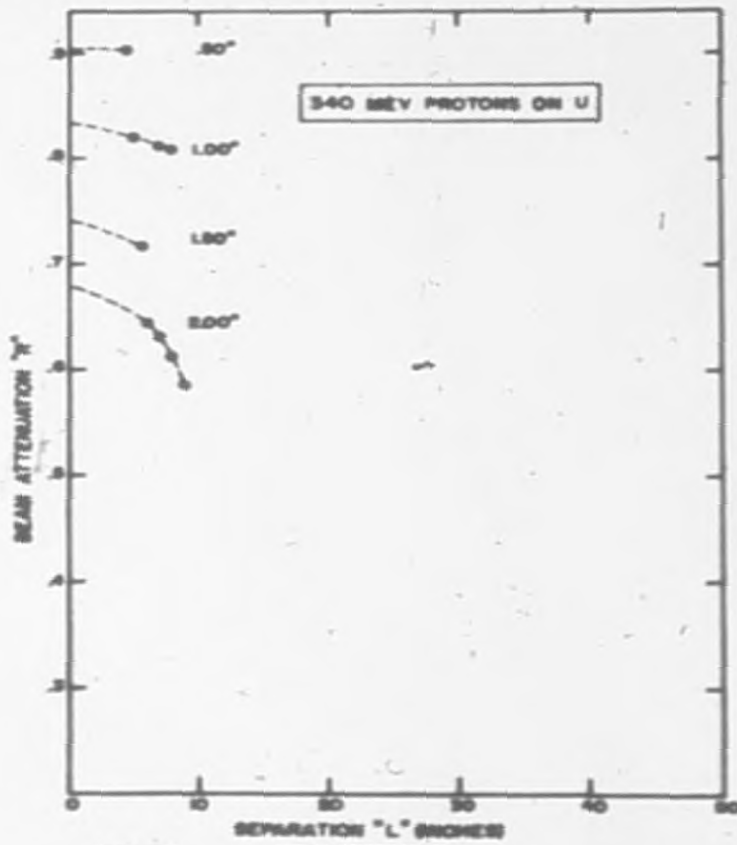
SECRET

MU-4696

2043-41



20K3-42

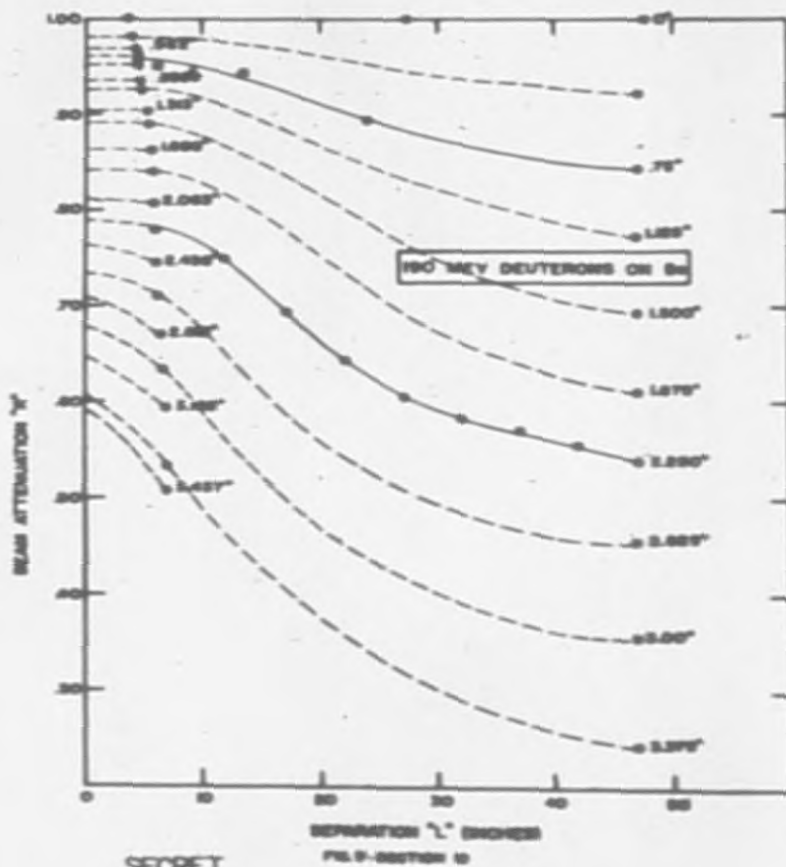


SECRET

FIG. 6 SECTION 49

ML-4887

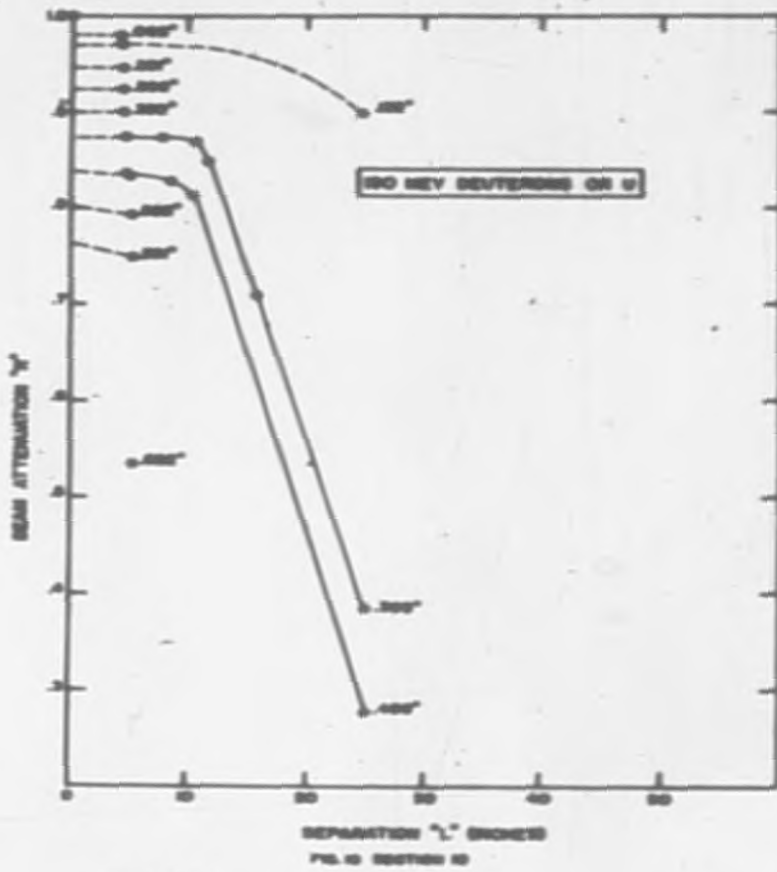
20K3-K3



SECRET

NU-6000

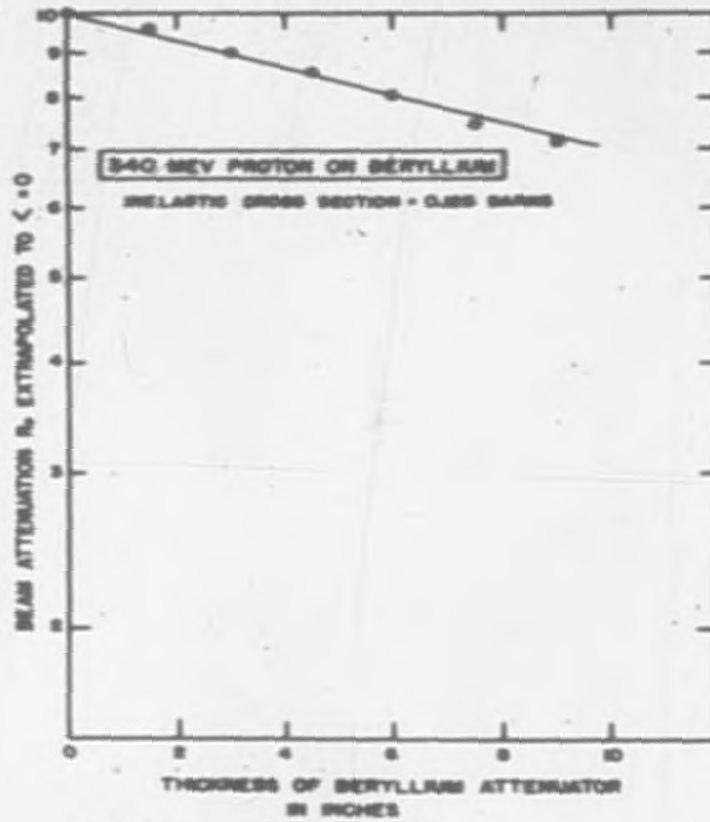
2043-44



SECRET

50-6000

2043-45



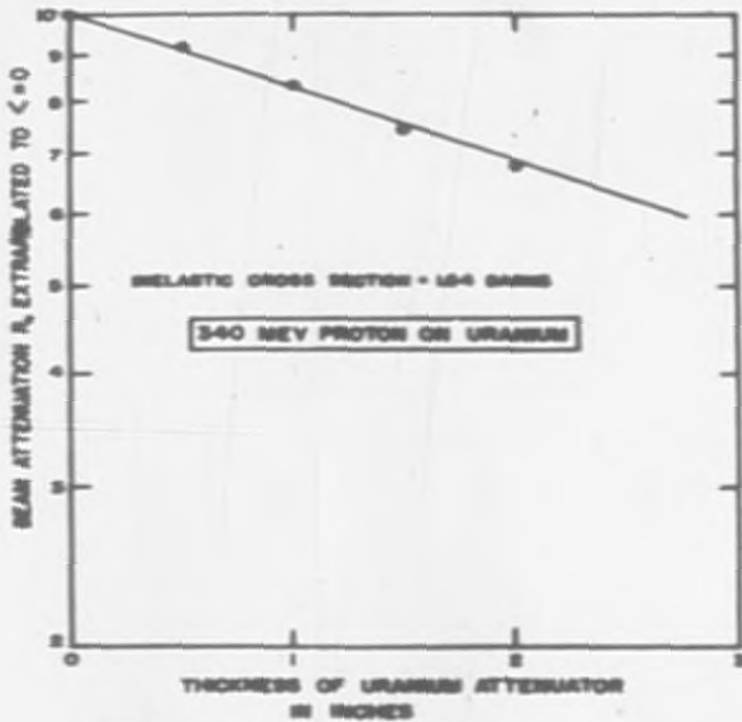
SECRET

FILE 8 SECTION 10

BU-4700

UNCLASSIFIED

2043-46



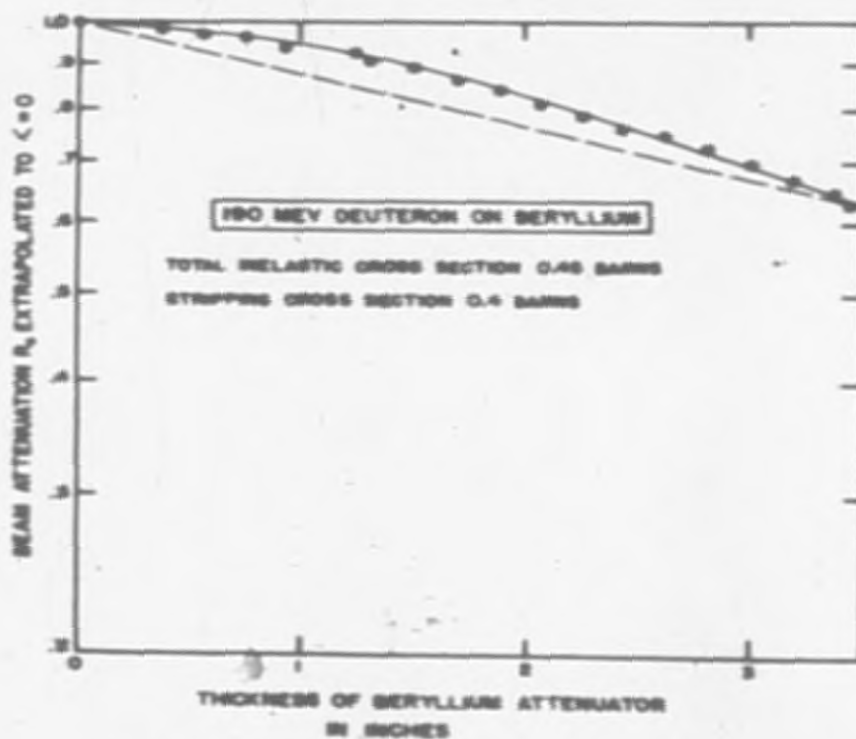
SECRET

FIG. 12 SECTION 10

NU-6701

UNCLASSIFIED

20K3-47



SECRET

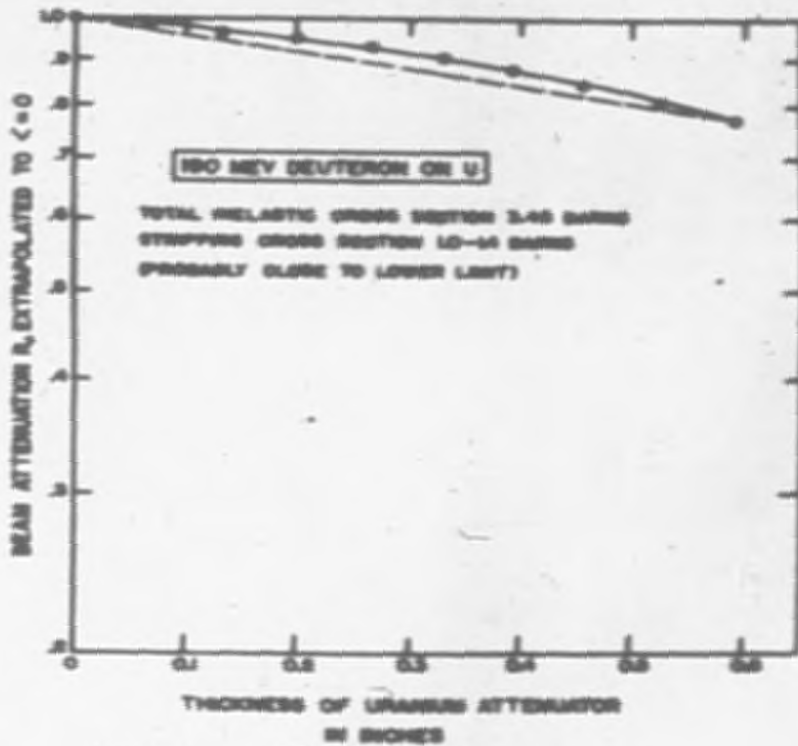
FIG. 13 SECTION 10

ML-6702

REPRODUCED FROM UCRL-2043

2043-48





SECRET

PL 14 SECTION 10

NU-4708

UNCLASSIFIED

3043-49

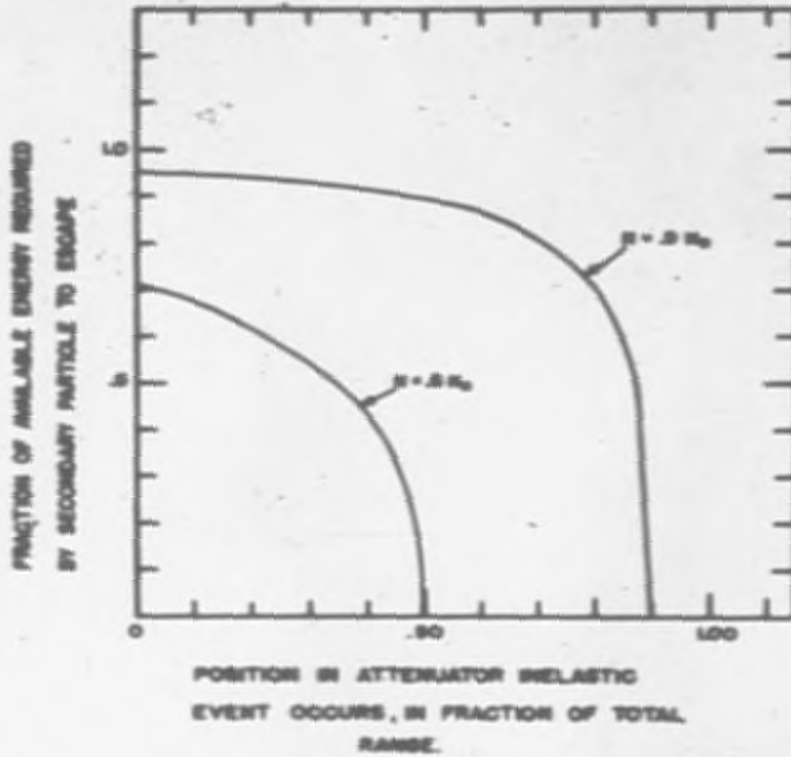


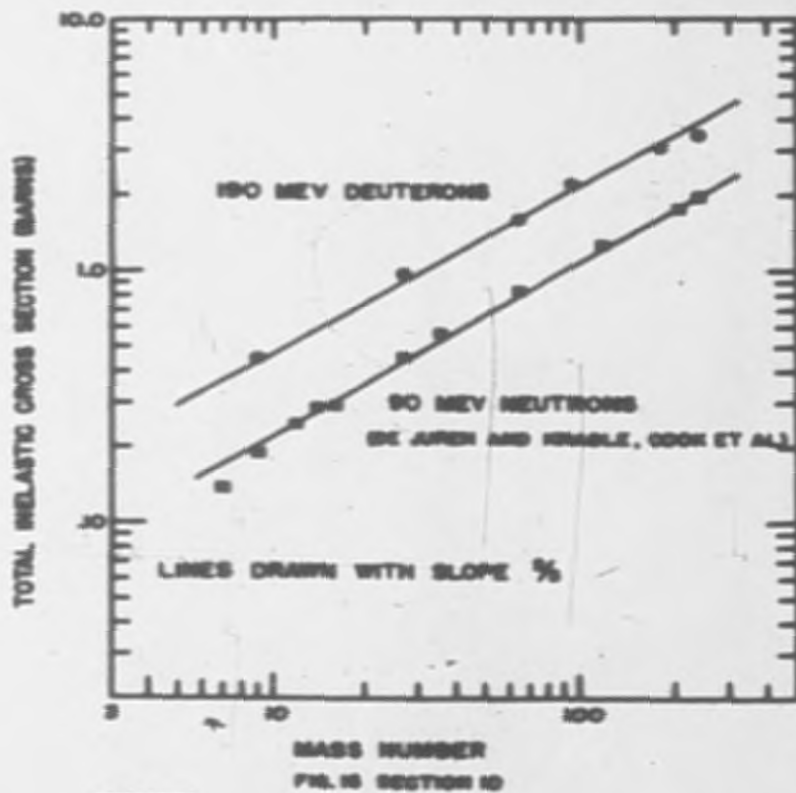
FIG. 15 SECTION 10

SECRET

BU-4704

DECLASSIFIED

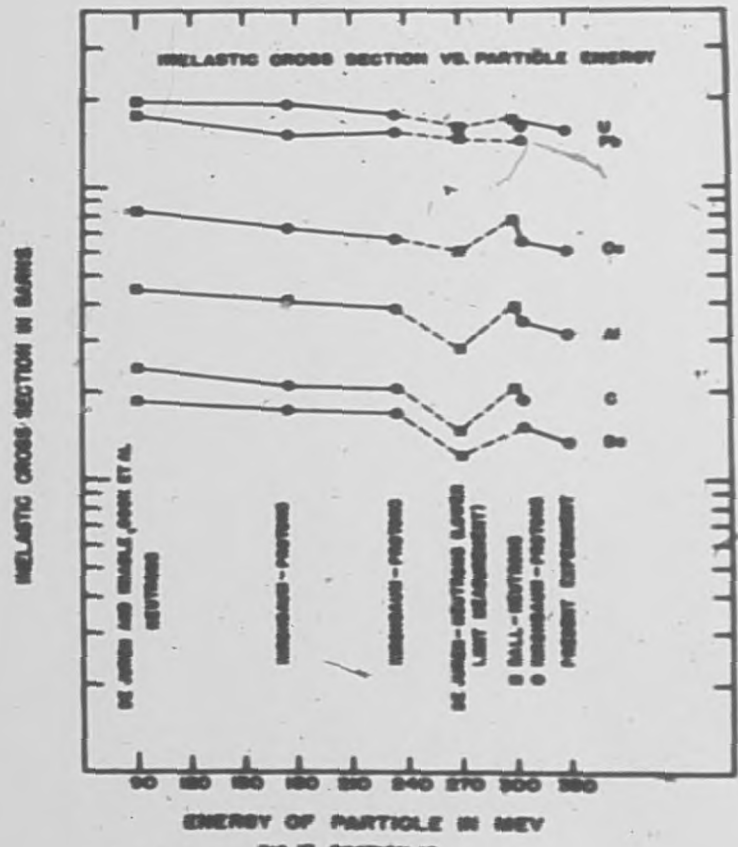
2043-50



SECRET

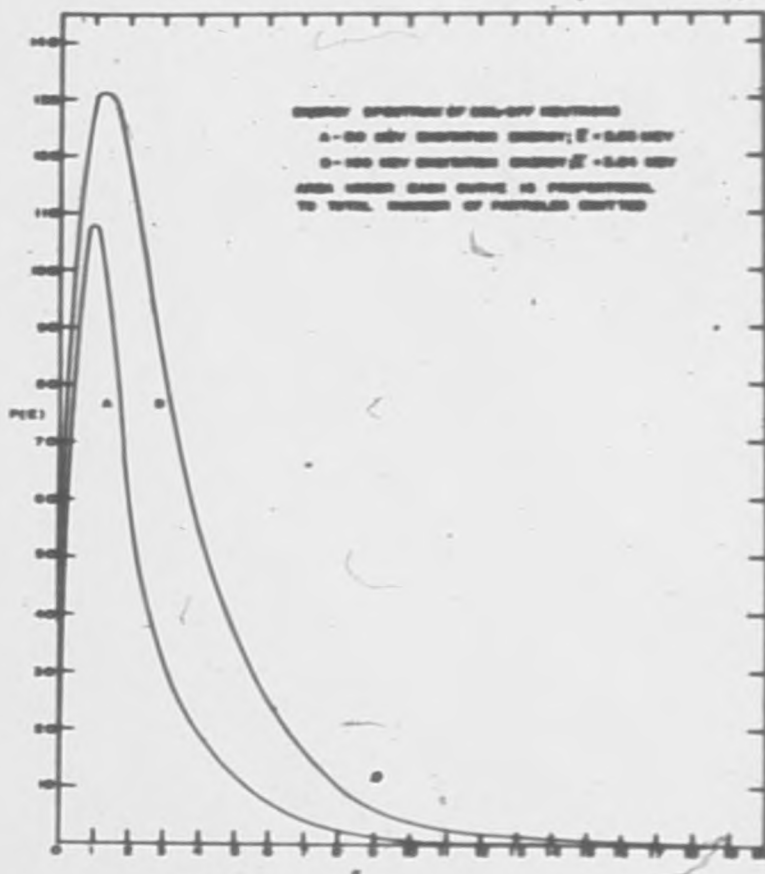
BU-4708

DECLASSIFIED 2043-51



SECRET  
 FIG. 17 SECTION 10  
 BR-6706

UNCLASSIFIED 2043-52

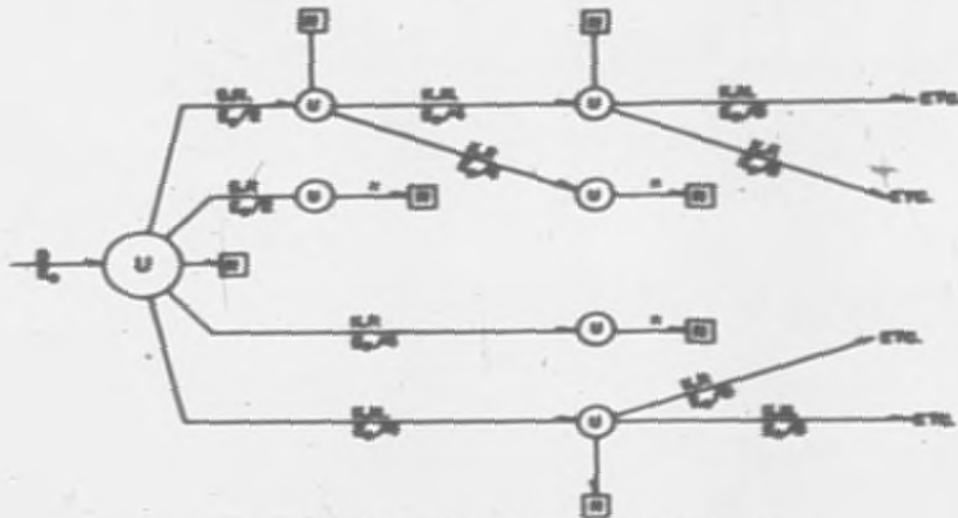


SECRET

FIG. 10 (PARTIAL OF)

100-4000

2043-53



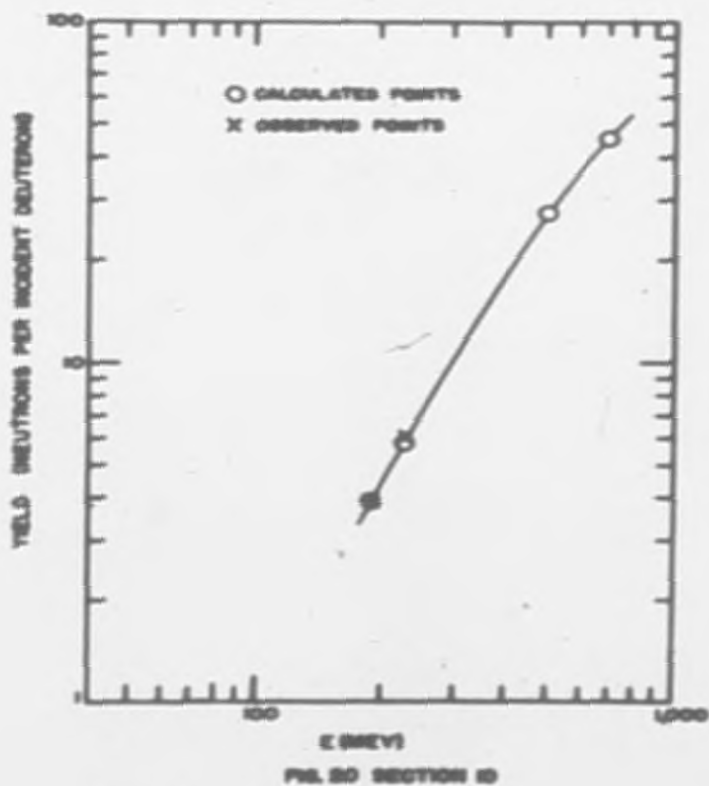
\* EXPERIMENTAL DATA USED INSTEAD OF CIRCUITS

SECRET

FIG. 10 SECTION 10

MU-4707

2043-54



SECRET

MU-4708

2043-55

## II. A-12 TARGET THEORETICAL AND ENGINEERING PHYSICS

D. H. Imhoff

W. H. Harker, C. C. Old, J. R. Dorfaldson, R. E. Nather,  
J. W. Flora, R. H. Graham, K. Bernstein, S. H. Fitch,  
A. E. Farnham, F. E. Bjorklund, W. E. Drummond, E. J. Strain  
CRDC

### Primary and Secondary Target Studies

#### Extrapolation of Neutron Yields from High Energy Charged Particle Bombardment of Solid Targets.

Recent studies involving extrapolation of neutron yields from deuteron and proton bombardment of solid uranium targets have indicated the increasing importance of secondary reactions with increasing energy. As a result, the previous extrapolations (UCRL-1164, UCRL-1389) predict yields too low at the higher energies. In this report an extrapolation with energy has been made by two different approaches.

The following processes contribute to the neutron yield in a solid uranium primary and secondary target.

1. Deuteron induced fission or spallation reactions in the primary target. The latest estimates of the cross sections involved indicate that of the total deuteron inelastic events, approximately 50 percent result in fission and the remainder in spallation events. Neutrons produced in the above reactions are of two general types, evaporated neutrons with an average energy of approximately 2-3 Mev and knock on and stripped neutrons with average energies considerably greater than the evaporated neutrons and with a wide spread in energy.
2. Secondary high energy reactions yielding both evaporated and knock on neutrons by fast fissions and spallation in the primary target. These reactions are caused by stripped protons and neutrons and knock on neutrons and protons of high energy.
3. Evaporated neutron induced fast fissions in uranium. The energy spectrum of evaporated neutrons has been measured experimentally at 190 Mev and found to be of average energy considerably above thermal fission neutron energy. The neutron production per fission should be similar to that of thermal fission and corresponds to what is termed the "fast effect" in reactor technology.
4. Stripped or exchange neutron induced fissions and spallation in the secondary target.
5. Evaporated or knock on neutron induced fast fissions in the secondary target.

In general the neutron yields obtained by charged particle bombardment can be attributed to two factors. In the first place, it is reasonable to assume

2043-56



that the number of neutrons produced from the foregoing reactions will be proportional to the number of neutrons which undergo an inelastic nuclear event before suffering an ionization death. The second factor is related to the fraction of deuteron energy which goes into nuclear processes. If one assumes that the amount of energy that is effective in producing neutrons is proportional to the average deuteron energy on collision and that the number of neutrons per Mev resulting from all processes is independent of deuteron energy, the following extrapolation results:

<u>Initial Deuteron Energy Mev</u>	<u>Ratio of Neutron Production</u>
190	1.0
350	4.4
500	9.4
700	16.7

It is apparent that the weakest assumption is the second. In order to be conservative the following energy extrapolation has been employed. The method represents a refinement of the extrapolation presented in UCRL-1164 and UCRL-1389. The assumption is made for the purpose of producing neutrons, a deuteron can be considered as two protons each of half the energy. This appears to be a conservative approach since a high energy neutron cascading from an initial impact is more effective in producing further neutrons than a proton since it does not suffer ionization losses. This assumption, however, allows the use of the 340 Mev experimental data since we are assuming that the number of neutrons produced by a proton is one-half the number produced by a deuteron of twice the energy.

If the theoretical curve thus obtained is normalized to the 190 Mev experimental point, the 340 Mev point is about 60 percent of the experimental value. In an attempt to use this concept to correlate the proton data, an effective differential cross section was derived which presumably includes secondary events and which was fitted to the experimental data at 190 and 340 Mev. If then a deuteron can be thought of as two protons each of half the energy an effective differential cross section for deuterons up to 680 Mev may be prepared from the empirical proton curve. This can then be employed to obtain an extrapolated yield which is 80 percent (at 700 Mev) of that obtained by the constant efficiency approach. Both extrapolations are given in Fig. 1, the second one as the solid curve.

It is felt that the second extrapolation is a more conservative one, since it appears to underestimate the effectiveness of the deuteron. Furthermore, this method gives results which are in agreement with the most recent UCRL work. Until further experimental and theoretical studies are made, it is believed that the second method gives a reasonable estimate of neutron yields at the higher energies.

2043-57

Modified Base Case Target

A two medium two energy group neutron diffusion study of the modified base case target has been completed. Briefly, the results indicate that per incident deuteron 8.7 atoms of plutonium are formed within the target, 5.1 neutrons escape from the target, and 2.6 thermal fissions occur.

The dimensions of the target components considered were as follows:

Primary Target

Plates -----0.045" U clad with ) Contained in two  
0.010" Zr on each side) rows of bayonet  
Coolant Channels -----0.100" water ) tubes

Secondary Target

0.200" U core plate separated by 0.150" water (9 rows) and  
0.320" U core plate separated by 0.100" water (12 rows)  
All plates clad with 0.010" Zr on each side.

Defining medium a to be one deuteron range and medium b to be all remaining material, the following nuclear parameter values were determined.

<u>Medium a</u>		<u>Medium b</u>	
f = 0.783	$L^2 = 6.61$	f = 0.891	$L^2 = 4.83$
p = 0.793	$\gamma = 42.1$	p = 0.559	$\gamma = 52.9$
E = 1.025	$\eta_1 = 3.09$	E = 1.075	$\eta_1 = 2.29$
n = 0.853	$\eta_3 = 0.709$	n = 0.853	$\eta_3 = 0.985$
k = 0.543	$\beta = 0.598$	k = 0.457	$\beta = 0.598$

Based on primary and secondary target efficiencies of 75 percent and 85 percent respectively, 12.0 neutrons per deuteron are created in primary events in the combined target. Fig. 2 shows the calculated fast and thermal flux profiles, while Table I summarized the results per deuteron incident on the target.

Table 1

<u>Quality</u>	<u>Primary (1 deut. range)</u>	<u>Secondary (all materials beyond one range)</u>	<u>Total Target</u>
Pu Prod. in Resonance Region	1.36	3.14	4.50
Pu Prod. In Thermal Region	1.87	2.37	4.24
Total Pu Production	3.23	5.51	8.74
Fast Neutrons Escaping	3.88	0.47	4.35
Thermal Neutrons Escaping	0.72	0.05	0.77
Total Neutrons Escaping	4.60	0.52	5.12
Thermal Fissions	1.11	1.52	2.63
Thermal Fission Heat Load(Mev)	210	290	500

Lattice StudiesSplit Lattice

As a method of reducing lattice inventory and decreasing the peak to average ratio of the radial heat distribution, a split lattice has been investigated. In this lattice the first few centimeters in the radial direction consist of a closely packed lattice which serves to reduce the streaming of neutrons into the cavity. The remainder of the lattice is chosen to have an optimum reproduction factor.

In the study a total lattice thickness of 30 cm was chosen. This is backed up by an infinite graphite reflector. The lattice is made up of 1/2 in. diameter uranium rods clad with 0.025 in. of aluminum. Table 2 below gives a comparison of the optimized split lattice as compared with the base case lattice.

Table 2

	<u>Split Lattice</u>	<u>Base Case Lattice</u>
Rod Diameter (U + Al)	1"	1"
Aluminum Cladding	0.025"	0.025"
Lattice Thickness		
Internal Section	10 cm	30 cm
External Section	20 cm	-----
Center to Center Rod Spacing		
Internal Section	1.25"	1.25"
External Section	1.375"	-----
Infinite Reflector Material	Graphite	Graphite
Total Number of Pu Atoms Produced Per Neutron Incident On Lattice	1.227	1.229
Peak to Average Radial Heat Load	1.65	1.73
Relative Metal Inventory	0.891	1.000

DECLASSIFIED

3043-59

As is seen from the table, the peak to average radial heat load can be reduced by 4.6 percent while the inventory is reduced by 11 percent with no resultant loss of production.

Figure 3 shows a, the fast and thermal flux distributions for this type of lattice.

#### Production in a Pellet Type Lattice.

Since some of the handling difficulties in the MTA lattice might be overcome by the use of fuel spheres rather than rods or slabs, some of the properties of such a lattice have been investigated.

Plutonium production and fissions per neutron incident on the lattice have been calculated as functions of the fuel sphere radius and porosity of the bed. The results of these calculations are shown in Figs. 4 and 5.

The lattices considered use uranium depleted as fuel. The cladding is aluminum and the moderator is light water. Calculations were carried out for lattices with 27 percent, 38 percent, and 47.5 percent voids which correspond to tightest, random, and loosest packing respectively.

Standard two group methods were used in the calculations.

To obtain the thermal utilization for use in the two group equations a set of diffusion equations with the usual boundary conditions were solved for clad spheres using the following approximations:

1. The moderator may be treated as a spherical shell.
2. Thermal neutrons are produced uniformly throughout the moderator and are not produced in either the fuel or cladding.

For thin cladding these equations give

$$\frac{1}{\Gamma} = F \times \frac{\Sigma_1 V_1}{\Sigma_0 V_0} \left[ 1 + \frac{D_2 d}{D_1} X_2^2 R_2 (R_2 - R_0) \right] + \frac{X_1 V_1 d}{4\pi R_2} + \frac{\Sigma_1 V_1 (R_2 - R_0)}{4\pi R_2 R_0 D_2}$$

$$\text{where } F = \frac{(X_0 R_0)^2}{3} \frac{\tanh X_0 R_0}{X_0 R_0 - \tanh X_0 R_0}$$

$$d = \frac{1 - X_1 R_1 \text{Coth } X_1 y}{1 - X_1^2 R_1 R_2 - X_1 y \text{Coth } X_1 y}$$

$$y = R_1 - R_2$$

The subscripts 0, 1, 2 refer to fuel, moderator, and cladding respectively.  $R_0$ ,  $R_1$ ,  $R_2$  are the radii of the fuel sphere, unit cell, and clad sphere.  $V_0$  is the fuel volume and  $V_1$  the volume of the moderator. The remaining symbols have the standard diffusion theory meaning.

Graphs of  $F$  vs  $X_0$ ,  $R_0$  and fast effect  $E$  vs  $X_0$ ,  $R_0$  are presented in Figs. 5 and 7. Inspection of Fig. 4 will show that to obtain good production with a reasonable sphere size a loose packed lattice must be used. Calculations were carried out for spheres with thicker cladding which would give a smaller fuel to moderator ratio. These calculations indicated that production dropped with increased cladding thickness. It is possible that some type of channeling such as a set of rods on which the fuel spheres rest may be used to attain uniform loose packing and high production. If this is done a correction will have to be made to account for absorption in the structural materials used and the resulting production will be somewhat lower than that shown in Fig. 4

#### Product Level Variation in A Pellet Type Lattice

A lattice fueled with spherical fuel elements offers the advantage of a more uniform product level than the rod lattices conceived at present. This more uniform product distribution might be achieved by removing the lattice charge, mixing it and then replacing it several times during the total irradiation period.

This process raises two questions; how many passes are necessary to insure a given degree of product level uniformly and what is the probability that a sphere will reach a product level high enough to make rupture of the element probable? These questions can be answered by treating the system statistically as a number of cells into which the balls are thrown at random, each ball remembering its past history.

Some results are given in Table 3 below; the fraction of spheres whose product level lies within thirty percent of the average is tabulated as a function of the number of times the spheres are removed, mixed, and replaced in a light water moderated lattice with a graphite reflector.

Table 3

<u>Number of Passes</u>	<u>Percent of Total Number of Spheres Whose g/t Level Lies Within 30 Percent of Average g/t Level</u>
3	75
4	87.5
5	93.8
6	96.0
8	96.9

UNCLASSIFIED

2043-61

The above figures are only indicative of the general trend since they represent a rough approximation in which only two cells were used. Further work is being performed to obtain more accurate results using many cells.

#### Light Water Moderated Aluminum Clad Slab Lattices

An aluminum clad slab lattice has been studied to determine the production of plutonium in the lattice. The basic design of such a lattice is given in Fig. 8. Depleted uranium XXXXXXXXXX is used in the plates, and the cladding is 25 mil aluminum sheets. This design is shown in Fig. 9. *white*

The problem was approached using two group diffusion theory for resonance and thermal energies in a finite lattice. Losses from the resonance group were taken as 0.09 neut./incident neut., and from the thermal group 0.30 neut./incident neut.

A maximum production was determined by optimizing the slab thickness and water to slab volume ratio. The productions and fissions both per incident neutron for a thickness of 5/8" and a volume ratio of 0.87 are given in Table 4. The base case rod lattice productions are also given for comparison.

Table 4  
Lattice Production and Fissions

	Slabs	Rods
Resonance Production	0.6267 n/in n	0.6650 n/in n
Thermal Production	0.6801	0.5910
Total Production	1.3068	1.2560
Fissions	0.4320 f/in n	0.3530 f/in n

#### Corrections for H<sub>2</sub>O Moderated Lattices

The high ratio of fuel to moderator required for optimum production in the MTA lattice will produce deviations from the neutron distribution predicted by diffusion theory. A series of corrections are being developed to take into account this close spacing of fuel elements. The corrections considered to date are those for resonance escape probability and those for fast effect.

**Resonance escape probability:** In the resonance region two types of absorption occur. First volume absorption of neutrons which are weakly absorbed and secondly surface absorption of those neutrons which energies coincide with the resonance energies of the fuel. To obtain an absorption cross section which will effectively take into account both types of absorption, the following formula is usually used.

$$\sigma_{\text{eff. Res.}} = 9.25 \left( 1 + \frac{2.5}{0.1 + M/S} \right)$$

Where M and S are the mass and surface area respectively of the fuel elements.

If the fuel elements are closely spaced they tend to shield each other and lead to a spectrum depleted of resonance energy neutrons thereby reducing resonance absorption. - To account for this the formula

$$\sigma_{\text{eff. Res.}} = 0.925 \left( 1 + \frac{2.5C}{0.1 + M/S} \right)$$

is used.

Where C is the ratio of the number of neutrons which reach the surface of the fuel element without collision in the actual lattice to the number which would reach the surface without collision if a single fuel element were embedded in an infinite body of moderator.

For an array of infinite plates this expression is

$$C = 1 - 2 E_3 \left( \frac{a}{\lambda} \right)$$

where

a = thickness of the moderator layer

$\lambda$  = scattering mean free path for resonance neutrons in the moderator

and

$$E_3(x) = \int_1^{\infty} \frac{e^{-x\xi}}{\xi^3} d\xi$$

The correction  $C = 1 - F$  for two infinite rods of Radius  $R_1$  with a center to center separation  $d$  is derived by Dancolf and Ginsburg in CP-2157.

$$\text{They obtain } F = \frac{R}{\rho} \int_{-\pi/2}^{\pi/2} d\theta \int_{-\pi/2}^{\pi/2} d\phi \frac{XX'}{\rho^3} K_{1,3} \left( \frac{\rho}{\lambda} \right)$$

where  $\rho$  is the distance between two surface elements, one on each rod.  $\theta$  and  $\phi$  are the angles from the line connecting the rod centers to the radius of each rod passing through the surface element under consideration

$$X = d \cos \phi - \rho [1 + \cos(\theta + \phi)]$$

$$X' = d \cos \theta - \rho [1 + \cos(\theta + \phi)]$$

$$\text{and } K_{1,3}(x) = \int_x^{\infty} dx \int_x^{\infty} dx \int_x^{\infty} dx K_0(x)$$

This integral must be evaluated by numerical methods.

In a square array the correction is  $1 - 4F$  and in a triangular array the correction is  $1 - 6F$ .

C for a plate lattice has been evaluated as a function of  $(a/\lambda)$  and evaluation of C for rod lattices is in progress.

UNCLASSIFIED

2043-63

Fast Effect

In a tightly packed water moderated lattice there is a large probability that a neutron will have its first collision in a fuel element other than the one in which it was born. This leads to a considerable increase in the fast effect. The usual expression for E is

$$E = \frac{1 - P + \frac{\sigma_i}{\sigma_t} P}{1 - P \frac{\nu \sigma_c + \sigma_a}{\sigma_t}}$$

where P = the probability that a neutron will make its first collision with the fuel material of the lattice and the remaining symbols have the usual meaning.

$P = P_{int} + P_{ext}$  where  $P_{int}$  is the probability that the first collision will take place in the fuel element in which the neutron is born and  $P_{ext}$  is the probability that the neutron will make its first collision in an external fuel element.

The expression for  $P_{ext}$  derived for plates is:

$$P_{ext} = \frac{a}{\lambda} \sum_{\text{all plates}} \left\{ E_3 \left[ \frac{n(d+a)+a}{\lambda} \right] + E_3 \left[ \frac{n(d+a)-a}{\lambda} \right] - 2E_3 \left[ \frac{n(d+a)}{\lambda} \right] \right\}$$

where d = thickness of moderator layers  
 a = thickness of plates  
 $\lambda$  = first collision mean free path for fission neutrons.

To obtain  $P_{ext}$  for cylinders a double integral must be evaluated by numerical methods.

A comparison for some typical results obtained with the new parameters to those obtained with the uncorrected parameters is given in Table 5.

Table 5

	<u>Old Parameters</u>	<u>Mod. Parameters</u>	<u>%Change</u>
Thermal Utilization	0.915	0.900	-0.55
Resonance escape prob.	0.630	0.637	+1.11
Fast fission effect	1.028	1.085	+5.54
Neutrons/fuel absorption	0.853	0.853	- - -
R = fPEN	0.505	0.536	+6.14
Production in infinite lattice	1.444	1.529	+5.89

2043-64



Natural Uranium Lattice

A preliminary survey of water moderated lattices loaded with natural uranium fuel rods has been performed, assuming the base case lattice geometry. The effects of both rod diameter and rod spacing were investigated. The characteristics of the maximum production natural uranium lattice are compared in Table 6 with those of the optimized base case lattice below.

Table 6


<u>Quantity</u>	<u>Natural Uranium</u>	<u>Base Case</u> <i>Optimized</i>
Percent U <sup>235</sup>	0.7113	1.00
Rod diameter (Inches)	0.75	0.025
Aluminum Cladding (Inches)	0.025	---
Coolant Annulus (Inches)	0.086	none
Process Tube (Al) (Inches)	0.058	---
End Cap Thickness (Al) (Inches)	0.10	---
Slug Length (Inches)	4.8	---
Center to Center Spacing (Inches)	1.25	1.25
Cell Arrangement	Triangular	Triangular
Reproduction Factor (k)	0.942	0.506
Thermal Utilization (f)	0.852	0.910
Resonance Escape Probability (P)	0.813	0.631
Pu Produced (atoms/incident neut)	3.79	1.26
Fissions Per Incident Neutron	3.14	0.36
Pu Production (moles/operating day)	12.8	3.62
Total Lattice Heat Load (MW)	2520	275

*delete*

The above table indicates that, although the lattice production increases by a factor of four, the lattice heat load increases by a factor of nine, which tends to discourage the use of natural uranium in the MTA assembly.

Evaluation of Increased Beam Energy and/or Increased Beam Currents

The new neutron yield energy extrapolation reported in CRD-T4A-126 indicates a greater neutron yield at high energies than the previous extrapolation. This fact points out the desirability of studying production machines using higher energy deuterons than the base case. The performance of an enlarged base case type target using 500 Mev deuterons was studied with two energy group neutron diffusion theory. The effect of increasing the beam current to one ampere was also studied. The significant results are reported in Table 7

*211* *OK* 

RECEIVED

2043-65

Table 7

Quantity	Base Case	Revised Base Case	1	2	4
Deuteron Energy Mev	350	350	500	350	500
Beam Current MA	500	500	500	1000	1000
Lattice					
Production mol/day	2.75	3.62	5.85	7.24	11.7
Production kg/yr	204	268	430	536	860
Processing Level gm/ton	520	700	700	700	700
Heat Load MW	210	275	440	550	880
Primary Target					
Production mol/day	2.25	1.94	4.35	3.88	8.7
Production kg/yr	167	144	320	288	640
Processing Level g/t	520	700	700	700	700
Heat Load MW	275	315	500	630	1000
Secondary Target					
Production Mols/day	1.30	1.15	2.8	2.30	5.6
Production kg/yr	96	85	210	170	420
Processing Level g/t	520	700	700	700	700
Heat Load MW	180	160	390	320	780
Total Production mol/day	6.3	6.71	13.0	13.42	26.0
Total Production kg/yr	467	497	960	994	1920
Total Heat Load MW	665	750	1330	1500	2660

### The Transport of Neutrons in Cylindrical Cavities

The MTA target assembly is a hollow cylinder surrounded by the lattice and reflector.

The variation of neutron flux inside this tube in the axial direction must be known in order that the leakage of neutrons out the beam hole can be calculated and the axial variation of production and heat loads in the lattice determined.

To accomplish this a mathematical description of the transport of neutrons in cylindrical cavities was formulated.

The physical model chosen is a cylindrical cavity of length  $L$  and diameter  $D$  imbedded in a semi infinite moderating slab extending from  $-∞$  to  $L$ . A plane neutron source is placed at the back of the cavity as shown in Fig. 8.

UNCLASSIFIED

2043-66

The following equations were obtained using two energy group diffusion theory.

$$\nabla^2 \phi_1(r, z) - K_1^2 \phi_1(r, z) + \frac{3k\Sigma_3}{\lambda_1 \rho} \phi_3(r, z) = \frac{3}{\lambda_1 \Delta} q(r, z)$$

$$\nabla^2 \phi_3(r, z) - K_3^2 \phi_3(r, z) + 3 \frac{\Sigma_1}{\lambda_3} \phi_1(r, z) = 0.$$

Where the subscript 1 refers to the fast group and 3 to the thermal group and  $q(r, z)$  is a first collision density in the moderator of neutrons originating in the plane source at the back of the cavity.

$\lambda$  is the first collision mean free path for neutrons coming from the source.

$K_1$  and  $K_3$  are the reciprocals of the fast and thermal diffusion length and the other symbols have the usual diffusion theory meaning.

Ordinary diffusion theory leads to the following equation for  $J_+(z)$ , the current from moderator to cavity.

$$J_+(z)_1 = \left[ \frac{\phi(r, z)}{\lambda} + \frac{\lambda}{6} \frac{\partial \phi(r, z)}{\partial r} \right]_{r=R}$$

The current from cavity to moderator  $J_-(z)$  will be the fraction of the total number of neutrons leaving the cavity walls which strike the element under consideration. Defining the probability that a neutron entering the cavity at  $z'$  will strike the element at  $z$  as  $K(|z-z'|)$ , then the number of neutrons leaving  $z'$  that enter at  $z$  is  $J_+(z')K(|z-z'|)dz'$  so that the total number entering at  $z$  is the integral of the contributions of this type over the entire emitting surface of the cavity.

$$\text{Thus } J_-(z) = \int_{\text{Surface of cavity}} K(|z-z'|) J_+(z') dz'$$

The exact boundary conditions which apply are,

$$J_{1-}(R, z) = \int_0^L J_{1+}(R, z') K(|z-z'|) dz'$$

$$J_{3-}(R, z) = \int_0^L J_{3+}(R, z') K(|z-z'|) dz'$$

$$\lim_{r \rightarrow 0} \phi_1(r, z) = 0$$

$$\lim_{r \rightarrow 0} \phi_3(r, z) = 0$$

$$J_{1+}(r, L) = 0$$

$$J_{3+}(r, L) = 0$$

UNCLASSIFIED

2043-67

Two boundary conditions are needed at  $x = 0$ . The conditions

$$\frac{\partial \phi_1(r, x)}{\partial x} \Big|_{x=0} = 0$$

$$\frac{\partial \phi_3(r, x)}{\partial x} \Big|_{x=0} = 0$$

are taken for convenience since the interest is primarily in the regions around the cavity. A more exact picture would be obtained by using albedo boundary conditions at the back of the cavity.

A solution has been obtained for this set of equations. Work is being done at present to break this solution down to a form that is amenable to calculations.

An approximate solution has been obtained using the following assumptions:

1. The transport of neutrons through the medium is primarily through the cavity and secondarily through the diffusion medium.
2. the body is non multiplying
3. the cavity's length is short enough so that the angle of incidence of the source neutrons will not vary greatly along the tube length.

Fig. 10 shows the epi-cadmium flux measured in cavity for a point source as compared to a theoretical curve obtained under the approximations given above.

The treatment of multiplying media is considered in CRD-T4A-140. To date no work has been done to obtain a solution of the resulting equations.

#### Study of Two Group Neutron Flux Calculations in Water Using a First Collision Source

**Introduction.** Neutron fluxes from a physical point source in water have been measured experimentally in order to verify the validity of two group flux calculations in water and to investigate the accuracy of a first collision source assumption. Flux traverses were made for neutrons having the indium resonance energy (1.44 ev) as representative of the fast group, and for thermal neutrons having energies below the absorption region of cadmium (which begins at about 0.4 ev).

**Experiment.** A polonium-beryllium neutron source, having an emissivity of  $1.25 \times 10^7$  neutrons per second as measured by Mound laboratory on April 14, 1952, was used in all experimental runs. In order to create an apparent first collision point source, the physical source was suspended at the center of an air-filled lucite sphere, which was immersed completely in a water tank. Thus the neutrons entered the water moderator in a direction normal to the cavity moderator interface.

DECLASSIFIED

2043-68

The source, a right circular cylinder 0.70 inches in diameter by 0.70 inches in height was supported, with its active center at the center of the sphere, which was five inches in inner diameter. The support consisted of a thin-walled aluminum shell, which was in turn supported by an aluminum wire attached to a lucite tamping bar sliding in a lucite sleeve. (See Fig. 11.) This bar and sleeve combination allowed the source to be retracted from the sphere. While the source was in place, the lucite tamping bar and sleeve matched the neutron characteristics of the water in which the entire assembly was immersed.

The water tank was a steel cylinder 3 feet, 4 inches in diameter by four feet in height. The sphere assembly was oriented in the center of the vessel by an aluminum bracket across the top supporting the lucite sleeve and tamping bar. Water temperatures were constant at  $22.0 \pm 1.0$  degrees centigrade.

Neutron flux distributions were measured at 1.44 ev and thermal energies by conventional indium foil techniques. All foils were in the form of circular sheets one-half inch in diameter and 0.005 inches in thickness mounted on lucite discs one inch in diameter. Foils were calibrated by irradiation, and activities were normalized to a standard foil. Resonance measurements were made by shielding the indium foil with a cadmium box 0.020 inches thick. Foils were supported normal to a radius of the sphere by a lucite bracket extending from the outer face of the sphere to the tank wall (see Fig. 12).

Beta activity was counted in standard end window G - M tubes and saturated activity calculated from the appropriate data. The counting procedures were the same as those described in the section of this report dealing with neutron flux measurements in and around cavities. The precision of the measurements is given as  $\pm 0.5$  percent.

Theory. If a first collision source of neutrons is assumed, the fast flux external to the sphere obeys the equation

$$(\nu^2 - K_1^2)\phi_1 = -\frac{3Q}{4\pi a^2} e^{-a/\lambda} \frac{1}{r^2} e^{-r/\lambda} \quad (1)$$

where:

- $\phi_1$  is the fast flux
- $K_1^2$  is the reciprocal of  $\bar{\tau}$ , the Fermi age or fast to thermal slowing down area
- $\lambda_1$  is the transport mean free path for the fast group
- $Q$  is the source term
- $\lambda$  is the first collision mean free path
- $r$  is the distance from the center of the sphere
- $a$  is the radius of the cavity surrounding the physical source; i. e. the inner radius of the lucite sphere, since as explained before, the lucite possesses the same neutron characteristics as does water.

RELEASED

2043-69

We may write equation (1) as

$$(\nabla^2 - K_1^2)\phi_1 = -C_1 \frac{1}{r^2} e^{-r/2} \quad (2)$$

$$\text{where } C_1 = \frac{3Q}{4\Delta^2 v} e^{-a/2} \quad = \text{constant}$$

The reduced form of equation (2) has two solutions,  $\phi_1 = 1/r e^{aK_1 r}$ . Solving the general equation by the variation of parameters method,  $\phi_1$  may be written

$$\phi_1 + A(r) \frac{e^{K_1 r}}{r} + B(r) \frac{e^{-K_1 r}}{r}$$

then

$$A(r) = \int -\frac{C_1}{2K_1 r} e^{-(1/2 + K_1)r} dr = \frac{C_1}{2K_1} [E_1(L_1 r) + a]$$

where  $E_1$  indicates one of a family of functions defined as

$$E_n(X) = \int_1^\infty e^{-xu} u^{-n} du$$

$n$  being = 1 in this case

$$L_1 \text{ is the sum } \frac{1}{\lambda} + K_1$$

$a$  is a constant of integration, to be determined by the boundary conditions on  $\phi_1$ .

Also

$$B(r) = \int \frac{C_1}{2K_1 r} e^{-(\frac{1}{2} - K_1)r} dr \\ = -\frac{C_1}{2K_1} [E_1(S_1 r) + \beta]$$

where  $S_1$  is the difference  $\frac{1}{2} - K_1$

$\beta$  is a constant analogous to  $a$ .

The fast flux is then

$$\phi_1 = \frac{C_1}{2K_1} \left\{ [E_1(L_1 r) + a] \frac{e^{K_1 r}}{r} - [E_1(S_1 r) + \beta] \frac{e^{-K_1 r}}{r} \right\} \quad (3)$$

We know that at  $r = \infty$ ,  $\phi_1$  has a finite bound, so that  $a = 0$  and

$$\phi_1 = \frac{C_1}{2K_1} \left\{ [E_1(L_1 r)] \frac{e^{K_1 r}}{r} - [E_1(S_1 r) + \beta] \frac{e^{-K_1 r}}{r} \right\}$$

UNCLASSIFIED

2043-70

The equation for the thermal flux uses the fast flux as a source term:

$$(\nabla^2 - K_3^2) \phi_3 = - \frac{3\Sigma_1}{\lambda_3} \phi_1 \quad (4)$$

where  $\phi_3$  is the thermal flux

- $K_3^2$  is the reciprocal of  $L^2$ , the thermal to zero energy slowing down area.  
 $\Sigma_1$  is the average cross section for removal from the fast group to the thermal group  
 $\lambda_3$  is the transport mean free path for the thermal group.

The solution to (4) is found by the same method used to obtain the fast flux, and the result is

$$\phi_3 = \frac{C_3}{(K_3^2 - K_1^2)r} \left\{ K_1 \left\langle [E_1(S_3r) + \delta] e^{-K_3r} - [E_1(L_3r)] e^{K_3r} \right\rangle - K_3 \left\langle [E_1(S_1r) + \beta] e^{-K_1r} - [E_1(L_1r)] e^{K_1r} \right\rangle \right\} \quad (5)$$

where  $C_3 = \frac{9\Sigma_1}{\lambda_1 K_1 \lambda_3 K_3} \frac{Q}{4\pi\Omega} e^{-a/\lambda} = \text{Constant}$

$$S_3 = \frac{1}{\Delta} - K_3$$

$$L_3 = \frac{1}{\Delta} + K_3$$

and where  $\delta$  is a constant which, like  $\beta$ , is determined by the initial conditions.

In order to determine  $\beta$  and  $\delta$ , the same condition is imposed on both fast and thermal fluxes. The moderator is aware of the neutrons only after they have been "created," so to speak, by their first collision in the moderator itself. It is not aware of a neutron source within the spherical cavity, since the neutrons make no collisions in the void, nor for the same reason does it see any thermalization in the cavity. Thus the boundary condition on both fast and thermal fluxes is that the same number of neutrons must enter the cavity as leave it. Mathematically this may be formulated in terms of the currents  $J^+$  and  $J^-$  across the cavity-moderator interface:

$$J^+(a) = \frac{\phi(a)}{4} + \frac{\Delta}{6} \frac{\partial \phi}{\partial r} \Big|_{r=a} \quad = \text{current entering cavity}$$

$$= J^-(a) = \frac{\phi(a)}{4} - \frac{\Delta}{6} \frac{\partial \phi}{\partial r} \Big|_{r=a} \quad = \text{current leaving cavity}$$

This means that  $\frac{\partial \phi}{\partial r} \Big|_{r=a} = 0$  for both  $\phi_1$  and  $\phi_3$ .

Setting  $\frac{\partial \phi}{\partial r} \Big|_{r=a} = 0$  and solving for  $\beta$ ,

$$\beta = \frac{1}{K_1 + 1/a} \left\{ e^{2K_1 a} [L_1 E_0(L_1 a) - (K_1 - \frac{1}{a}) E_1(L_1 a)] - S_1 E_0(S_1 a) \right\} - E_1(S_1 a)$$

Here  $E_0(x)$  belongs to same family of functions as  $E_1(x)$ , defined previously. Similarly, solving

$$\begin{aligned} \frac{\partial \phi_3}{\partial r} \Big|_{r=a} = 0 \text{ for } \delta, \\ \delta = \frac{1}{K_3 + 1/a} \left\{ e^{2K_3 a} [L_3 E_0(L_3 a) - (K_3 - \frac{1}{a}) E_1(L_3 a)] - S_3 E_0(S_3 a) + \frac{K_3}{K_1} e^{(K_3 - K_1)a} \left\langle [E_1(S_1 a) + \beta] (K_1 + \frac{1}{a}) + S_1 E_0(S_1 a) \right\rangle + \frac{K_1}{K_1} e^{(K_3 + K_1)a} \left\langle (K_1 - \frac{1}{a}) E_1(L_1 a) - L_1 E_0(L_1 a) \right\rangle \right\} - E_1(S_3 a) \end{aligned}$$

Calculations. Curves for the fast and thermal fluxes have been calculated using two values of  $\tau$  (48 cm<sup>2</sup> and 50 cm<sup>2</sup>) and three values of  $\lambda$  (5.0 cm, 5.7 cm, and 6.5 cm). The best fit to the experimental points was obtained with  $\tau = 48$  cm<sup>2</sup> and  $\lambda = 5.0$  cm. This fit is shown in Fig. 13. For comparison, a two group calculation using a boundary source is shown for the fast flux, using the same values of  $\tau$  and  $\lambda$  and normalized for the same total flux.  $L^2$  was taken as 8.117 cm<sup>2</sup> for all three curves.

Conclusions. The agreement obtained between theory and experiment demonstrates the validity of two group flux calculations for neutrons in water, provided that a first collision source is assumed. The significance of this assumption with relation to the A-12 is that for neutrons leaving the cavity near the target (where the direction of entry into the lattice is approximately normal to the cavity-lattice interface) the lattice flux will have a first collision source. The flux at the interface will be very much less than for a comparable boundary source, and the predicted neutron losses to the cavity will consequently be reduced an appreciable amount.

Summary. A rather thorough mapping of the neutron flux both inside and around a cylindrical cavity was completed during the quarter. The flux contours form an interesting picture, as the flux falls off more slowly along the cavity than



in the water, and is very flat across the cavity. This work was done in the prototype tank.

Data were taken with the prototype tank heated to about 60°C, to compare results with those normally obtained at about 20°C. The change in both thermal and resonance flux was easily observed. The experiment was undertaken to determine how carefully the tank temperature must be controlled; the conclusion was that plus or minus 5°C would cause no detectable change in flux.

Preliminary studies on a method of measuring the disadvantage factor are proceeding.

In the large tank, a determination of the migration area was completed. The work, done with a large polonium-beryllium neutron source, resulted in a measured age to indium resonance of 56.6 cm<sup>2</sup>, and a total migration area of 65.7 cm<sup>2</sup>.

The cavity and rotating plane source to be used in the large tank were constructed during this period, and will be used during the next quarter.

In Zn<sup>65</sup> activity in a copper plate bombarded with protons by the Accelerator Division was counted, and the beam profile determined. The targets had been in so long under different conditions that the activity was greatly smeared out, and the experimental work useful only as a development of the method.

#### Migration Area of Polonium Beryllium Neutrons in Water

In the initial phases of an experiment to study the variation of neutron fluxes in cavities surrounded by moderating and absorbing media, radial distributions of neutrons from a polonium beryllium source were studied in water. Cadmium covered indium resonance and bare indium detectors were employed.

From these data it was possible to calculate the "age" of neutrons from birth in the polonium alpha beryllium reaction to capture at the 1.44 ev resonance of indium and the total migration area to capture at thermal energies. The geometry of the experiment approximated a point source in an infinite sea of moderator.

Neutron age to indium resonance with the source employed was measured as 56.6 cm<sup>2</sup> and the migration area to total indium activation as 65.7 cm<sup>2</sup>.

#### Experimental Procedure

Nine nickel plated aluminum capsules, each containing 27.47 curies of polonium and 0.85 grams of beryllium were employed as neutron sources. The average individual source emissivity was  $6.46 \times 10^7$  neutrons per second measured May 8, 1952 by Mound Laboratory. These sources were mounted with centers on the circumference of a circle 1.25 inches in diameter to simulate a point source (see Fig. 14). They were held in a lucite cylinder.

The experiments were conducted in a 2000 gallon distilled water tank six feet, six inches in diameter and nine feet in height (see Fig. 15). Conductivity of the distilled water averaged approximately 180,000 ohms per centimeter during the experiment. The point source container was inserted into a vertical guide tube on the central axis of the tank. This tube, two inches inside diameter and having a quarter inch wall, was drilled through its walls at frequent intervals to allow water to fill the volume not occupied by the point source container. It was also "gun-bored" to minimize clearance between the source container and its inner wall. This clearance was 0.008 in. diameter.

The source container was held forty-two inches below the top surface of the water by lucite locking pins which allowed the source to be lowered to the bottom of the tube while foils were being positioned.

A lucite foil support bracket was supported (see Fig. 12) radially from the source support tube to the tank wall. Individual foils were supported on lucite discs, one inch in diameter by one-sixteenth inch thick. These discs were supported vertically by the support bracket, and the bracket loaded with foils was slipped into end holders which held the foils in line with the active center of the source.

The irradiation procedure was as follows: The source was lowered to the base of the tank, the loaded foil support bracket was slipped into the end holders, then the source was raised to foil level. The foils were removed by strings attached to individual foil support discs, those close in to the source being removed first.

The source was raised to foils level in less than five seconds which was small compared to the minimum irradiation time of fifteen minutes. Foils were separated at least one inch to minimize mutual interaction.

The foils themselves were half inch discs of indium metal 0.005 inches thick. Those to be used bare were cemented directly to the lucite support discs with dilute Duco cement. Those to be used as resonance detectors were enclosed in circular cadmium boxes with a 0.020 inch wall. The boxes were then cemented to the lucite discs. Bare foils were counted as exposed with the support discs acting as planchets. Covered foils were removed from the cadmium boxes and counted on similar lucite planchets.

Standard end window GM tubes and scalars were used for beta counting.

#### Data and Calculations

Variation of saturated counting rate with distance from the source is shown in Fig. 16. The products  $A_0 r^2$  and  $A_0 r^4$  were plotted against  $r$  for both bare and cadmium covered indium data. The areas under the curves to the outer limit of the data were integrated by planimeter. Exponential decrease without limit was assumed beyond the data with the average slope determined from the last fifteen centimeters of the  $A_0 r^2$  curve and this area calculated by formal integration. The  $A_0 r^4$  curve did not appear as a true exponential, so the slope of the approximating exponential to infinity was calculated from the outermost data. The area beyond the data accounted for less than 4 percent of the total.

The curve between the source center and innermost measurement was approximated by assuming the parabolic relationship between  $r$  and  $A_0 r^2$ .

A correction for the large physical size of the group of sources was made by choosing an arbitrary position along the foil traverse line and calculating from geometrical considerations, the contribution of each of the nine individual sources on a foil at that point. This showed an apparent center 0.18 cm closer to the foils than the geometric center.

The mean squares of the distance to activation were calculated from:

$$\bar{r}^2 = \frac{4\pi \int_0^a A_0^4 dr}{4\pi \int_0^a A_0^2 dr}$$

and the corresponding migration areas from

$$M^2 = \frac{\bar{r}^2}{6}$$

The migration area for thermal neutrons was calculated as 65.7 cm<sup>2</sup> and to indium resonance, which is the age ( $\tau_{in}$ ) to indium resonance as 56.6 cm<sup>2</sup>.

This shows close agreement with the data of other investigators since

$$M^2 - \tau_{in} = \tau_{in+th} + L^2$$

From this experiment:  $\tau_{in+th} + L^2 = 65.7 - 56.6 = 9.1 \text{ cm}^2$

From other data:  $\tau_{in+th} + L^2 = 1.0 + 8.1 = 9.1 \text{ cm}^2$

#### Disadvantage Factor

An investigation was begun to study neutron fluxes in fuel rods surrounded by moderator. To check analytical methods, an absorbing rather than a multiplying medium was chosen for the rod. This structure was simulated by lucite tubes surrounded by water and filled with an aqueous solution of cadmium sulphate. By varying the concentration of Cd SO<sub>4</sub>, the ratio of the absorption to total cross section ( $a$ ) of the rod media can be varied from 0 to 0.75.

The first detector employed was a strip of indium metal mounted diametrically across the rod. A flux depression was observed by counting portions of the strip through a collimating block. Due to gamma penetration of the block and flux depression by the indium itself, the disadvantage factor, peak to average flux appeared smaller than expected.

Gold wires mounted axially are now being studied as detectors.

REPRODUCED FROM  
UCRL-2043-75

2043-75

### Neutron Flux In and Around Cavities

Neutron flux measurements were made using a lucite cavity mounted in a 250 gallon tank, 40 in. in diameter and 48 in. in height (Fig. 17). Tap water was continuously circulated through the tank and adjusted to the proper height. The cavity, a 26 in. long cylindrical tube of lucite 4-3/4 in. inside diameter, with a 1/8 in. wall, was supported in the center of the tank by an aluminum bar. It was immersed to a depth of 23-3/4 in. to give a length to diameter ratio (L/D) of five for the cavity. During irradiation periods a 25 curie polonium-beryllium source was located coaxially with the cylinder with its center at the bottom boundary of the cavity.

Indium foils, 1/2 in. in diameter and 5 mils thick bare for the detection of resonance plus thermal neutrons, and cadmium covered for the detection of resonance neutrons alone, were used in the experiment. The thermal flux was obtained by subtraction of the cadmium covered foil data from the bare foil data. The foils were mounted on discs for ease of handling and for identification purposes. Lucite discs 1/16 in. thick and 1 in. in diameter were used for bare foil measurements in water. Flux perturbation by this amount of lucite is negligible. Aluminum discs 12 mils thick and 1 in. in diameter were used for bare foil measurements in air, since aluminum gives very little flux perturbation. The foils for use in cadmium covers were mounted on 1/2 in. diameter thin aluminum discs which were then placed inside cadmium boxes already mounted on lucite or aluminum 1 in. discs for exposure in water or air. Foils were supported in the tank by a horizontal traverse rod made of lucite which was in turn supported at the cavity and tank wall in several positions at different elevations. In addition to these multiple horizontal traverses a vertical traverse was made which allowed data to be taken very close to the cylinder wall. The supporting material for foils in the cavity was made of aluminum and consisted of vertical bars slotted to accept the aluminum mounting discs. These vertical bars were adjusted to various positions to obtain data in the form of multiple vertical traverses.

The irradiation of foils in the tank was accomplished as follows. The source was removed to a safe distance while the foils were placed. The irradiation was begun by positioning the source and ended after sufficient exposure by removing the source. The foils were then retrieved. The sequence was somewhat different for the foils in the cavity since the source was inaccessible in this case. The irradiation was accomplished by simply inserting the holder assembly into the cavity with the source already in position. The assembly was then removed after a sufficient exposure time, and the foils recovered.

The radioactive foils were washed with carbon tetrachloride, and counted with end window geiger tube detectors connected to atomic multiscalers. The foils were placed during counting time on aluminum shelves inserted into the lucite assemblies supporting the tubes and mounted inside of aluminum lined lead pigs. A minimum of 10,000 counts was obtained for an experiment point for a 1 percent statistical error. Most foils, however, were counted more than this. The raw data was corrected for background, tube dead-time and source decay. Counter sensitivity was checked by counting a standard at least once a day.

The data are collected in the form of bare and cadmium covered indium horizontal and vertical traverses. Examples are included (Figs. 18 and 19) for

the case of bare indium foils yielding resonance plus thermal neutron flux. It is possible to derive a cross section of neutron flux from these traverses in the form of a profile or contour map of isoflux lines (Fig. 20). The profile gives a physical picture of the effect of a cavity on the neutron flux. The gradient up the cavity is about half that in water and so causes the isoflux lines to be distorted upward in the vicinity of the cavity. The closer to the cavity the greater is the distortion, resulting in rather a steep slope at the boundary of the cavity. The discontinuity of slope in the isoflux curves at the boundary is the result of the steep gradient on the water side of the boundary and the flat flux giving no gradient inside the cavity.

### Mark I Beam Profile

The Accelerator Division has been concerned with the determination of the profile and general characteristics of the Mark I proton beam. As one method of measurement, the Engineering Physics Group has undertaken the counting of a radioactive copper plate which was exposed to the accelerator beam.

Protons on copper give the reaction  $Cu^{65}(p,n)Zn^{65}$  with a threshold energy of 2.16 Mev. The  $Zn^{65}$  is radioactive so measurements may be made of the activity per unit area over the surface of the plate. The beam profile may be obtained from these measurements assuming that the activity per unit area is proportional to the number of protons incident on the area.

The copper plate was cut into 1 in. strips marked off into 1 in. squares. Seven-eighths inch discs were then punched from the center of these squares. The columns of squares were labeled with letters A-Z, AA-JJ and the rows labeled with numbers 1 - 36, so that each disc was identified by a letter and a number.

The discs were counted with a thallium activated sodium iodide scintillation crystal in conjunction with a 5817 photomultiplier tube. The pulses, amplified by a preamplifier were sent into a nuclear scaler. Corrections made for all data include coincidence correction, background correction, and daily sensitivity correction. The background was determined every night and the sensitivity variation determined by counting a standard disc (Y - 18) at least once a day.

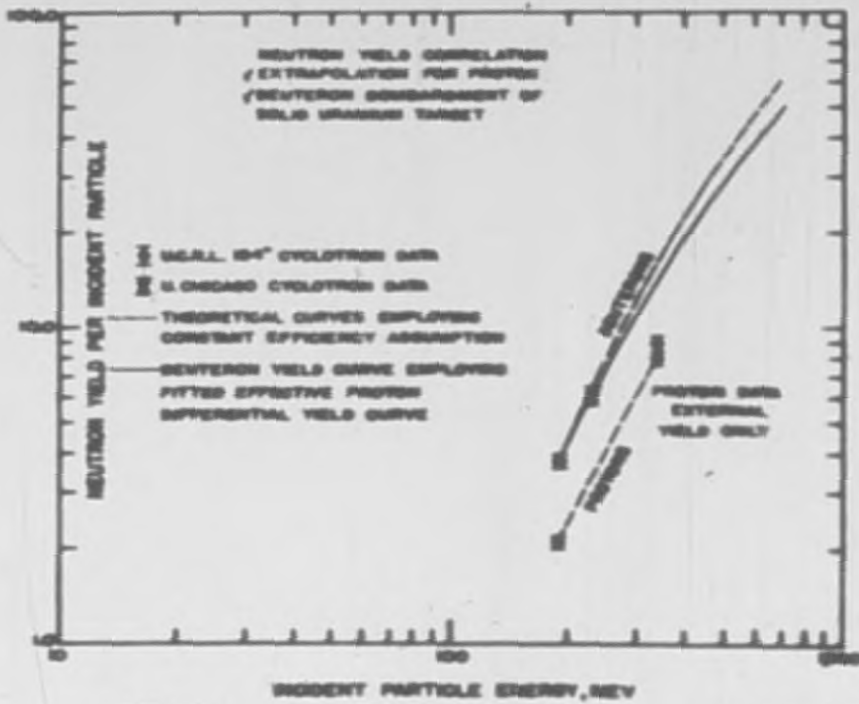
The identity of the active isotope was established by measurement of the energy of the emitted gamma rays. This was done using two independent methods, a gamma-ray spectrometer, and an absorption curve through lead.

The data are presented in the form of horizontal and vertical profiles (Figs. 21 and 22) and in a contour map (Fig. 23) derived from the profiles. The contours are given in measured counts per minute as taken from the original data. Analysis of the data shows spread out, irregular curves indicating that the beam wandered during operation. The irregularity in addition to the lack of knowledge of constancy or homogeneity of beam energy precluded the possibility of any reliable estimate of beam energy. Without an accurate knowledge of beam energy it is impossible to determine the integrated beam current, since the  $Cu^{65}(p,n)Zn^{65}$  reaction cross-section is strongly energy dependent.

Even though the results of the experiment are not conclusive, experimental techniques have been developed which will be very useful in future studies. It may be possible in a planned experiment to determine accurate instantaneous beam profiles, beam energy, and integrated beam current.

REPRODUCED FROM  
UCRL-2043-78

2043-78



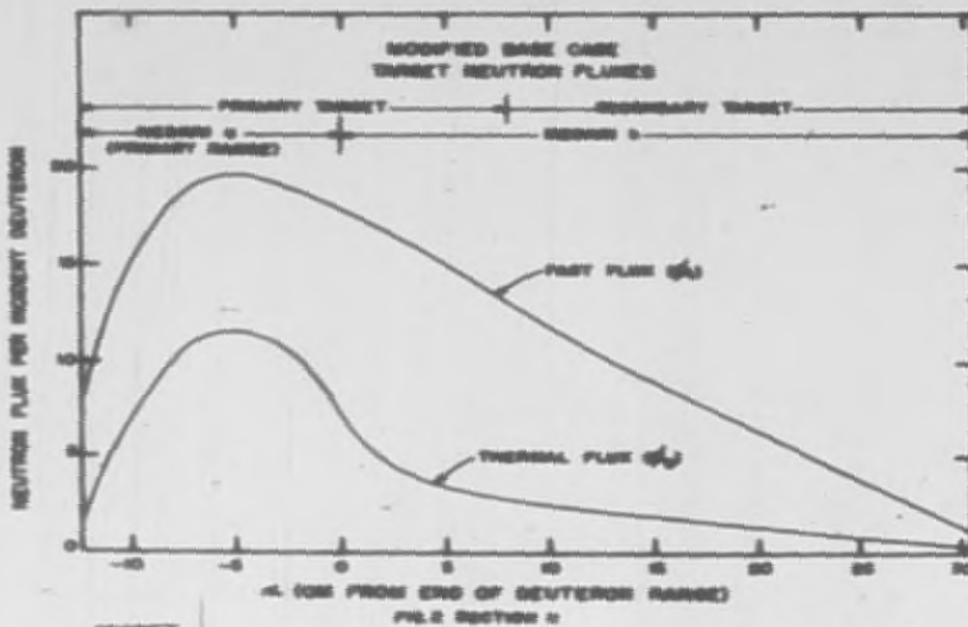
SECRET

PL. 1 SECTION 2

50-6706

CONFIDENTIAL

2043-77



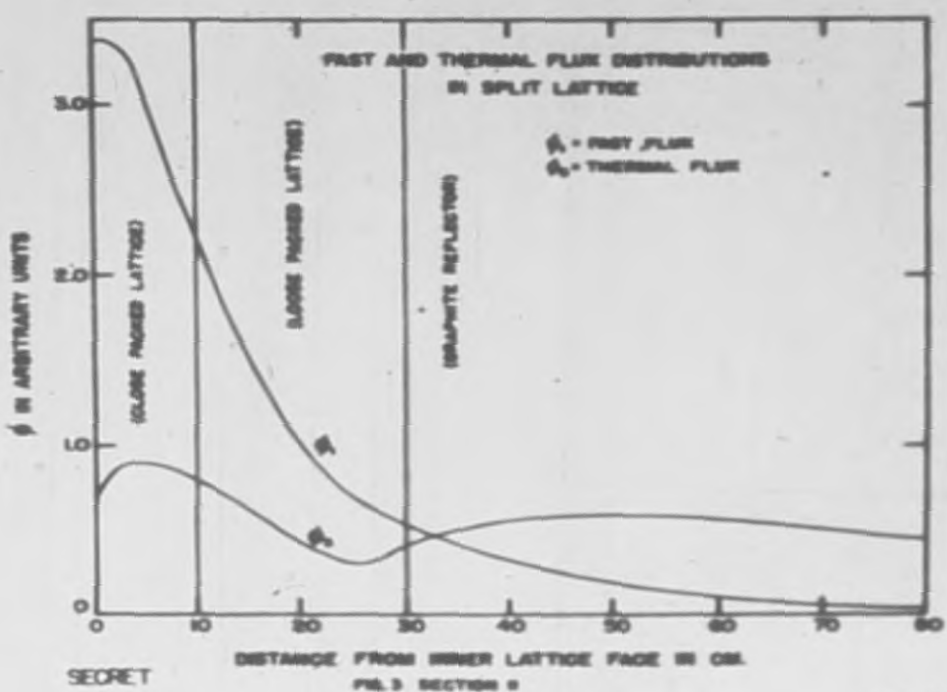
SECRET

DU-4700

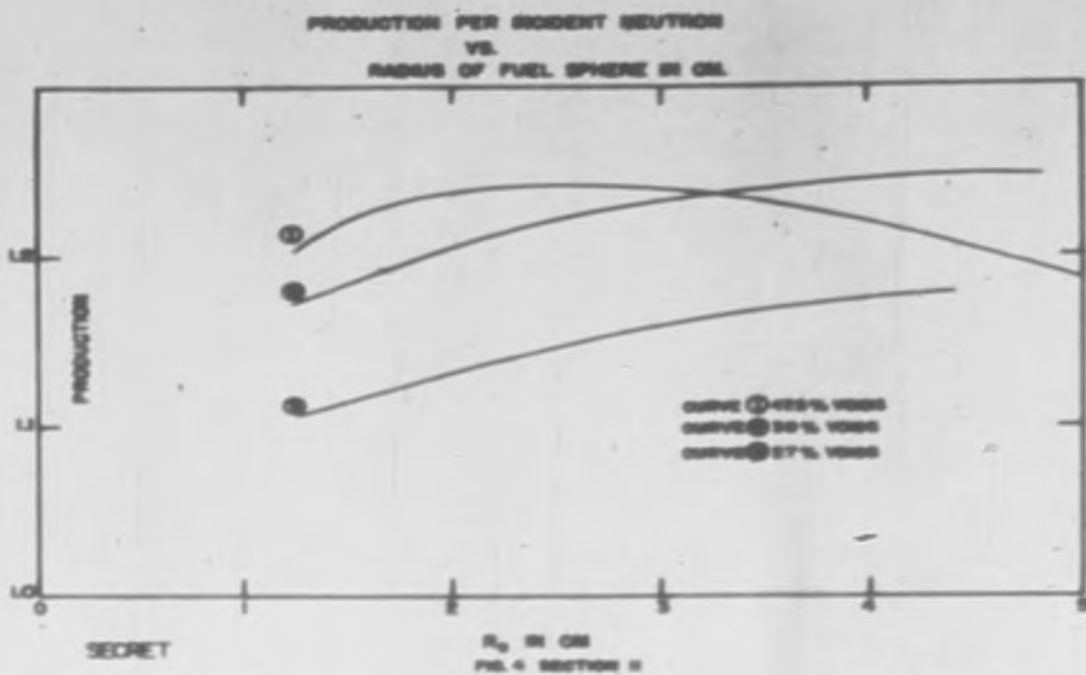


2043-80





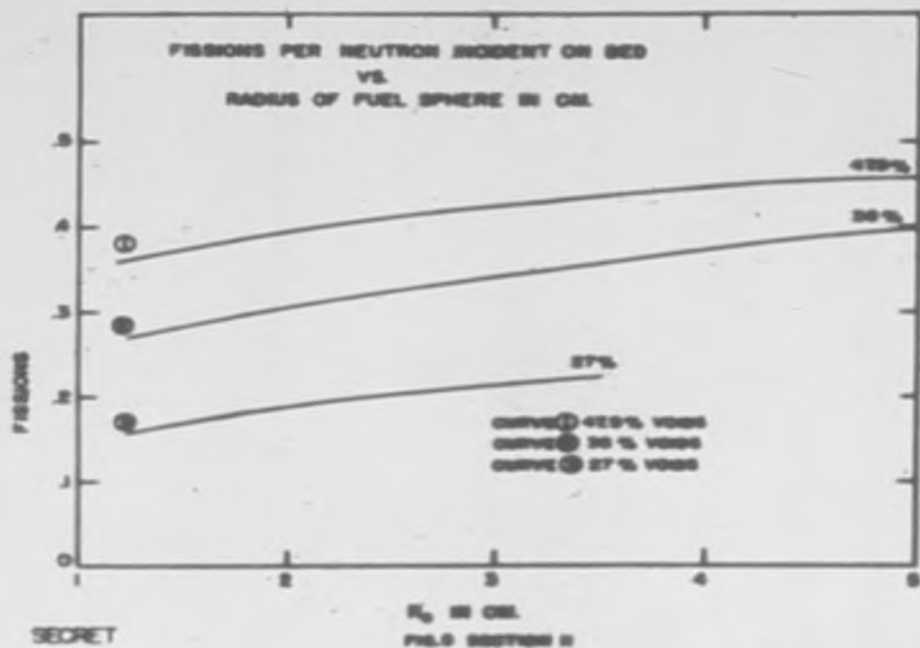
2043-P1



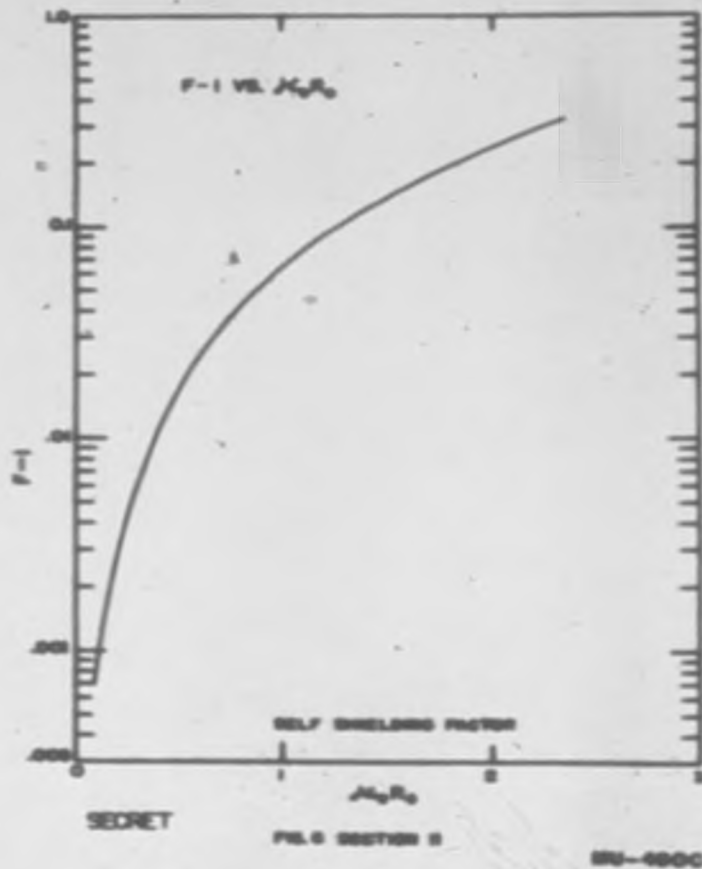
MS-4798

SECRET

2043.82

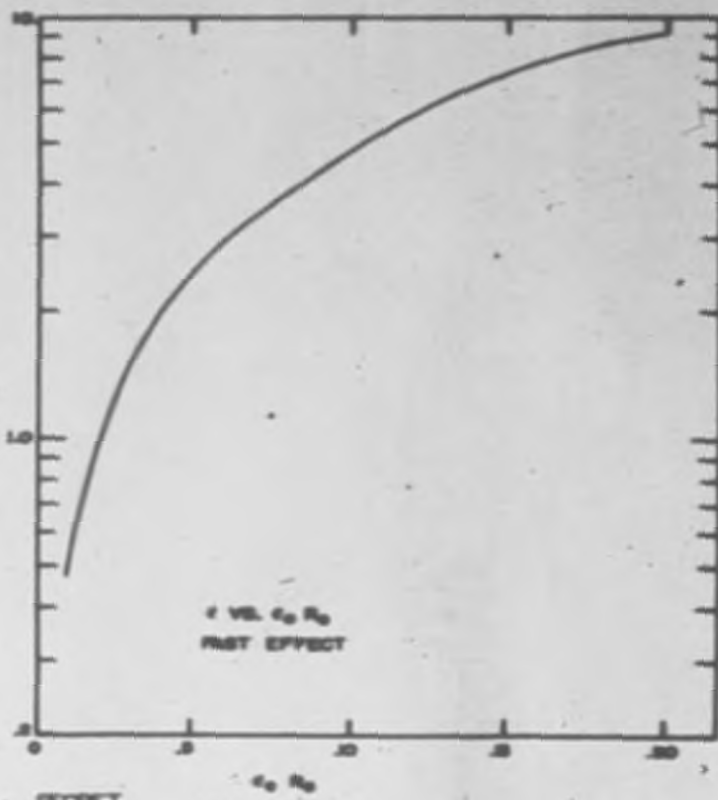


3043-83



SECRET

2043-84



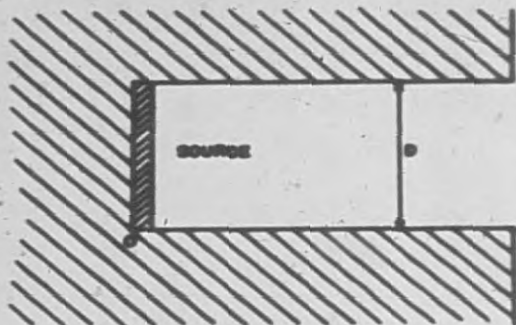
SECRET

PL 7 SECTION 2

89-4801

DECLASSIFIED

2043-85



CYLINDRICAL CAVITY OF LENGTH L AND DIAMETER  
D IMBEDDED IN SEM-INFINITE MODERATING SLAB  
EXTENDING FROM L TO D.

FIG. 8 SECTION II



BASIC DESIGN OF MTR LATTICE

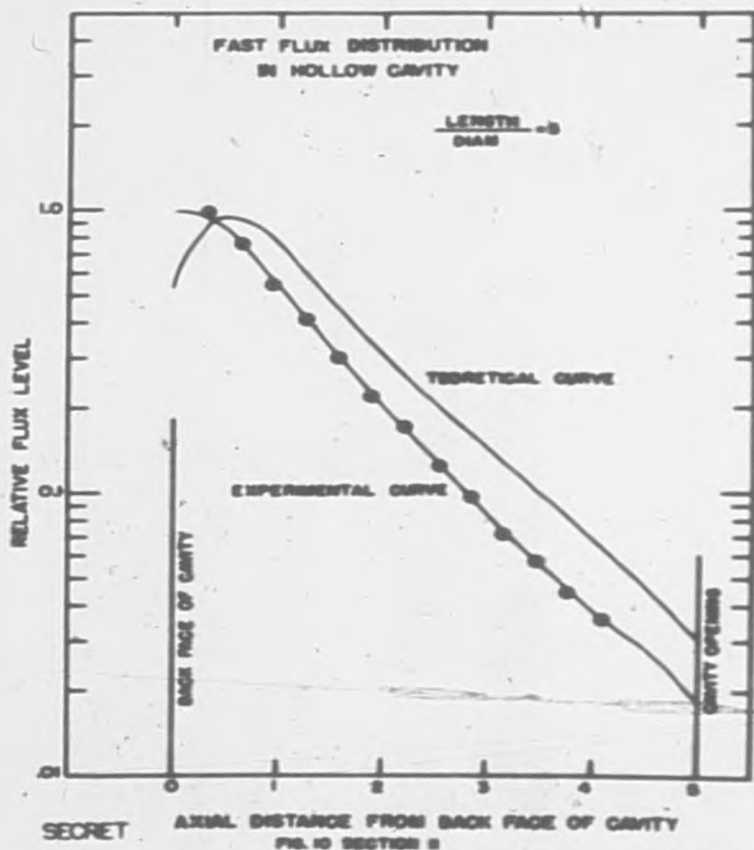
FIG. 9 SECTION II

SECRET

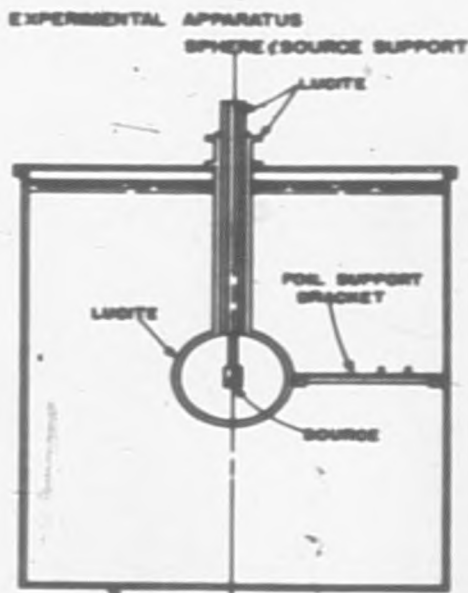
NU-4802

UCRL-2043

2043-86



9043-81



SECRET

4'-0" DIA. x 5'-0" HIGH TUBE  
FILM SECTION II

NU-6804

2043-88



EXPERIMENTAL APPARATUS  
EXTERNAL FOIL SUPPORT BRACKET

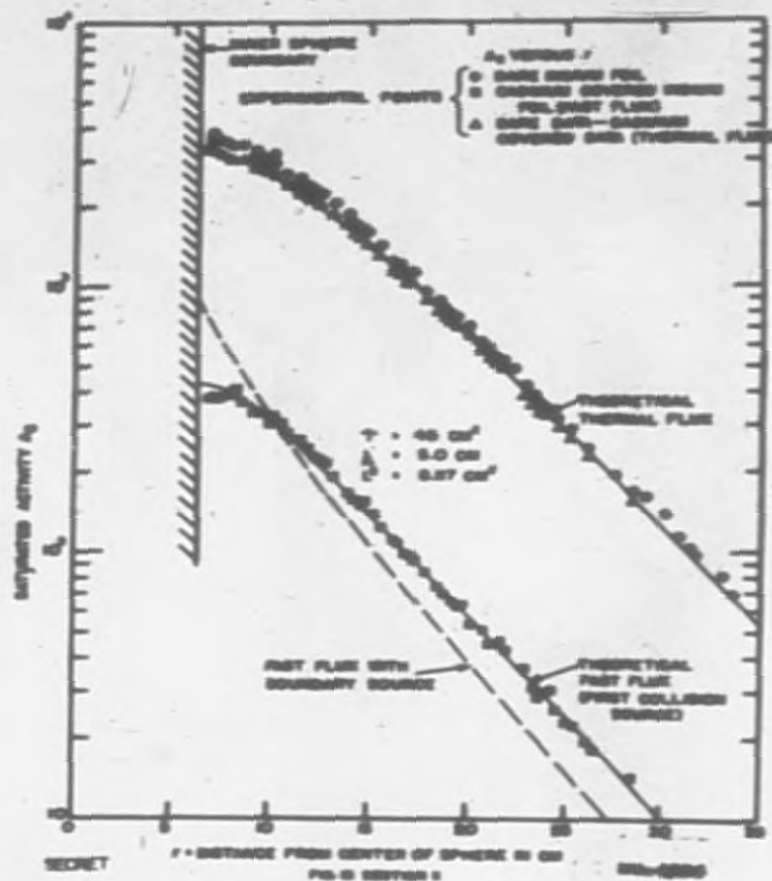


SECRET

FILE SECTION 9

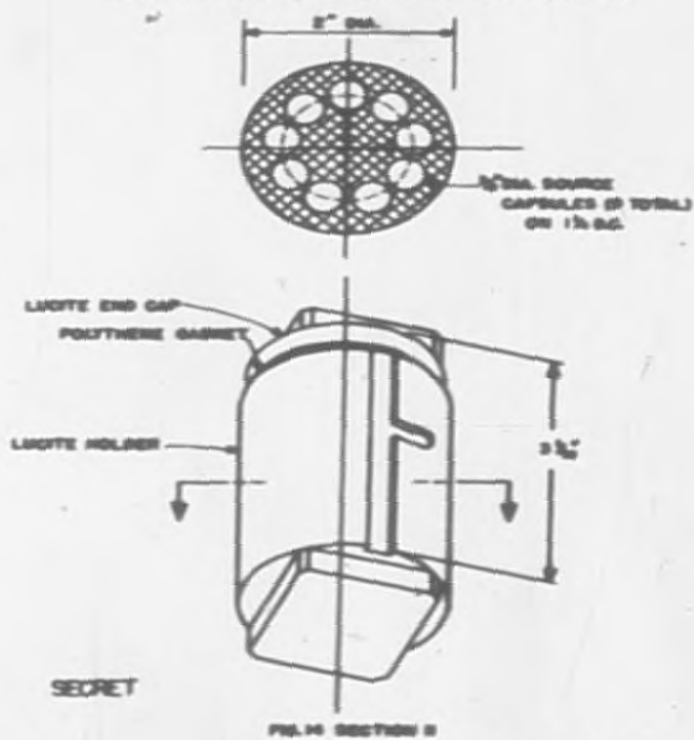
MU-4805

2043-89



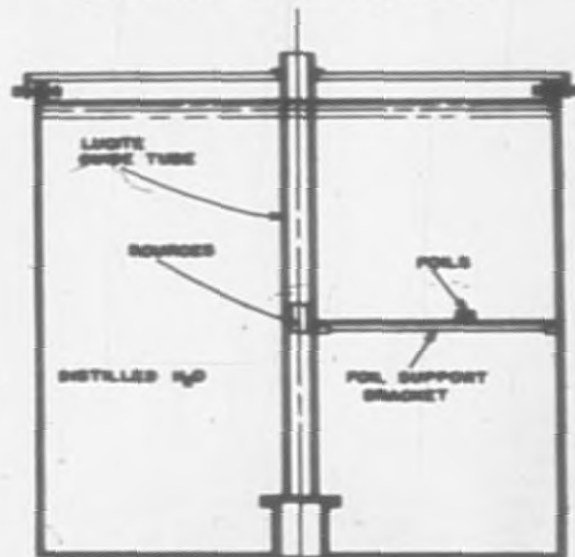
2043-90

EXPERIMENTAL APPARATUS SOURCE CONTAINER



2043-91

EXPERIMENTAL APPARATUS ASSEMBLY

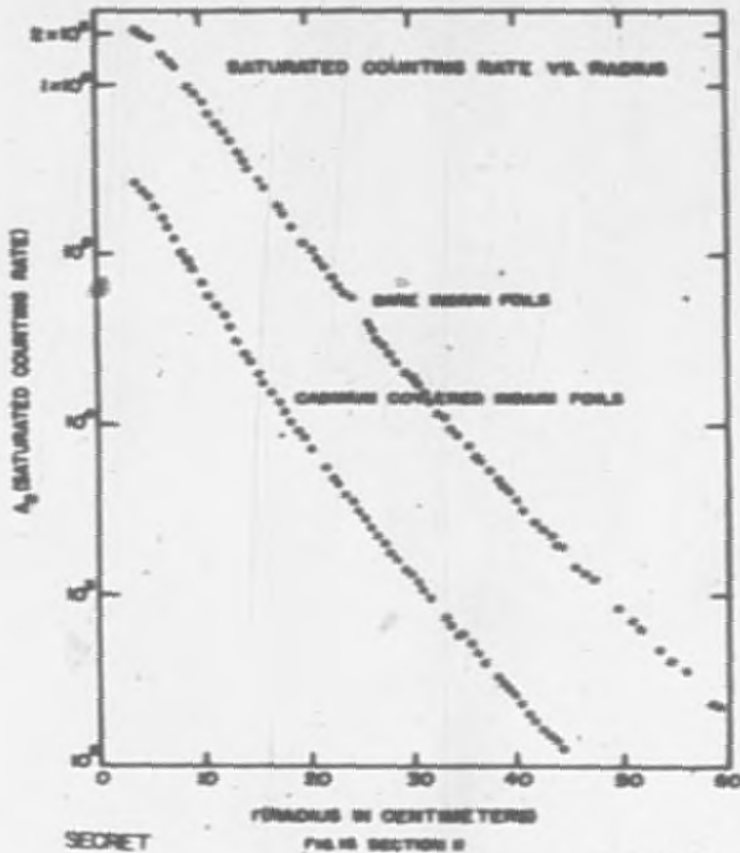


SECRET

FILE SECTION 8

8U-4808

2043-92



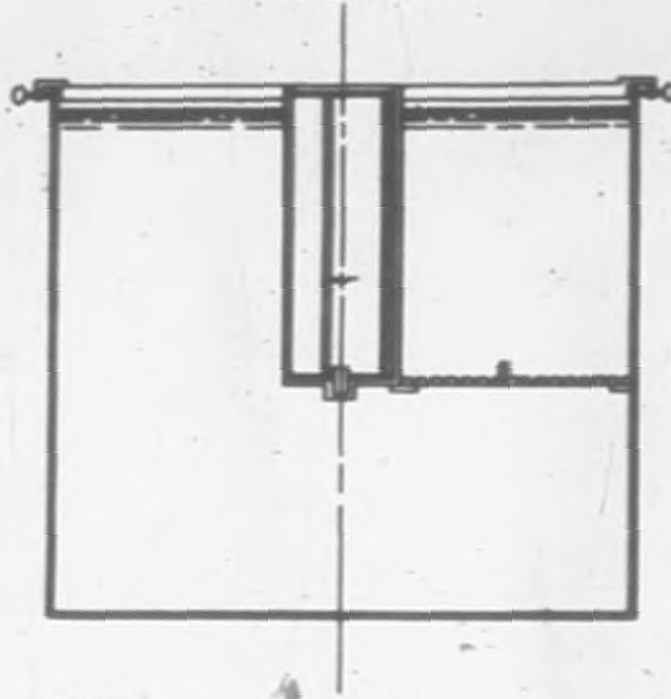
SECRET

FILM SECTION II

2043-93

2043-93

4 1/2" CAVITY - 1/2" = 5  
PROTOTYPE TANK

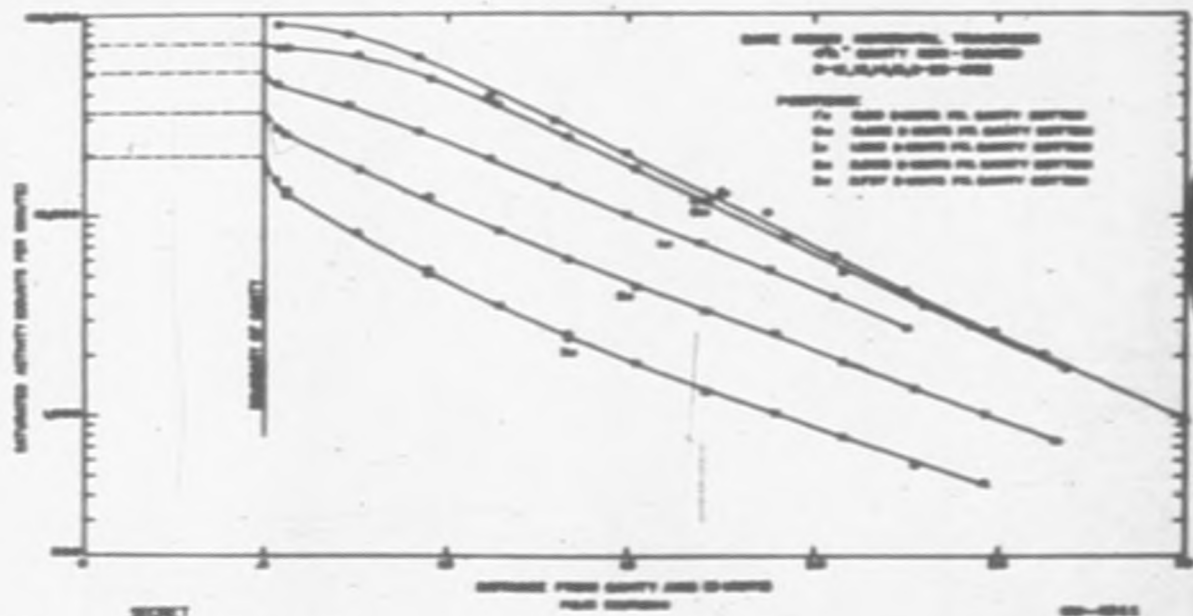


SECRET

FIG. 17 SECTION II

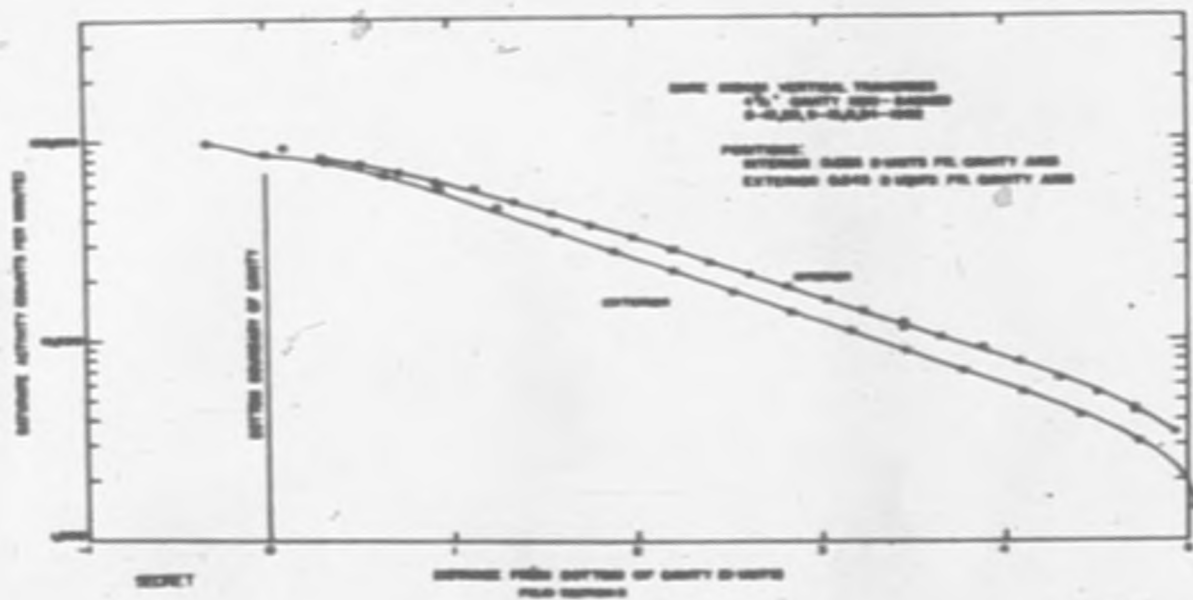
MU-4810

2043-94



CONFIDENTIAL

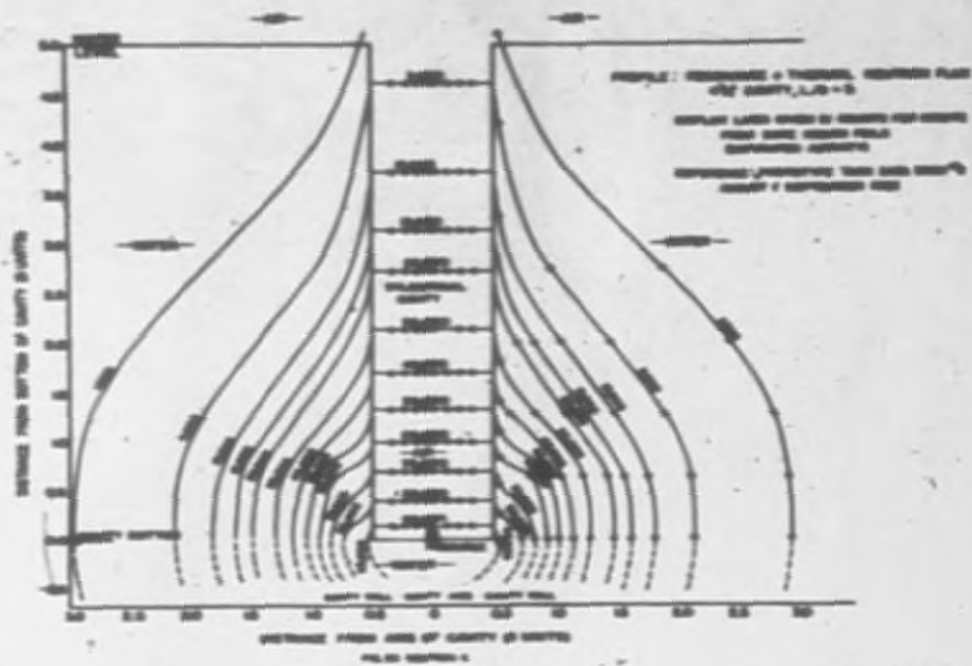
2043-75



100-4010

2043-98



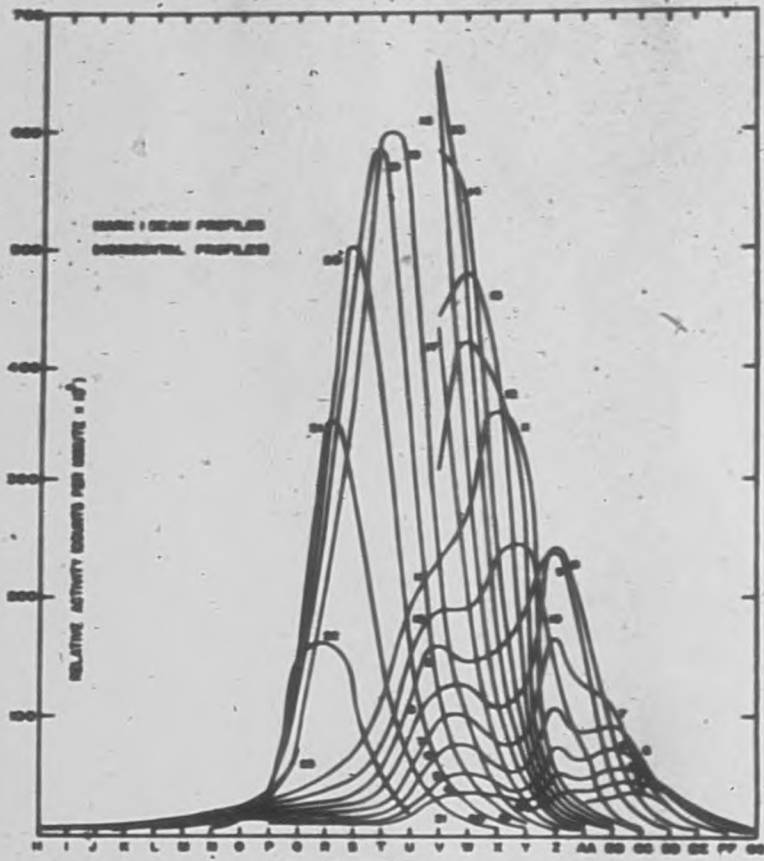


SECRET

UCAL-2013

CONFIDENTIAL

2043-97

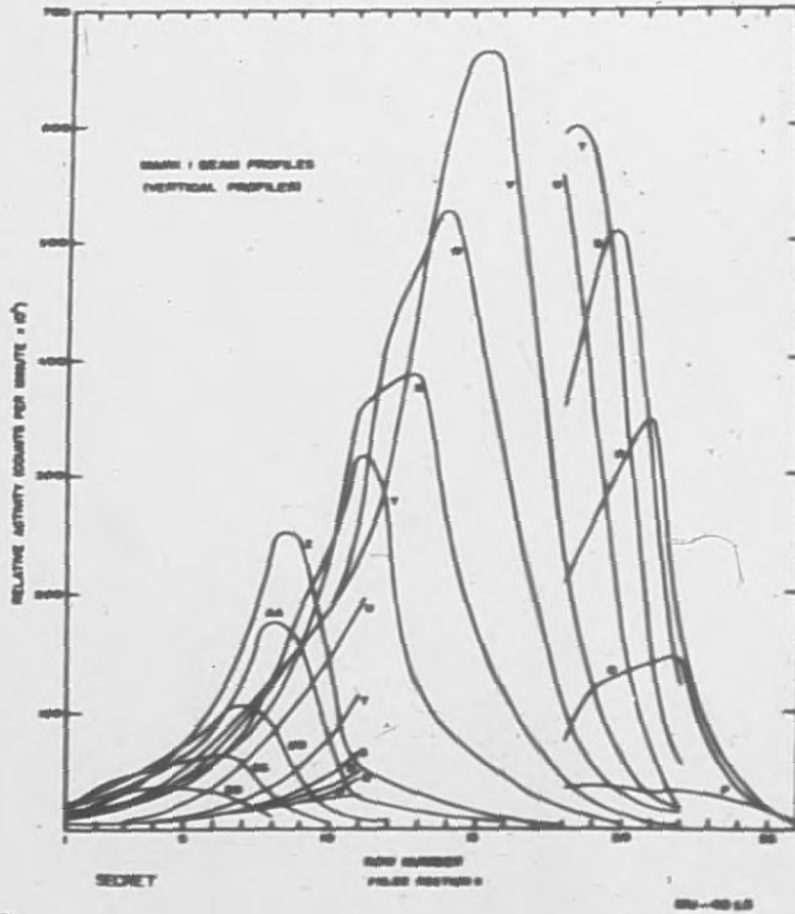


SECRET

COLUMN LETTER  
FILE NUMBER

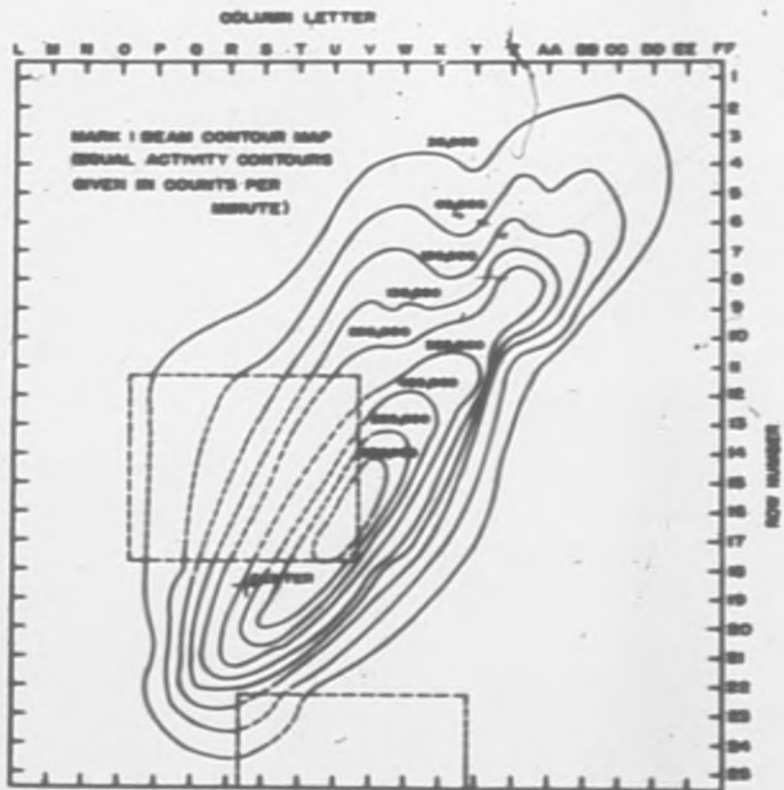
50-4004

2043-98



REPRODUCED

2043-99



FILES SECTION 8

SECRET

50-6816

2043-100

## 12. NUCLEAR CHEMISTRY

K. Street  
CRDCFission and Capture in A-12 TargetsR. E. Batsel, G. H. Coleman, W. W. Crane, R. S. Gilbert  
H. G. Hickf, W. H. Hutchin, and G. M. Idings  
CRDCP. C. Stevenson  
UCRL

Studies of the fission and capture events produced by 190 Mev deuteron irradiation of uranium blocks with beryllium and uranium primaries were continued. The studies included measurements for irradiations of unmoderated blocks 12 inches x 12 inches perpendicular to the beam and bombardments of a 3 foot x 3 foot moderated block arrangement. A more accurate measurement of the counting yield of  $\text{Np}^{239}$  was made; this giving a better value for the number of capture events included in the various target configurations.

Moderated Block Study

A moderated uranium block (3 foot x 3 foot x 5 inches thick in uranium) was bombarded with 190 Mev deuterons and the distribution of fission and capture events studied. The first portion of the target was made up of sixteen 1/16 inch x 3 foot x 3 foot sections of uranium alternated with 3/32 inch polyethylene to approximate the effect of water cooling in an A-12 primary target. The second and third portions of the target were made up of 1/2 inch x 1/2 inch by 12 in. uranium bars interspersed laterally and along the centerline with 3/32 inch polyethylene strips and sheets.

Samples of uranium were placed radially from the center of the target at various depths in the configuration, and the number of fission and capture events per gram of uranium was measured. By integrating the number of fission and capture events radially and in depth, it was possible to calculate the total number of fissions and captures occurring in the target arrangement. The results are shown in Figs. 1 and 2 and are summarized as follows:

Fissions

Primary (1st 9/16 in. of Uranium)	0.25 fissions/deuteron
Secondary	0.80 fissions/deuteron
TOTAL FISSIONS	<u>1.05 fissions/deuteron</u>

Captures

Primary (1st 9/16 in. of Uranium)	0.20 captures/deuteron
Secondary	0.90 captures/deuteron
TOTAL CAPTURES	<u>1.10 captures/deuteron</u>

### Unmoderated Block Studies

The measurements of the total number of fission and capture events induced by 190 Mev deuteron irradiations of unmoderated uranium blocks with beryllium and uranium primaries are now complete for the blocks 12 inches x 12 inches perpendicular to the beam and of varying depth. The results are summarized in Table 1 for the measurements outside the water tank, and these results can be compared with values given in the quarterly report, December 1951, January and February 1952, for the same configurations measured inside the water tank. As will be discussed in the following section, the capture numbers reported previous to this report should be corrected by multiplying by a factor of approximately 1.25 due to a better determination of the counting yield of  $\text{Np}^{239}$ . Examples of the fission and capture distributions of a uranium primary uranium secondary outside the water tank are shown in Figs. 3 and 4.

**TABLE 1**

Total Fissions and Captures In  
12 Inch x 12 Inch Unmoderated  
Targets Outside Water Tank

Configuration	Total Captures Per Deuteron	Total Fissions/Deuteron	
		Primary	Total
5-5/8 in. Uranium Secondary (Uranium Primary)	0.35	0.25	0.55
11-1/4 in. Uranium Secondary (Uranium Primary)	0.65	0.25	0.60
5-5/8 in. Uranium Secondary (Beryllium Primary)	0.35		0.45
10-1/8 in. Uranium Secondary (Beryllium Primary)	0.70		0.65

### Redetermination of Counting Yield of $\text{Np}^{239}$

Because of the importance of the counting yield of  $\text{Np}^{239}$  in determining proper capture numbers within the target configurations, it was decided to re-measure the number of disintegrations per observed count for  $\text{Np}^{239}$ . A sample of depleted uranium was irradiated in the Oak Ridge Pile to produce  $\text{Np}^{239}$ . The  $\text{Np}^{239}$  was separated chemically, standard solutions made up, and aliquots taken to determine the number of counts of  $\text{Np}^{239}$  present. After the  $\text{Np}^{239}$  had decayed for several half-lives, the  $\text{Pu}^{239}$  which is the decay product

was detectable by its alpha radioactivity. By counting the  $\text{Pu}^{239}$  alpha particles, it was possible to get a number for converting observed counts of  $\text{Np}^{239}$  taken in the standard counting arrangements to actual atoms of  $\text{Pu}^{239}$  which would be present on decay. This could be interpreted in terms of disintegrations of  $\text{Np}^{239}$  per observed count. The new value is  $\sim 1.25$  (average for the counting arrangements) times higher than the old value. Thus, the number of captures per deuteron given for configurations previous to this report should be corrected by a factor of 1.25.

### Isotopic Composition In Primary and Secondary Targets

W. W. T. Crane, G. M. <sup>CRDC</sup>Idings, and R. L. Tellefsen

The shipment of  $\text{Np}^{237}$  requested from the General Electric Company at Richland, Washington was received. The group processed some 30 liters of solution in which the  $\text{Np}^{237}$  was contained, and separated 1.4 grams of  $\text{Np}^{237}$ . From considerations as to the amount of material expected, the 1.4 grams was recovered without loss.

The  $\text{Np}^{237}$  is to be used in studying its capture cross section as compared to the capture cross section of  $\text{U}^{238}$  in the various target configurations. The  $\text{Np}^{237}(n, \gamma)\text{Np}^{238}$  reaction leads to  $\text{Pu}^{238}$  which is an undesirable contaminant in  $\text{Pu}^{239}$  produced in an MTA type target.

A one gram sample of  $\text{Th}^{230}\text{O}_2$  requested has been received from the Oak Ridge National Laboratory, and 0.7 gram of the material was purified and packaged for irradiation in the MTR at Arco. The  $\text{Th}^{230}$  will produce  $\text{Pa}^{231}$  by the following reaction:



The  $\text{Pa}^{231}$  is to be used to study the ratio of its capture cross section to that of  $\text{Th}^{232}$  in the various thorium block configurations. The  $\text{Pa}^{231}(n, \gamma)\text{Pa}^{232}$  reaction leads to  $\text{U}^{232}$  which is undesirable in  $\text{U}^{233}$ .

In order to check the validity of the extrapolation of the  $\text{U}^{238}(d, p2n)\text{U}^{237}$  and  $\text{U}^{238}(d, 2pn\beta^-)\text{U}^{237}$  reactions from 190 Mev to higher deuteron energies, the excitation functions for the  $(d, 2pn\beta^-)$ ,  $(d, 2np)$ ,  $(n, 2n)$ , and  $(p, pn)$  reactions on  $\text{U}^{238}$  have been completed in the high energy region. A plot of these reaction cross sections versus energy is shown in Fig. 5.

As can be seen in Fig. 5, all of the reaction cross sections appear to be comparable to the energy region around 90 Mev where the reaction is probably due to single nucleon-nucleon collisions or knock on reactions. The shape of the  $(p, pn)$  reaction excitation function shows the extrapolation of the  $(d, 2pn\beta^-)$  reaction cross section to higher energies is reasonably good. (d, 2np)

Fission Product Distribution at High Energies for Uranium and Thorium

M. Linder and R. N. Osborne  
CRDC

Three reports have been completed since the last quarterly report. These are:

1. CRD-T1-148 "Cross Section For The Reaction  $Al^{27}(\alpha, \alpha' 2p)nNa^{24}$ "
2. CRD-T1-139 "Energy-Dependence of Cross-Section For the Reaction  $C^{12}(\alpha, \alpha n)C^{11}$ "
3. CRD-T1-150 "Neutron-Deficient Isotopes of Cesium and Barium"

A fourth report, entitled "Some Studies Of The Products Of The High-Energy Fission Process," has been completed and is being submitted as a CRD-T report. This treatment included study of the cross sections for formation, at various energies, of  $Ni^{66}$ ,  $Ba^{131}$ ,  $Ba^{139}$ ,  $Ag^{111}$ , and  $Zr^{97}$  from alpha-particle, proton, and deuteron bombardments of uranium and thorium. The results have been interpreted on the basis of the Goeckhermann-Perlman model of high-energy fission.

$Ba^{128}$  has been definitely established as a product of fission of uranium bombardment with 340 Mev protons. The cross-section of 0.2 mb is consistent with the interpretation of formation of neutron-deficient fission products discussed above.

An extensive program for the study of the products of spallation of uranium and thorium has been undertaken. Serious difficulties have been encountered in working out satisfactory chemical separations for such products as protactinium, thorium, actinium and radium in the carrier-free state. This is necessary because of the importance of pulse-analysis of alpha-particle groups in identification of various isotopes.

Absolute Beta Counting

P. C. Stevenson  
UCRL

R. S. Gilbert, H. G. Hicks and W. H. Hutchin  
CRDC

Work on the problem of absolute beta counting has pointed out the following effects: air and counter window absorption of radiation, backscattering of the sample mount, absorption of radiation by the sample material (self-absorption), scattering of radiation by the sample material. The first two of these effects have been measured and correlated, the other three effects are as yet incompletely determined. A more complete discussion of this problem has been prepared for distribution as a CRD-T report.

2043-10K



Separation of Tantalum and Niobium by Solvent Extraction

P. C. Stevenson  
UCRL

R. S. Gilbert, H. G. Hicks, and W. H. Hatchin  
CRDC

In order to extend the high energy studies of fission and spallation reactions in uranium and thorium, it has been necessary to perfect new methods of radiochemical purification of various elements. Of particular interest is the separation of tantalum and niobium by differential extraction into diisopropyl ketone from mineral acid-hydrofluoric acid aqueous solutions.

About one milligram of inactive tantalum or niobium along with the tracer ( $Ta^{182}$  or  $Nb^{95}$ ) was added to the aqueous phase containing known amounts of acids, and the volume adjusted to 1 ml. An equal volume of diisopropyl ketone was added to the tube, and the mixture stirred for one minute. The phases were centrifuged, and equal aliquots of each phase placed into machined teflon cups for counting. Distribution coefficients of tantalum and niobium were measured by counting the gamma radiation from  $Ta^{182}$  and  $Nb^{95}$  in a single channel pulse analyzer using a thallium-activated sodium-iodide crystal.

Ratios of distribution coefficients of tantalum and niobium were measured (Table 2) and the extraction behavior of tantalum studied in some detail (Figs. 6, 7 and 8)

TABLE 2

Relative Extractabilities of Tantalum  
And Niobium Into Diisopropyl Ketone

Acid Concentrations	Element	Extraction Coefficient	Ratio of Extraction Coefficients, Ta/Nb
HCL 3.70M	Ta	4.3	91
HF 0.40M	Nb	0.047	
HNO <sub>3</sub> 3.92M	Ta	3.8	880
HF 0.40M	Nb	0.0043	
H <sub>2</sub> SO <sub>4</sub> 4.50M	Ta	19.0	160
HF 0.40M	Nb	0.12	
HClO <sub>4</sub> 4.61M	Ta	9.0	290
HF 0.40M	Nb	0.031	

A detailed study of niobium behavior was not made, for niobium extracted well when the hydrofluoric acid concentration reach about 6M. Accurate volume measurement and maintenance of a given known concentration of hydrofluoric acid could not be assured at these concentrations in glass apparatus.

The extraction of tantalum into diisopropyl ketone from 5 M  $H_2SO_4$ -0.40 M HF aqueous solution proved to be a very specific chemical property of tantalum. In addition to niobium, Se(VI) and Te(VI) tended to accompany the tantalum. Se(IV), Te(IV), Si, Sn(IV), Ti(IV), Mn(II), Zr(IV), Hf(IV), Fe(III), Sb(III), and Sb(V) did not accompany the tantalum.

#### Instrumentation

G. D. O'Kelly, J. D. Olsen,  
J. K. Tarrant and P. W. Maguire  
CRDC

#### Pulse Height Analyser Program

After making numerous modifications on UCRL cathode-ray pulse height selector circuits, the 20 channel pulse height analyzer was made to perform as well as the cathode-ray tubes would permit. The Elec. Engineering Dept. of UCRL has cooperated with the Allen B. Dumont Laboratories in an attempt to manufacture a better cathode-ray pulse height selector tube, with at least a 2 percent tolerance on the channel width and negligible interaction between adjacent channels. Thus far, a satisfactory tube has not been produced, and there is no reason to assume one will be available within the next few months. Extending the range of a 20 channel cathode-ray pulse analyzer by moving the analyzer across a spectrum 20 units at a time is an awkward and unreliable procedure, especially in routine operation. Once the utility of a multichannel analyzer was established in the group, thinking began to center on an enlarged unit of 40 to 50 channels.

Two alternatives for a multichannel pulse height analyzer was considered; first, the expansion of the existing analyzer to 40 channels, and second, the construction of an entirely new pulse height selecting system designed by A. Ghiorso and A. E. Larsh of UCRL. After considering the complexity, expense and maintenance requirements of the cathode-ray units, the first alternative was rejected in favor of the Ghiorso-Larsh system, which is extremely stable and also rather easily built. The cost of this unit, including self-contained power supplies, registers and pulse height selectors for 50 channels only costs \$30.00 per channel, if all parts are purchased. However, utilizing parts on hand, a 50-channel analyzer was constructed by this group at a cost of about \$450.00. The analyzer has been installed in the Building 4 counting racks and is in the "trouble-shooting" stage, which should be completed in about a week's time.

#### Scintillation Spectroscopy

Although the group has been occupied most recently with the pulse analyzer program, considerable work has been done with scintillation spectroscopy. The Borkowski technique uses NaI crystals with ground surfaces, packed in a diffusely reflecting bed of white, dry, MgO. It has been found that the crystal should be shaped to fit the curved face of the photomultiplier tube, making the optical seal at the interface with clear white petrolatum. Using light pipes for this purpose gives poor energy resolution. Typical detectors yield 10 percent full width at half maximum for the photoelectron peak of the 0.67 Mev  $Cs^{137}$  gamma-ray.

If a carefully selected photomultiplier tube is used, a resolution of 8.4 percent can be obtained for the same gamma-ray. Some difficulty was experienced in maintaining this resolution over a period of several days, even when the MgO was oven-dried. However, it was found that the seals around the assembly were not air-tight, and moist air had entered the detector head, deteriorating the hygroscopic crystal. With improved seals, one such detector has remained stable for five days at this writing.

#### Beta-Ray Spectrometer

Because of the higher priority of the work described above, the completion of the beta-ray spectrometer proceeded more slowly than was anticipated.

The motor-generator set installed for the magnet supply was found to have been designed in such a way that the electronic regulator could not function normally. Fortunately, another unit was available for stock which appears to perform satisfactorily.

The automatic counting control equipment is complete and in working conditions. A new magnet sweep unit is under construction, which should avoid contact difficulties encountered in the present unit. As soon as this component is complete, the spectrometer should be ready for fully automatic operation.

Meanwhile, positioning of the ring focus baffle will proceed, recording data manually.

#### Automatic Sample Counter

A new model of the automatic sample counter has been drawn up by the UCRL Mechanical Engineering Department, and is under construction. Positioning of the sample is accomplished by mating two precisely machined cams, instead of the present less accurate system of the microswitch controlling a drive motor and solenoid brake. As soon as operational data on this device are available, a full report will be prepared.

#### Corrosion Studies

W. R. Balkwell, L. M. Litz, and S. A. Ring  
CRDC

#### Zirconium

Two series of experiments have been performed in which zirconium foils bombarded with 190 Mev deuterons have been immersed for varying periods of time in doubly distilled water at 300°C in one set and at 280°C in the other set. In the runs at 300°C, stainless steel liners were used to contain the water in the high pressure autoclave. In the runs at 280°C, aluminum liners were used.

Table 3 summarizes the data obtained on the corrosion of the zirconium foils and the activity transferred to the walls of the steel container at 300°C. It is seen that the average rate of attack of the zirconium over the first 27 days was approximately five times that of the succeeding 34 days, indicating the formation of a protective film. The rate of transfer of activity, expressed as a function of that accumulated in the first six day period, was also found to fall off very rapidly.

Table 4 gives the data pertaining to the runs at 280°C. The rapid decrease in the rate of attack on the zirconium was also observed here with the total attack in the first 40.5 days being only 82 percent of that in the first 27 days at 300°C. However, the rate of transfer of activity was not observed to fall off as rapidly at the lower temperature as at the higher.

After running for 40.5 days at 280°C using aluminum liners, a nine day run was made at this temperature in a stainless steel liner. The rate of attack of the zirconium foils was about the same as in aluminum, but the transfer of activity to the liner apparently dropped off. A run was then made with the same foils at 300°C for 13 days. The rate of attack on the zirconium over this period was about four times that for the preceding nine day period at 280°C. The data for these last two runs is also given in Table 4.

Table 5 lists the specific activities found in the water after each of the first set of runs at 300°C. The activity is expressed as the percentage of the total for each element found in the entire set of ten foils after dissolving them following the conclusion of this series of runs. This percentage was obtained from the ratio of the counting rates of the relative samples at comparable times. The total activity in the foils for each element is listed in Table 6. These values were obtained from the counting rate of the chemically separated sample corrected for chemical yield and an approximated counting efficiency for the major radiation involved. Table 7 lists the relative activities found in the acid solutions used to remove the radioactivity from the stainless steel liners.

It is seen that strontium and yttrium contribute the largest amount of activity transferred out of the foils with rubidium and selenium next in order of intensity. Although the fraction of the total selenium and arsenic removed from the foils was relatively large, the total amounts presented are small. The fact that very little zirconium or niobium is found in the water or on the walls of the container indicates that the mode of transfer is probably a leaching of the more soluble spallation products from the insoluble zirconium oxide corrosion film.

Based on the weight gain of the foils in this set of runs, a total of 0.2 percent of the foil was attacked. Only the fractions of strontium and selenium leached out of the foils approach this figure, with the total amount of selenium found being appreciably in excess. This would indicate that some of the selenium in the metal underneath the corrosion film diffused out through the film and would, therefore, indicate an appreciably higher diffusion coefficient for this element than for most of the others in this system.

TABLE 3

Corrosion of Zirconium in 300°C Water -  
Contamination of Container by Transferred Radioactivity

Container Material - Type 307 Stainless Steel

Run No.	Length Of Run Days	Zr Foil Weight Gain mg/cm <sup>2</sup>	Weight Gain mg/cm <sup>2</sup> , mo.	Zr Attacked mils/mo.	Container $\beta$ of A	Activity $\beta$ of A/day
7A	6)				100	100
7B	8)					
7C	13)	0.079	0.088	0.0039	14.3	10.7
7D	34	0.019	0.017	0.0008	4.0	1.9
					5.8	1.0

TABLE 4

Corrosion of Zirconium in 280°C Water -  
Corrosion of Aluminum Container and Contamination by Transferred Radioactivity

Container Material - Type 28 Aluminum

Run No.	Length of Run Days	Zr Foil Weight Gain		Zr Attacked mils/mo.	Container Activity		Container Weight Gain	
		mg/cm <sup>2</sup>	mg/cm <sup>2</sup> mo.		% of A	% of A/day	mg/cm <sup>2</sup>	mg/cm <sup>2</sup> mo.
11A	3.1	0.0394	0.386	0.0173	100**	100	1.86	18.2
11B	6.1	0.0112	0.058	0.0026	86	43.2	3.6	17.7
11C	11.8	0.0008	0.002	0.0001	64	16.7	11.0	28.0
11D	20.5	0.0137	0.020	0.0009	~60	~10.5	~35.0	~51.0
Container Material - Type 347 Stainless Steel								
11E	9.0	0.0024	0.008	0.00036	5	1.7	1.9	4.00
11F*	13.1	0.0145	0.033	0.0015	8	1.8	0	0

\* Note: Temperature of Run No. 11F was 300°C

\*\* Note: Activity Deposited in Run No. 11A was 20 Percent of that Deposited in Run No. 7A

2043-110

DCRL-3043

TABLE 5

Radioactivity Transferred From Zirconium  
Foil To Surrounding Water At 300°C

Container -- Type 347 Stainless Steel

Run No.	Duration, Days	Radioactivity, % of Total In Foils*						
		Nb	Zr	Y	SR	Rb	Se	As
7A	6	$1 \times 10^{-3}$	$1 \times 10^{-4}$	$1.8 \times 10^{-3}$	$8.8 \times 10^{-2}$	-	$8.1 \times 10^{-2}$	$3 \times 10^{-2}$
7B	8	-	$3.7 \times 10^{-4}$	$8.9 \times 10^{-4}$	$3.9 \times 10^{-3}$	-	$5.1 \times 10^{-1}$	-
7C	13	-	-	$1 \times 10^{-4}$	$3.0 \times 10^{-3}$	-	$7.9 \times 10^{-2}$	$3 \times 10^{-2}$
7D	34	-	$1 \times 10^{-4}$	$7.9 \times 10^{-4}$	$2.8 \times 10^{-3}$	$4.0 \times 10^{-2}$	-	$3 \times 10^{-2}$
TOTAL	61	-	-	$3.5 \times 10^{-3}$	$8.9 \times 10^{-3}$	-	-	-

\* Note: Lower Limit of Activity Determined by Ability To Count On Geiger Counter

2043-111

TABLE 6

Radioactivity Levels For Longer-Lived Isotopes  
Of Zirconium Spallation Products For Run Zr-7

Bombardment Data:

Date 4/20/52 - 4/21/52  
 Time 23:13 - 02:53  
 Duration, Minutes 220  
 Target 10 - 0.005 in. x 1.25 in. x 1.625 in. -  
 Perpendicular to 1/4 in. edge  
 Bombarding Particles 190 MEV Deuterons

Spallation Product	Probable Isotope	Half-Life Days	Radiation Energy (MEV)	Assumed Counting Efficiency, %	Activity, c/m*	
					7/28/52	9/28/52
Nb	Nb <sup>91</sup>	64	0.1 e <sup>-</sup>	4.06	3.58x10 <sup>6</sup>	1.34x10 <sup>6</sup>
	Nb <sup>95</sup>	35	0.15 $\beta^-$ , 0.76 $\gamma$			
Zr	Zr <sup>88</sup>	85	0.48, e <sup>-</sup>	0.68	3.52x10 <sup>8</sup>	2.60x10 <sup>8</sup>
Y	Y <sup>88</sup>	104	x-ray, 0.9, 18 $\gamma$	0.0379 (Shelf 5)	1.78x10 <sup>9</sup>	1.06x10 <sup>9</sup>
	Y <sup>91</sup>	57	1.5 $\beta^-$			
Sr	Sr <sup>82</sup>	25.5	3.15 $\beta^+$ , 4.15e <sup>-</sup>	0.643 (Shelf 5)	1.01x10 <sup>8</sup>	2.98x10 <sup>7</sup>
	Sr <sup>85</sup>	65	x-ray, .5 $\gamma$			
	Sr <sup>89</sup>	53	1.5 $\beta^-$			
Rb	Rb <sup>83</sup>	83	x-ray, .4, .15 $\gamma$	4.06	-	1.77x10 <sup>7</sup>
	Rb <sup>84</sup>	34	x-ray, 1.5 $\beta^+$ , .8			
	Rb <sup>86</sup>	19.5	1.8 $\beta^-$ , 1.1 $\gamma$			
Se	Se <sup>175</sup>	127	x-ray, .1, .4 $\gamma$	0.18	6.71x10 <sup>6</sup>	4.81x10 <sup>6</sup>
As	As <sup>73</sup>	76	x-ray, .05 $\gamma$	4.06	1.46x10 <sup>5</sup>	2.83x10 <sup>3</sup>
	As <sup>74</sup>	17.5	1.5, .9 $\beta^-$ , .6 $\gamma$			

\*Note: Activity Corrected Only For Chemical Yield and Assumed Counting Efficiency For Shelf 2 Unless Noted Otherwise



TABLE 7

Radioactivity Transferred From Zirconium Foils To Stainless Steel Container At 300°C

Run Duration, No. Days	Total Activity % of A	Wash Solution	% of Activity Removed	Radioactivity in Wash, % of Total in Foils*						
				Nb	Zr	Y	Sr	Rb	Se	As
7A 6	100	6N HCl	57.2	-	-	2.0x10 <sup>-3</sup>	-	-	3.1x10 <sup>-1</sup>	-
		8N HNO <sub>3</sub>	17.8	1x10 <sup>-3</sup>	-	1x10 <sup>-4</sup>	1.0x10 <sup>-3</sup>	-	1.2x10 <sup>-1</sup>	7.8x10 <sup>-2</sup>
		6N HCl	24.3	1x10 <sup>-3</sup>	1x10 <sup>-4</sup>	2.5x10 <sup>-4</sup>	7.1x10 <sup>-3</sup>	-	-	-
7B 8	14.3	6N HCl	67.9	-	-	-	-	-	-	-
		8N HNO <sub>3</sub>	27.9	-	-	2.1x10 <sup>-4</sup>	4x10 <sup>-5</sup>	1x10 <sup>-3</sup>	3.1x10 <sup>-1</sup>	2.0
<u>Activity Found On Underside of Autoclave Closure In Run 7A</u>										
		6N HCl	85.6	1x10 <sup>-3</sup>	-	2.3x10 <sup>-3</sup>	1.3x10 <sup>-2</sup>	-	3.5	3x10 <sup>-2</sup>

\*Note: Lower Limit of Activity Determined by Ability To Count On Geiger Counter

-114-

UCRL-2043

2043-113

From Tables 6 and 7, it is seen that roughly comparable amounts of activity are found on the wall of the container and in the water. That on the steel wall was very difficult to remove even with both hot and cold applications of the indicated wash solutions.

Quite a bit of activity was also found on the underside of the closure of the autoclave as may be seen from Table 7. This closure was not in contact with the liquid water at all but was at the top of the system about ten inches above the water level. It was appreciably cooler than the section containing the water and probably acted as a condenser of the water vapor. Although the high selenium content found on it may be due to the volatility of this element, it must be emphasized that the yttrium and strontium reached this surface by diffusion through the liquid film on the walls of the autoclave.

Figure 9 shows the measured gross decay of the activity deposited on the wall of the container during run No. 11A at 280°C. The first point on the decay curve was taken four days after the foils were bombarded. Figure 10 is a similar decay curve for the gross activity in a zirconium foil bombarded edge on the 190 Mev deuterons. This curve was started about six hours after the end of the bombardment.

#### Aluminum

In the series of runs at 280°C, where aluminum liners were used to contain the water, very severe attack on these liners was observed as indicated by the last two columns of Table 4. As the time of immersion was increased, the average rate of attack went up rapidly. In Run 11D, with 20.5 days immersion at 280°C, the liner swelled so badly it could not be removed from the autoclave and had to be dissolved out.

Accompanying this oxidation of the aluminum liners was a correspondingly great evolution of hydrogen gas. Figure 11 shows the residual gas pressure in the autoclave after it had been cooled to room temperature at the end of each run. Mass spectrographic analysis showed the gas to be pure hydrogen.

The pH of the water at the end of these runs was about 6.5. This is a little lower than in the case of the higher temperature runs with steel liners which usually end up at about 6.8.

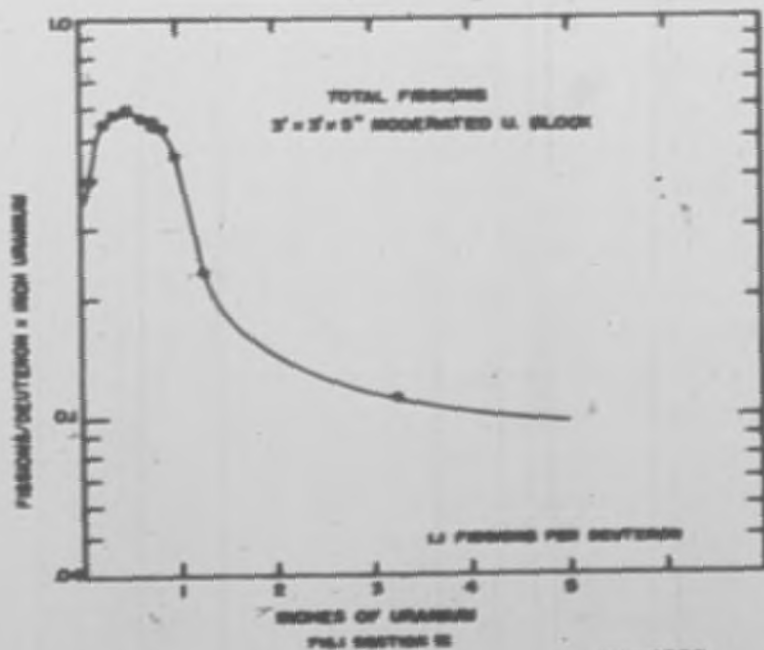
#### Zirconium Spallation Products

W. R. Balkwell, L. M. Lits and S. A. Ring  
CRDC

Twelve bombardments have been made on the 184-inch cyclotron at various deuteron energies from 30 to 190 Mev to obtain the excitation functions for the longer lived zirconium spallation products of Nb, Zr, Y, Sr, Rh, and Se. Work is also being done to characterize two previously unreported isotopes of yttrium,  $Y^{83}$  and  $Y^{85}$ .

Also, in the course of this work, the previously unreported isotope  $Rb^{82m}$  was separated from the 25.5 day parent  $Sr^{82}$  and was found to have a 1.25 minute half-life. It decays with the emission of the 3.15 Mev positron to stable  $Kr^{82}$ . This chain does not go through the 6.3 hour  $Rb^{82}$  isomer.

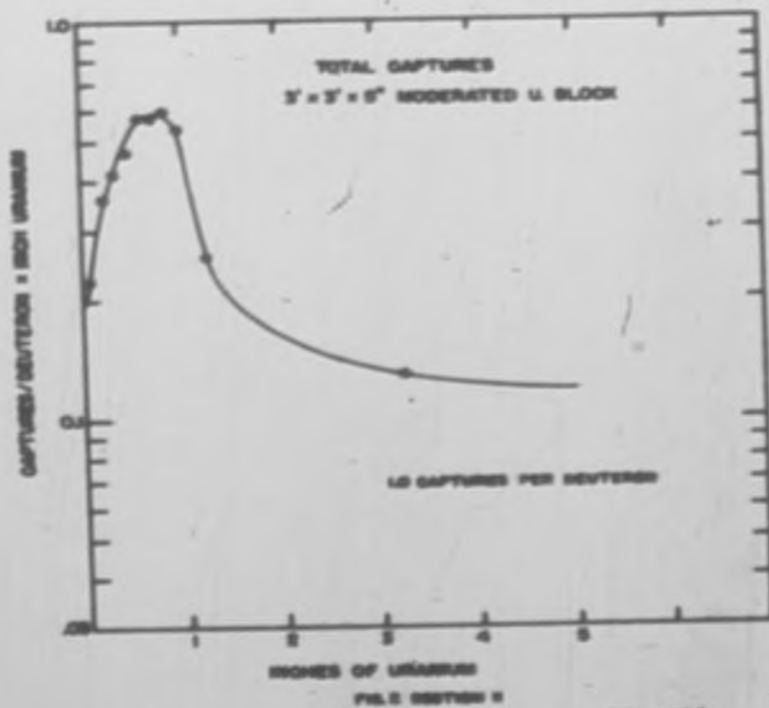
2043-11F



SECRET

EU-4022

2043-115

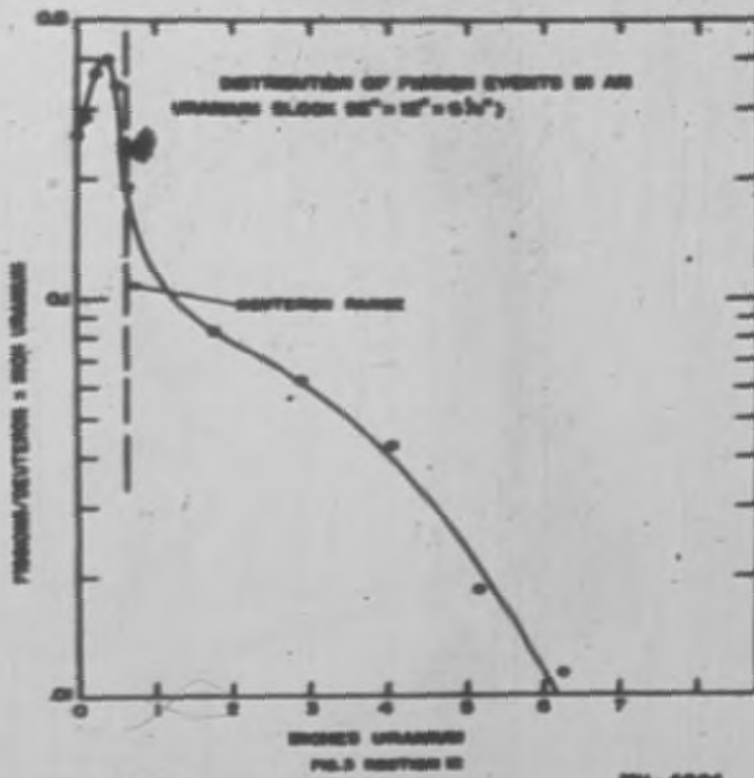


SECRET

FILE SECTION 2

50-4823

2043-116



REF ID: A72877

2043-117

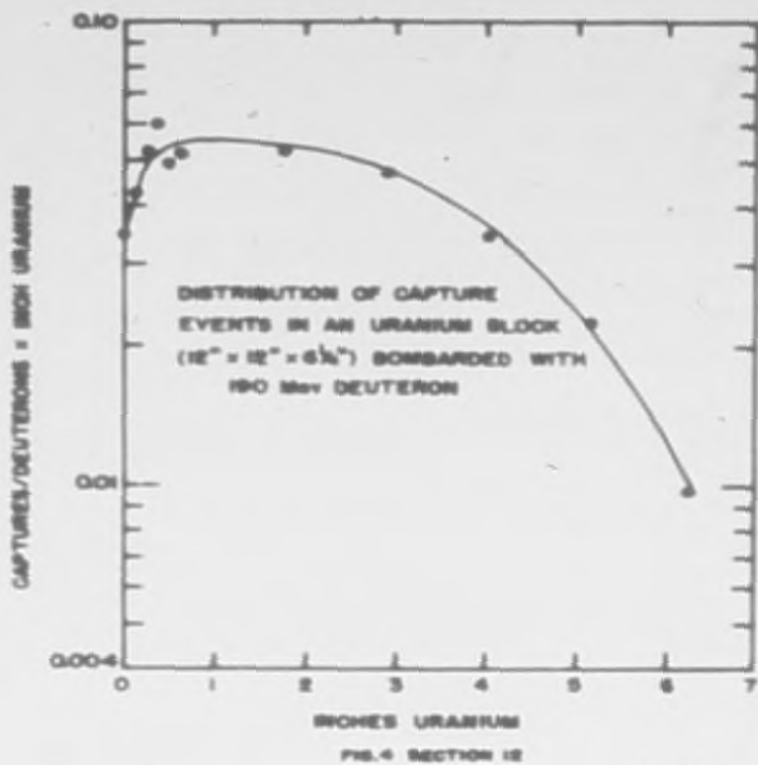
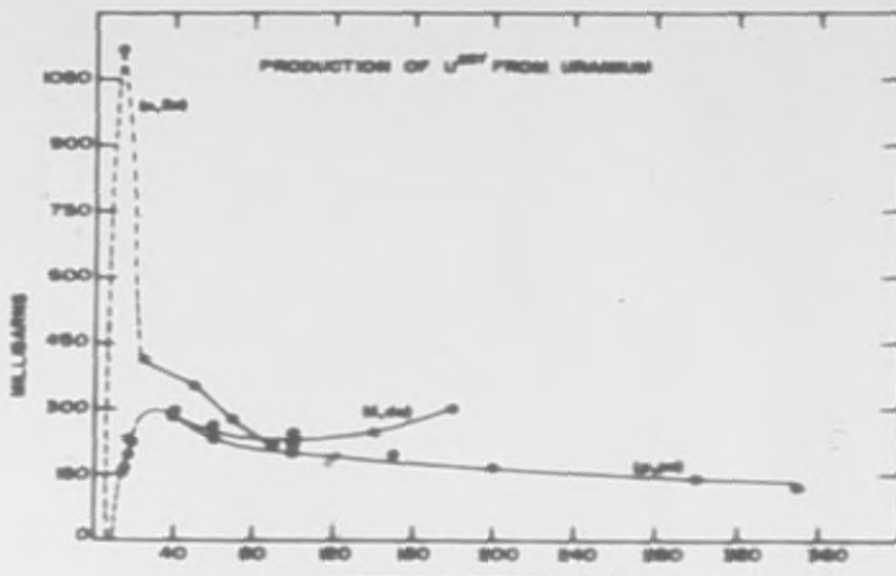


FIG. 4 SECTION 12

SECRET

BU-4825

2043-118



SECRET

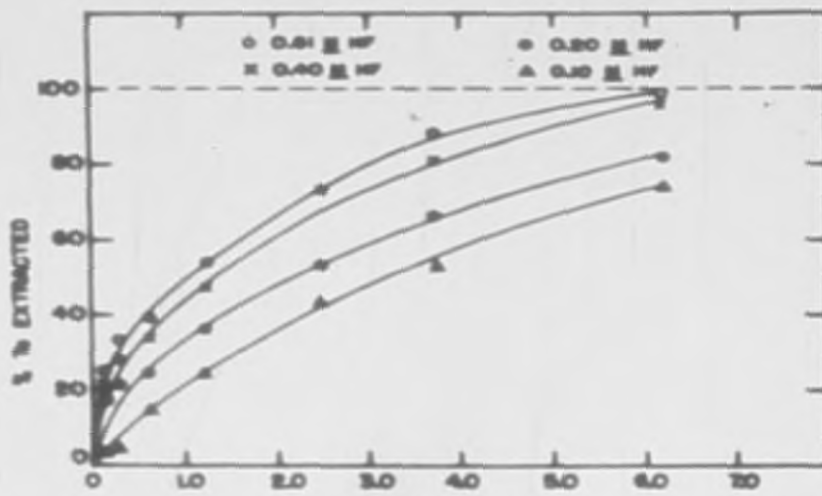
PAL 5 SECTION 2

NU-4026

REPRODUCED

2043-119

EXTRACTABILITY OF TANTALUM IN THE SYSTEM  
HCl - HF - DIISOPROPYL KETONE AS A FUNCTION OF HCl CONCENTRATION



SECRET

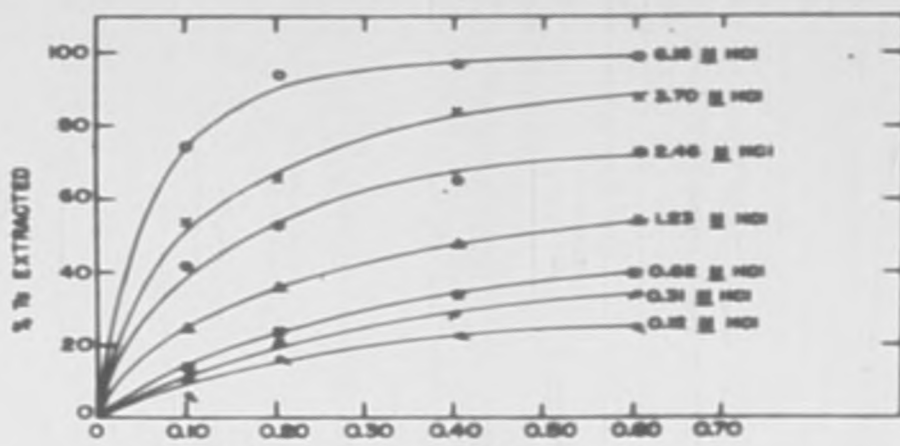
FIG. 6 SECTION II

MU-4827

2043-120



EXTRACTABILITY OF TANTALUM IN THE SYSTEM  
HCl - HF - DIISOPROPYL KETONE AS A FUNCTION OF HF CONCENTRATION



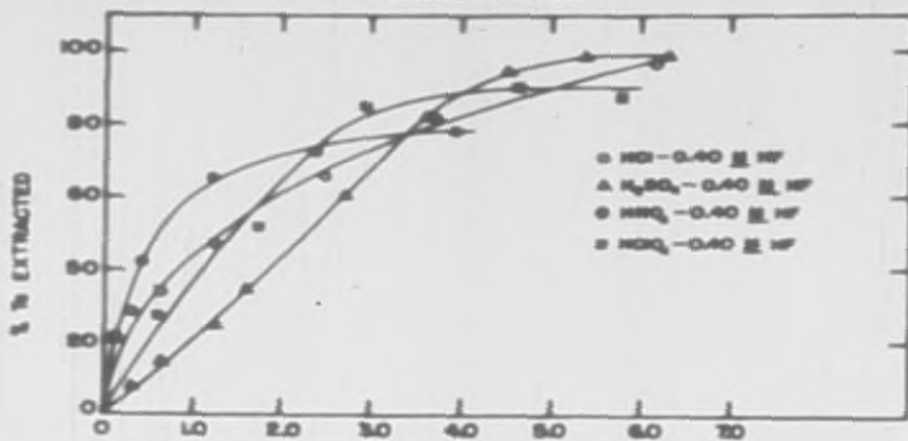
SECRET

PLANT SECTION 12

80-4828

2043-121

EXTRACTABILITY OF TANTALUM IN THE SYSTEM  
MINERAL ACID - MF - DIISOPROPYL KETONE AS A FUNCTION OF MINERAL ACID  
CONCENTRATION



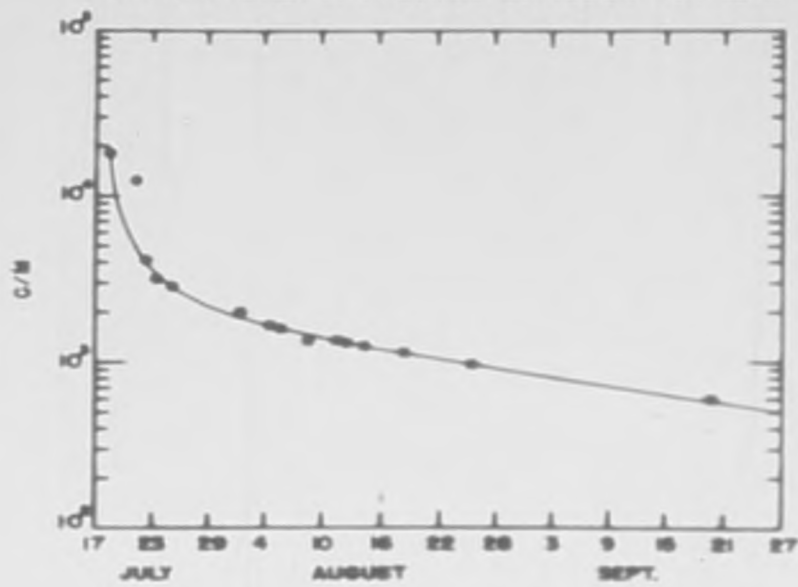
SECRET

ACID MOLARITY  
FIG. 8 SECTION II

MU-4829

2043-122

GROSS DECAY OF ACTIVITY TRANSFERRED TO  
ALUMINUM LINER IN ZIRCONIUM CORROSION RUN NE11A



SECRET

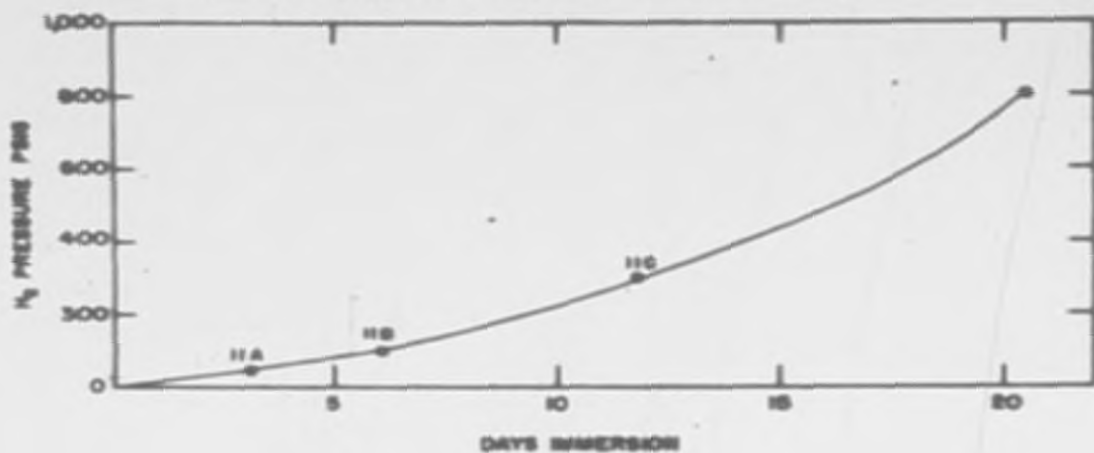
FIG. 9 SECTION 12

MU-4630

2043-123



HYDROGEN EVOLUTION FROM ALUMINUM IN 230°C WATER



SECRET

FIG. 4 SECTION 10

MU-4632

2043-125

## 13. TARGET DEVELOPMENT

Target Analysis

R. L. McKisson, R. M. Morning, M. F. Katzer,  
N. R. LeRoy, J. L. Smith, and A. R. Snyder  
CRDC

Blister Problem in Clad Plates

Limiting sizes of cladding flaws (blisters) have been determined for the standard A-12 primary target fuel plate (0.045 inch U clad on both sides with 0.010 inch Zr). The computations are based on an internal heat generation rate,  $W$ , of 40 KW/cu. in.; a constant  $h = 5000$  BTU/hr. sq. ft.; and a maximum allowable uranium temperature of  $1800^{\circ}\text{F}$ . The solution to the problem was carried out under the direction of Mr. N. C. Ostrander, and his results are given in LWS-24549. The maximum allowable diameter of the surface flaw for the conditions above is 0.20 inches; and the maximum end-flaw or edge-flaw length is about 0.07 inches.

Calorimetric Measurement

The feasibility study of the calorimetric measurement of the heat released in a bare uranium primary target in the 190 Mev deuteron beam is complete. Two 184-inch cyclotron runs were made and the pertinent data is given in Table 1.

Table 1

Feasibility Study Data

<u>Quantity</u> <u>Date</u>	<u>Run No. 1</u> <u>6-20-52</u>	<u>Run No. 2</u> <u>7-1-52</u>
Length Of Irradiation, Min	56.0	42.3
Beam Current, Amps*	$1.81 \times 10^{-9} \pm 7$ percent	$2.56 \times 10^{-9} \pm 7$ percent
Incident Beam Energy, Mev/d	189al percent	189al percent
Collected Beam Energy, Mev/d**	189al0 percent	183al0 percent

\* The error in the beam current is estimated because the foil geometry used was not identical with that for which the foils were calibrated.

\*\* These errors would be reduced to about  $\pm 5$  percent by calibration of the beam monitoring foil for the geometry of the experiment. Such a calibration was not warranted for this experiment because it was designed only to test the feasibility of getting reproducible data.

The agreement between the collected beam energies indicates that this type of measurement is feasible and a new calorimeter is being built to measure the rate of energy release of 190 Mev deuterons as a function of depth into a uranium primary target. It consists of five approximately one-fifth range, 2 inch diameter, uranium discs aligned with the beam. Each disc has a three-element thermopile for temperature monitoring, and a nichrome heater wire applied to one face for use in calibration. The discs are supported on lucite stand-off insulators and are mounted inside an aluminum radiation shield which is within, and concentric with, an aluminized lucite radiation shield. This shield is supported on three lucite stand-off insulators from the rear end-plate of the cylindrical vacuum chamber. The beam will be monitored by the use of a 0.005 inch aluminum foil placed ahead of the first uranium disc. In addition, there is an 0.005 inch uranium foil attached to each disc to monitor fission events throughout the target.

From the calorimetric data in each disc, the fission event data from the uranium foils, the range-energy curve, and the total cross section, one can estimate the type and number of heat-producing reactions in the uranium primary target for 190 Mev deuterons. Such data is fundamental to the study of target heating in A-12.

#### Experimental Probe

The bursting pressure tests on window designed for the experimental probe for the Radiation Effects Group indicate that a 0.003 inch flat stainless steel window whose span is 1.6 inches will sustain a static pressure of 100 psc. This gives a safety factor of about three over the design operating pressure. The use of a flat window simplifies the probe design and, in addition, the wider window allows a longer sample length to be used. The design of the probe is continuing based on the use of a flat window and detailing of the components is under way on this 30 Mev deuteron probe.

Preliminary studies have been initiated for the design of a similar probe for use in the 15 Mev proton beam.

Rate of energy loss vs range curves have been prepared for the ionization energy loss of 15 Mev protons on aluminum, stainless steel, and zirconium. These are useful in designing and interpreting results of irradiation experiments for the 15 Mev proton beam.

#### Design Development

T. H. Batser, J. C. Ekvall, B. W. Eia, R. C. Gerber  
J. W. May, L. B. Robbins, and J. E. Viscardi  
CRDC

#### General

The main effort of the group during this quarter was continued work on the target design using depleted uranium (0.3 percent  $U^{235}$ ) on the primary, secondary and lattice sections, moderated and cooled by light water. The primary target

intercepts the deuteron beam near the closed end of the vacuum vessel. High-energy neutrons from deuteron events in the primary are absorbed in a secondary target located at the closed end of the vacuum vessel. Fission energy neutrons from the first two targets are absorbed in the lattice, which is essentially a water-uranium blanket surrounding the primary and secondary targets. Long flat plates of zirconium-clad uranium are utilized for basic fuel assemblies in the primary and secondary targets, and long rods of aluminum-clad uranium are employed in the lattice.

Important changes in the general design described in the last quarterly report are: (1) the adoption of full-sine spiral sweeping; (2) the addition of a graphite reflector to the lattice; (3) a two-region lattice with a lower fuel content in the outer region; and (4) a planned processing level of 700 grams of plutonium per ton of uranium. Some of the important engineering design conditions are summarized in Table 2.

TABLE 2  
DESIGN CONDITIONS

	<u>Primary</u>	<u>Secondary</u>	<u>Lattice</u>
Production, Moles/Day	2.2	1.3	4.1
Uranium Inventory, Tons	20	100	700
Uranium Consumption, Tons/Year	235	137	434
Heat Load	310 MW	180 MW	310 MW
Coolant Flow	31,000 gpm	37,000 gpm	60,000 gpm
Temperature In	100°F	100°F	100°F
Temperature Out	173°F	140°F	136°F
Pressure In	400 psi	120 psi	40 psi
Pressure Out	65 psi	50 psi	atm.
Velocity (ft/sec)	30	20	5

#### Primary Target

The basic plan of parallel plate fuel elements supported by the inner tube of the bayonet tube has not been changed. Studies are continuing on varying plate thickness, tube diameter, tube spacing, tube material and the fraction of the secondary-target uranium that might advantageously be transferred to the primary. A recent analysis indicates that the uranium core thickness of the plates can be increased from the 0.045 in. reported last quarter to about 0.100 in. without excessive thermal stresses, thereby improving target efficiency and flow conditions. Detailed work on header design shows that tube center-to-center distance should be increased to at least 9 inches. Several header designs are being considered to support the two rows of tubes and manifold water to them during operation and during fuel removal. Plates will have to be removed from the tubes at regular intervals to process the fuel, but tube removal will depend on radiation damage. Various designs place different emphasis on the ease of



removing plates and replacing tubes. One design has cylindrical inlet and outlet headers with the outer bayonet tubes bolted or pressed into the bottom of the lower header and the inside bayonet tubes and plate bundles supported by the upper headers, so that the entire primary target must be removed, as a unit, breaking the vacuum and replacing all the tubes with each unloading. A modified design allows removal of individual plate assemblies, but the headers and all tubes are handled as a unit if any tube needs replacing. Work has been started on a header design with independent tube connections to allow withdrawal of plate bundles separately and individual tube removal after the plate bundle is out. A detailed estimate of the relative handling time for arrangements with individual manifolding and integral manifolding must be made before the designs can be finally evaluated.

Work is in progress to study the design of the intersection of the vacuum vessel and the primary target. A rectangular vacuum extension of the main vessel to house the tube array would provide the least welding and most support for the vessel, but a series of extended sleeves may be required to meet shielding and production requirement.

Fill-sine sweeping of the beam has reduced the maximum heat load in the target. The tubes and the contained plate assemblies will be varied in length to approximate the overall circular area swept by the deuteron beam.

#### Secondary Target

The secondary, located at or just beyond the end of the vacuum vessel, will be contained in a rectangular tank divided into rectangular compartments that support plate assemblies and channel cooling water. A study is in progress to compare a tank integral with the vacuum vessel with a tank separated from the vessel by a thin water space. The integral tank improves vessel strength and reduced the amount of parasitic absorbing material. The separate tank will allow reconstruction or replacement of the tank with a minimum of shutdown time. Adequate cooling of the tank wall and the end plate of the vacuum vessel will be provided by natural convection if a 1/4 in. gap is left between the units. Forced cooling may be required for the internal stiffeners in the vessel end.

Cyclic thermal loads in the secondary-target plates have been studied, but the solution of the problem of transient thermal stresses was too involved to be used for varying design parameters. These plates will be designed for steady-state stresses and checked with the transient equations.

#### Lattice

The base-case lattice design uses rods supported circumferentially around the vacuum vessel with the rod axis parallel to the vessel axis. The rods are arranged in a flexible ladder with their ends, like rungs, linked together in chains, which slide in semicircumferential guides built into a movable structure (C-frame). The inner four rows of rods are spaced to approximate 1.25 inch

equilateral triangular setting of centers and the outer five rows spaced to approximate 1;375 inch setting of centers. The resultant spacing normal to the coolant flow path gives a pattern that varies from in-line to staggered array and is repetitive for each 60° of arc. Cooling water flows in perpendicular to the rod axis through two ducts 60° and 180° from the top of the C-frame and flows out through two other ducts 60° and 180° from the bottom of the C-frame. The lattice is backed up by a 2 foot graphite reflector, the main C-frame structure and a water shield.

Recent studies indicate that a "no-cavitation" design criterion would be slightly more restrictive than the "no-boiling" criterion heretofore adapted, and maximum permissible temperature of the rod surface has had to be slightly reduced. More detailed analyses tend to show that past estimates of cooling-water pressure drops through the lattice C-frames have been too conservative, i. e., larger than necessary. However, recently increased estimates of production and heat loads in the lattice have revised the cooling requirements upward. The net effect on flow and pressure drop is being studied.

The traveling carriage for handling C-frames has been revised. The mechanism to move the C-frames on and off the carriage has been changed from a chain-driven type to a rack-and-pinion device, which is hydraulically driven, in order to provide more precise control of the motion and location of the C-frame.

#### Window for 350 Mev 0.5-Ampere Beam

The design of a water-cooled aluminum-alloy window for the deuteron beam appears theoretically feasible. Layout studies indicate that it is possible to locate the window between the lattice and the precessor when the target is 160 feet from the last drift tube. The window will comprise three sheets of 61S-T6 clad aluminum alloy, each 0.064 in. thick, welded up into a sandwich with a corrugated sheet between two plane sheets to form many parallel 3/8 in. water channels. The combined thermal and pressure stresses with a 50 psi pressure differential across the window would be 15,000 psi. Maximum metal surface temperature would be approximately 280°F with water velocities as high as 40 feet per second. Inlet water pressure for non-boiling conditions would be about 80 psi. The attenuation of the beam by the window would result in a loss of about 9 percent of potential production.

The composite window can be fabricated by spot welding. Successful tests have been conducted on plug welds on 0.064 in. 61S-T6 aluminum. The mechanical design has features allowing pre-installation tests for structural soundness, vacuum tightness and pressure loading. It also provides for remote removal and replacement.

A preliminary investigation into the evaporative cooling of a single-layer window has been made. For the swept beam diameters of around 7 or 8 feet the peak heat flux is about 300,000 Btu/hr-ft<sup>2</sup>. Evaporative cooling appears possible at this flux level, but further study will be required before the method can be definitely proposed.

### Handling and Storage

Handling and storage comprise operations required to move fuel material through the target area until it is delivered to a chemical processing area. Since the treatment of such problems must be coordinated with target area design, the successful solutions will vary with changes in target design emphasis. A series of area layouts has been completed during the quarter, resulting in confirmation of the plan to extend the target area water tank in the direction of the beam to provide water shielding and natural convection cooling for all the fuel material. The areas are separated by a concrete shield wall above the water level and possibly by a concrete barrier in the water tank. The walls shield neutrons from the targets and gammas from the coolant systems, thereby allowing work in the storage area during acceleration operation. Two underwater openings are provided below the dividing shield wall to permit passage of the C-frame carriages from one area to the other, and possibly there will be a separate opening for moving a carriage that transports primary and secondary targets between the two areas. The C-frame unloading machine is located in an inner tank in the center of the storage area where it can receive C-frames from either side of the target. A turn table is installed at the end of each set of tracks to change the direction of travel of the C-frame carriages, so that they may run from each side on connecting cross tracks to the unloading machine tank entrance. Racks are provided between the unloading machine and the shield wall for storage of primary and secondary targets. Disassembly and packaging areas are included at the other end of the storage tank for preparing the fuel units for transportation to the chemical processing area.

An investigation of natural convective cooling of the primary and secondary targets has resulted in a major change in the type of cooling planned for the target material. Calculations show that natural convective cooling will suffice, and the latest area layouts are planned for it. Shutdown heat will be removed from the storage tank by evaporation, make-up water and a small amount of forced circulation through a heat exchange unit. A report "Convective Cooling of Primary and Secondary Targets In Storage," CRD-TI-160, will soon be issued, describing the calculation and summarizing the results.

### Vacuum Vessel

A preliminary design specification on the vacuum vessel was completed and issued as CRD-TI-143. Discussions of the reasons motivating the specifications were included for the guidance of the eventual designers. A study of the literature on the corrosivity of aluminum alloys and on the effects of irradiation upon the properties of materials has been made in this connection, and a brief discussion of these subjects has also been included in the design specification.

### Alternative Designs

Studies of the heat transfer and fluid flow characteristics of a packed-bed lattice have indicated the feasibility of using clad uranium balls as the lattice fuel elements with the heat loads anticipated in the base case. A calculation on

UNCLASSIFIED

2043-131

production with the use of 2 inch diameter spheres has shown that the efficiency is nearly the same as for the rod lattice design. Preliminary layouts indicate that simpler handling, storage and target area arrangements are possible with packed-bed lattices.

Analyses of packed-bed primary and secondary targets have been started, but the heat transfer loads are more severe in these cases and no firm conclusions have been drawn yet, although there is reason to think that they will be feasible, subject perhaps to the use of hollow spheres in the primary target.

### Target Design

G. W. Brown and F. J. Duvall  
CRDC

#### Target Plates

In an effort to explain the dimensional instability of the zirconium clad uranium target specimens used in the thermal cycler tests, preliminary calculations indicated that two isotropic materials when bonded together would grow upon thermal cycling. In order to verify the theory copper strips clad with zirconium were fabricated at Oak Ridge and tested in a thermal cycler. These strips exhibited growth and warpage in much the same manner as did the clad uranium strips.

A theory of growth of uranium which was extended to include any bi-phasic combination has been proposed in CRD-TI-164. This theory is based on the different rates of expansion of the two phases and upon the decreasing yield stress with increasing temperature.

#### Lattice Study Program

A stress analysis and modification of design was made of a lucite frame structure for supporting uranium slugs in an apparatus for radiation experiments.

#### Clad Spheres

An analysis of the thermal stresses in clad spheres was made to determine their suitability as a target element.

#### Mark I Target

A review of the thermal stresses was completed. Stresses in the bismuth or the cantilever beam test were determined; a relationship between beam deflection and temperature fluctuation in the target was determined for equal uniaxial stresses.

#### "C" Frame

Work was done in conjunction with the design group on the deflection of the lattice supporting structure.

2043-132

An investigation was made of the elastic stability of their aluminum panels, used for holding the uranium fuel rods in the "C" frame.

Experimental Engineering

P. J. Charley, E. G. Cope, P. W. Osborne,  
J. A. Quinville, C. J. Schoens and J. W. Shortall  
CRDC

Experimental Engineering Building

Due to the altered status of the A-12 program, the expenditure request previously submitted to management for the engineering of this structure will be revised. During the quarter a study of the feasibility of utilizing a portion of the A and R Building for the experimental facilities was completed. It was felt that while sufficient floor area is available here, the lack of sufficient power, the fire hazard inherent in this wooden building, and the necessity of carrying on classified work in this presently unrestricted location (among other things), show that active consideration should still be given to the construction of a new building.

500 KVA Resistance Thermal Cycler

A tentative program for this resistance cycler has been completed. Specifications for necessary indicating and recording instruments (which will be used initially with the cycler) have been prepared. Funds for the purchase of these instruments are not yet available. Either a new expenditure request or a revision to the original resistance cycler request will be prepared.

Recent computations by the theoretical groups have shown that a sphere bed lattice for the MTA may have many advantages, but since very little is known about the heat transfer properties of sphere beds with internal heat generation, a program for determining these unknowns has been started. It has been ascertained that the power supply for the 500 KVA cycler could be utilized to provide internal heat generation in a four inch tube packed with metallic spheres, perhaps up to 600 watts per cubic inch. The 60 cycle power supply would provide fairly uniform heating (as contrasted to the "skin effect" of the more common high frequency induction heating apparatus), but the design so far considered would operate at a power factor as low as 20 percent. Design work on this project is continuing.

Pretest: Special Irradiation Experiment No. 1

A device has been constructed which will cycle small pieces of metal between various temperatures. Cycling is accomplished by dipping the strip alternately in lead (nominally at 500°C) and "Aroclor" heat transfer medium (at 100°C). It has been shown at other AEC sites that the distortion of uranium resulting from such a cycle can be correlated roughly with that obtained upon irradiation. Since it was necessary to predict if the target element to be irradiated in the MTR would be satisfactory from the standpoint of cladding quality

2043-133

and maximum distortion obtainable, it was felt that the pretest using this cycle would prove acceptable. It has been demonstrated that this analogy is not applicable to the case of zirconium clad uranium plates. Samples of alpha uranium, beta uranium, and copper -- all clad with zirconium were cycled up to 1000 times between 500°C and 100°C. The appearance of all samples after testing was very similar. The results of this series of tests led to the formulation of a theory (CRD-TI-164) to describe the action of anisotropic materials and clad elements when subjected to thermal cycling. Thus the distortion due to the "bi-metallic strip" action explained by the above theory will obscure any distortion due to the uranium alone. It is evident that under certain conditions of cladding and core thickness any bi- or tri-metallic specimen constructed of materials with differing properties will distort when subjected to sufficiently severe alternating temperature levels.

In order to complete the pretest as presently planned, it will be necessary to cycle bare alloyed uranium specimens. Because of the oxidation and corrosion of the sample, such tests cannot be carried out on the existing apparatus. Accordingly an expenditure request has been prepared for the dilatometer which will permit very accurate distortion or expansion measurements while the sample is heated in a protective atmosphere. This equipment will also be used to further the work on the theory mentioned above.

#### Hydraulic System

A revised program for this equipment has been prepared. Since the original objectives of this program have changed to some extent, it was felt advisable to submit a new expenditure request based on the new situation. This request has now been prepared and will be included with that for the Experimental Engineering Building.

A method has been found which is felt will prove valuable in determining flow velocities and patterns in narrow channels such as are presently proposed for an MTA primary target. The method uses a phosphorescent powder suspended in the coolant which flows through a passage fabricated from a transparent material. A thin collimated beam of triggered ultra violet light of high intensity is sent through the coolant, exciting a visible band in the phosphor which is swept downstream by the moving water. This band will reflect the velocities and velocity distributions in the water. Such a method eliminated the unavoidable disturbances which would be incurred due to the insertion of probes or other usual means of measuring velocity. A search for a suitable phosphorescent powder is now underway, and an experimental verification of this method is planned.

#### Miscellaneous

In some cases it will be necessary to establish the temperature of a heated zirconium or zirconium clad sample. In such cases, the space available for thermocouple wires may be so limited that one wire may be the maximum permitted. Accordingly a determination is being made of the thermoelectric potential of zirconium versus alumel and constantan. The Zr-Alumel couple appears to yield a very usable potential of  $28 \times 10^{-3}$  m. v. /°C over the range 0-100°C.

#### 14. MATERIALS RESEARCH

##### Physical Metallurgy

C. C. Woolsey, J. P. Frankel, M. Bettman,  
M. L. Buehler, D. I. Martin, T. E. Stephens,  
and W. W. Walker  
CRDC

##### Dimensional Instability of Uranium

In a recent publication Burke et al. have summarized the development of analytical and experimental approaches to the problem of the dimensional stability of uranium. The theory proposed by Burke to explain the growth of uranium postulates that overall growth of specimens subjected to thermal cycling is due to the differential expansion of adjacent disoriented crystals permitted by grain boundary relaxation during the temperature increase. In discussing this "mechanism" of growth Burke was able to explain, qualitatively, why the effects were dependent on the magnitude of the temperature variation and the "hot-tank" temperature, as well as on heating and cooling rates.

There are, however, certain difficulties associated with the concept of differential growth of various grains; the most important of these would seem to be the resulting internal discontinuities. While differential growth was demonstrated in the case of bicrystals, it is difficult to explain how a polycrystalline conglomerate can allow the opening up of "holes" at the ends of shortened grains. The restraining effect of the surrounding grains must be shown to be compatible with the postulated deformations of the proposed theory before too much further work proceeds. This was first pointed out to the writers by Dr. Max Bettman of Livermore Research Laboratories. Micrographic work by Boas and Honeycombe revealed slip lines in adjacent grains, but no relative displacement of the grains during thermal cycling. This indicated a need for a theory of growth which did not require grain boundary relaxation.

Fortunately there is such an alternative "mechanism" that has the same advantage as that proposed by Burke, while at the same time it pictures all grains as growing at the same rate. In this way there are no questions of compatibility.

In the previous theory, the only effect of the postulated grain boundary slip was to relax the restraints that the less expansive crystals exerted on those tending to expand more, during temperature rise. In the present proposal it is submitted that the decrease of yield strength of uranium with increasing temperature would have the same effect.

A theory has been proposed to explain the dimensional stability of uranium subjected to thermal cycling. The theory proposed differs from existing theory in that the crystals of uranium are all presumed to grow at the same rate, no differential growth, such as allowed by grain boundary relaxation, being required. The proposed theory has been discussed in detail in CRD-T1-164, "An Alternative Mechanism of the Dimensional Instability of Uranium," by J. P. Frankel and G. W. Brown.

The theory is easily extended to the problem of the dimensional instability of multimetallic plates. The instability of composite metal components, quite apart from the inherent instability of the component metals, was predicted on the basis of this theory and confirmed in the laboratory.

It was found that copper plates clad on both sides by zirconium grew approximately the same amount of thermal cycling as did similarly clad a rolled uranium.  $\beta$  treated uranium plates clad with zirconium also grew approximately the same amount. In all cases severe warping was manifest.

#### Chemical Metallurgy

M. H. Boyer, R. F. Russi, and P. O. Strom  
CRDC

Experimental work has been done on the corrosion of aluminum alloys by water at 350°F. Alloys investigated were the following: alclad 75S-0, alclad 24S-T3, 61S-T3 and 52S. The first four were studied both as isolated specimens and coupled with stainless steel and zirconium.

In all cases, relatively high initial rates of attack were observed, gradually decreasing to a much lower value, which then remained fairly constant throughout the test period. For the first four alloys, initial values of about 3 mil per year were obtained, falling off after about one week to constant values of about 0.2 to 0.5 mil per year. In no case did the corrosion rate appear to be affected by coupling to stainless steel or zirconium.

The alloy 52S showed higher rates, an initial value of about 6 mil per year being observed, which subsequently decreased to about 2 mil per year.

Longest test periods were 1464 hours for the first four alloys and 673 hours for the 52S. Water was air saturated at the time of addition to the corrosion bomb and was changed periodically to minimize effects due to variation of pH. Temperature was 350°F in all cases through the tests.

#### Irradiation Experiments

W. E. Browning, S. E. Bramer, W. M. Haussler,  
R. A. Heckman, J. Palmer, R. V. Steele, S. V. Zinso,  
and S. Siegel  
CRDC

The target assembly for static irradiations of test specimens of the MTA at Livermore had previously been designed. Detailing of the irradiation thimble which is a part of this assembly was begun. Installation detailing was started for the complex helium and water cooling systems for the test targets. Special tests were performed to optimize dimensions and the operating conditions of sub-assemblies of the irradiation equipment. However, the design was advanced



far enough so that construction will be started as soon as the expenditure request covering this equipment is approved.

Studies were made to determine the effect on the tensile properties of the vibration caused in the test specimens by the high velocity cooling gas. Tensile specimens of 2S-0 aluminum were exposed to an air stream with the same flow characteristics as the stream of helium to which the test samples will be subjected during irradiations. Results showed that 0.013 in. thick specimens exposed for as long as 336 hours showed no change in tensile properties. In a similar experiment, 0.005 in. thick specimens were exposed for 95 hours and there was some slight indication of work hardening. This result is being checked in runs of longer duration.

Rupture tests on 0.003 in. thick stainless steel windows were performed and the results showed that a window sufficiently wide for the proposed test specimens will afford useful, reliable service in the irradiation equipment. In one particular design, a 1-5/8 in. wide window was found to sustain a differential pressure of 100 psi. This compares favorably with the design pressure differential of 30 psi.

Fabrication of the equipment to be used for the irradiation of Zr-clad uranium plates in the Material Testing Reactor was nearly completed. Completion of this equipment was not expedited because the clad plates were not available when originally planned. Since the MTR has actually been operated at fluxes as high as  $5 \times 10^{14}$  neutrons per square centimeter per second, it is possible to use specimens containing natural uranium and still accumulate the required burn-up in a reasonable length of time. The irradiation will be performed shortly after the test plates are delivered and pretested.

The experiment to determine the effects of radiation on the water-corrosion of aluminum, previously delayed by lack of machine shop time, has been scheduled for irradiation in the Berkeley 60-inch cyclotron. The first bombardment will be performed within the next month.

A literature survey was made on the performance of 41 organic materials in neutron fluxes ranging from  $10^7$  to  $10^{13}$  fast neutrons per square centimeter per second. The expected useful life of each of these materials in terms of conservative design and limiting design was expressed as a function of the location in the MTA accelerator with respect to the target. The results of this survey were presented in a formal report, CRD-TI-147.

## 15. A-12 CHEMICAL PROCESS STUDIES

Process Research

W. H. McVey, E. L. Anderson, P. L. Auer, F. J. Brutschy,  
R. E. Elson, R. H. Gercke, W. H. Ludwig, and K. L. Mattern  
CRDC

Uranium-Zirconium Dissolution

Studies on the dissolution of simulated zirconium clad uranium plates have continued. Minimum total hydrofluoric acid to total zirconium ratios and the corresponding minimum final nitric acid concentrations required for complete solution of zirconium metal without the formation of insoluble zirconium precipitates have been established. For the dissolution of zirconium metal in the absence of uranium, the relation between the minimum total fluoride to zirconium ratio and minimum final nitric acid to produce a stable solution may be expressed as  $2.8 - (\text{HNO}_3)/4 = (\text{HF})/(\text{Zr})$  where the concentrations are expressed in moles per liter of solution. The simultaneous dissolution of zirconium and uranium metals in hydrofluoric-nitric acid mixtures requires slightly higher fluoride to zirconium ratios or higher final nitric acid concentrations to produce stable solutions since the formation of the uranyl fluoride complex reduces the effective fluoride concentration somewhat. For example, the analogous relationship for a stable solution in which the final uranium concentration is 1.35 M is given by:  $3.1 - (\text{HNO}_3)/4 = (\text{HF})/(\text{Zr})$ .

Synthetic feed solutions containing uranium, zirconium, hydrofluoric and nitric acids have been contacted with 30 percent tributyl phosphate in carbon tetrachloride. The uranium extraction is essentially unaffected by the presence of zirconium and hydrofluoric acid and the zirconium is separated by a factor of greater than  $10^4$  from the uranium on one batch extraction with no scrub. A typical feed solution had the following composition: 1.35 M UNH, 0.4 M Zr (IV), 1.0 M total HF and 2.5 M  $\text{HNO}_3$ .

Both platinum and gold metals have been found to be unsatisfactory materials for constructing dissolvers for the dissolution of zirconium in hydrofluoric-nitric acid mixtures. The presence of either noble metal causes the zirconium metal to ignite with a brilliant flash toward the end of the dissolution, presumably due to a gold or platinum catalyzed zirconium metal reaction with a nitrogen oxide. The noble metals are unchanged after the reaction.

Purex Studies

Because considerable savings in inventory costs can be attained by reducing the cooling period before processing the irradiated fuel elements, investigation of the behavior of specific short lived fission products in Purex was initiated. Since 8 day iodine becomes important at short cooling times, and since there is some evidence that iodine tends to follow the organic phase in purex systems, a study of this element was undertaken.

Experimental work was carried out using two sources of radio-iodine; one source contained carrier iodine and the other was carrier free. While the carrier free iodine studies were probably more nearly representative of dissolved fuel conditions the results using carrier free iodine did not agree with the carrier experiments and were not reproducible in themselves. This is undoubtedly due to the extremely low concentration of iodine in the carrier free case with the resultant greater effect of minute traces of impurities.

The experimental results using radio-iodine with carrier iodine showed that elemental iodine is highly distributed in favor of the organic phase as expected. The distribution ratio of elemental iodine into pure carbon tetrachloride was of the order of 100 and into 30 percent tributyl phosphate in carbon tetrachloride was even higher. Experiments with macro concentrations of iodine indicated from spectral changes that there is compound formation or solvation of iodine by tributyl phosphate. On continued contact of iodine in 30 percent TBP,  $CCl_4$ , the distribution ratio of iodine decreases to a value of 7.5, which is due to the oxidation of elemental iodine to iodic acid which has a distribution ratio of approximately 7.

This indicates that with short cooling periods iodine will present a problem in the present flowsheets, particularly in solvent recovery since the iodine largely follows the organic phase throughout. The work was done by our representative at ANL.

Our representative at Oak Ridge has reported on Purex research in connection with temperature effects and the behavior of Np (V) in TBP aqueous two phase systems. An inverse dependence of the uranium distribution ratio with temperature has been observed while the distribution ratio for plutonium (IV), nitric acid and gross fission products increase sharply with temperatures.

A purex feed was spiked with Np (V) and its behavior was studied through a batch counter current Purex run. While 20 percent of the neptunium extracted, it was removed in the scrub section with an overall DF of 100.

Two reports on high energy bombardment induced fission and spallation products are being issued. The first deals with calculated fission and spallation product distributions expected in 350 Mev deuteron bombarded uranium as a function of irradiation and cooling times and the other gives experimental results obtained by our representative at ANL on the behavior in current purex at certain of the new fission products which were devised from high energy cyclotron bombardment.

2043-139

### Process Development

T. E. Hicks, J. L. Bloom, L. D. Christensen, J. M. Davis,  
L. M. Guenther, S. J. Horn, J. Jost, A. L. Lindsay, Jr.,  
W. J. Luke, R. W. Robinson, B. Rubin, and G. R. Tully, Jr.  
CRDC

#### Building Number 25

Steel doors were installed in Building 25, a guard was posted, and work was started on classified chemical and chemical engineering problems. All gloved boxes are ready for installation on completion of an auxiliary exhaust system for the boxes, but studies involving radioactive materials other than uranium or thorium cannot be started until this system is completed. The fume hoods for the laboratory had not been received by the end of the quarter, but all other major construction items have been completed.

#### Mini Mixer Settlers

A new fluorothene body for the miniature mixer settler having 3/8 inch square chambers instead of 1/4 inch chamber was tested for hydraulic performance. Twelve runs were made with 30 percent TBP in kerosene vs 2 M HNO<sub>3</sub>. Notably superior performance was noted over the 1/4 inch chamber body but because of the interdependence between stirring and pumping of the impellers, too much pumping of the heavy phase occurred at speeds required for adequate mixing. Also control of the heavy phase interface in the final stage by use of an adjustable weir was poor, and contributed to instability by causing irregular flow of the heavy phase. In order to correct these difficulties, the impellers were modified so that the throw-out holes are higher than the overflow passage; this has the effect of decreasing the pumping rate at high stirrer speeds. Good regulation of the heavy phase interface was achieved by use of a conductivity probe inserted in the final stage. This probe detects the difference in conductivity between the organic and aqueous phases, and through the use of an electronic amplifier and relay, operates a solenoid valve in the heavy phase overflow line. Further improvements include baffles in the bottoms of each mixing chamber to increase mixing and raising of the floor level of the mixing chamber to eliminate pockets of unstirred heavy phase.

Several runs were made using the system water-butanol succinic acid to check extraction efficiency. While the data were not entirely conclusive it was indicated that the stage efficiency is greater than 70 percent and probably is close to 100 percent. It is now felt that the hydraulic behavior is satisfactory with different liquids over a wide range of flow rates, and installation of a mini mixer settler in a shielded box has commenced. Auxiliary equipment such as miniature valves and syringe pumps is now being fabricated.

#### Homopolar Motors

In conjunction with the design and testing of the miniature mixer settler a need has arisen for a small, compact and reliable motor to drive the stirrers.

2043-190

A unique homopolar motor of extremely simple design has been developed recently which meets many of our requirements. The motor consists of a solid metal disc rotor spinning in a pool of mercury, the whole mechanism being in a magnetic field. A direct current of several amperes at a fraction of a volt is passed through the rotor shaft and out through the mercury at the edge of the disc, causing the rotor to turn. The speed of the motor can be varied by changing the current passing through the rotor.

The presence of copper oxide in the mercury arising from amalgamation of copper parts, has caused erratic behavior of the motor after extended periods of operation. This problem can be solved by using metals that amalgamate slowly or by preventing oxidation. Accordingly, various models of the motor constructed of copper, stainless steel, or nickel or chromium plated parts have been subjected to a series of short duration and life tests. It is indicated that the motors are capable of maintaining a constant speed to  $\pm 5$  percent for as long as 180 hours. Additional mechanical, electrical, and corrosion phenomena are being studied to improve operation of the motors.

#### Midi Mixer Settlers

The midi scaler mixer settler in Berkeley was operated using thorium nitrate - 30 percent TBP kerosene in order to determine the operating characteristics of the mixer settler with this system. A 0.50 molar thorium nitrate solution containing a small amount of fluoride ion from the dissolution procedure was contacted with a kerosene solution containing 30 percent TBP and 0.5 M in the  $\text{HNO}_3$  in a ten stage end-fed mixer settler. At organic/aqueous flow rates of 30/8 ml/min respectively, the waste stream contained  $1.5 \times 10^{-3}$  M thorium which represents a 99.8 percent recovery. The overall performance of the unit was considered satisfactory and efficiency was comparable to previous experience in extracting plutonium.

A limited program to more fully investigate the behavior of the mixer settler with this system was therefore initiated, and three ten-stage extraction runs were made at an aqueous thorium feed rate of 15 ml/min with organic/aqueous flow ratios of 2, 4, and 6. The aqueous feed in each case was 0.705 M Th and 0.473 M  $\text{HNO}_3$  while the organic extractant was 30 percent TBP - 70 percent kerosene and 0.535 M  $\text{HNO}_3$ . Thorium losses for the respective ratios were 12, 0.08, and  $10^{-3}$  percent respectively.

Aqueous waste stream concentrations for the latter two runs were  $5.6 \times 10^{-4}$  M Th and  $10^{-5}$  M Th respectively. Sufficient further data will be taken to attempt a correlation of several of the variables concerned in thorium extractions.

#### Midi Mixer Settler Prototype

A four stage mixer settler prototype has been operated to enable data to be assembled for design of larger units. Types of internal baffles and screens and their locations were varied using the 30 percent TBP kerosene - 2M  $\text{HNO}_3$  system.

A satisfactory combination of baffle screens, impellers, and stirring speeds was found which allows wide latitude of liquids and flow rates. Uranium was then added to the system, and extraction efficiencies approaching 100 percent were achieved on extracting uranium into 30 percent TBP - kerosene. Efficiency of 60 percent was obtained when re-extracting into the water.

At du Pont's request, recommendations were made for modifying the Savannah River mixer settlers to obtain increases in throughput and broaden the otherwise narrow critical speed range of their mixer pumps. Based on our experience with the prototype mixer settlers and especially its successful actions on their most difficultly handled stream, specific baffles and screens were suggested for installation in their settling sections.

#### Horizontal Pulse Column

A center pulsed horizontal column 1 in. diameter by 4 ft. long containing 20 perforated S-shaped plates was constructed and hydraulically tested using water-carbon tetrachloride. The dependence of maximum flow rates on the pulse magnitude are being studied. It is interesting to note that the transferred pulse volume of the two phases is not equal, being about 50 percent greater for the lighter phase than for the heavier. This means that the maximum flow rate of the light phase is 50 percent greater than that of the heavier phase. At 38 pulses/min water flow rates of 75 - 125 ml/min were observed under maximum operating conditions.

In order to check extraction efficiency several runs were made using the water-butanol-succinic acid system. Under conditions of maximum operable amplitude and frequency the LETS (length of an equivalent theoretical stage) varied from 5.6 to 12 inches, depending on flowrate. This indicates that the horizontal column operates in the same range of efficiencies as the more conventional vertical pulse columns and offers promise of being a useful contractor since it does not need the expensive headroom required by the vertical columns.

#### Equipment Testing

Studies are underway to test the performance of pumps, check valves, air spargers, solenoid valves, quick-connect fittings, spray wash rings for tanks, and other components to be installed in the cells in Building 21. It has been found that skinner stainless steel solenoid valves show little or no leakage after 15,000 cycles of operation and that they will probably be serviceable in the uses contemplated for them.

#### Equipment

Lead shielded containers for shipping Hanford dissolver solutions and Hanford slugs were designed by us and fabricated at Livermore. These are now ready for use. Drawings and specifications for additional gloved and shielded boxes have been completed, and a list of general laboratory equipment and supplies for Building 21 has been compiled. These will be ordered on approval of funds for that purpose.

Process Design

L. R. Michels, D. L. Fry, M. C. Feldman, E. J. Haven,  
R. J. McCarter, H. Schneider, J. L. Schwennesen, K. G. Steyer,  
and R. D. Chaffe  
CRDC

Equipment schematic flowsheets for the feed preparation, solvent extraction, solvent and acid recovery, and waste processing sections of the Purex No. 3 process have been prepared and are currently being reviewed and revised. These flowsheets are based on the materials flowsheet described in the Quarterly Progress Report for the period ending May, 1952. The equipment schematics represent the initial step in the scoping of the Purex Process.

A study has been completed to determine the storage capacity required for U-237 decay in a purex plant processing A-12 product. The study indicates that 1. Decay storage can be placed most advantageously after the concentration step prior to the second uranium extraction cycle, 2. An estimated 60-day hold-up capacity would be required in processing material irradiated under the conditions of the A-12 revised plutonium base case, 3. Segregation of UNH solutions according to the source of irradiation would not be warranted on the basis of U-237 content.

A number of economic evaluations have been completed and are described briefly in the following paragraphs.

- a) The economic merit of recovering nitric acid from dissolver off-gases in the Purex Process was studied. No incentive exists for acid recovery at uranium-processing rates below about five tons per operating day.
- b) A preliminary investigation of the economic justification for continuous dissolving in the Purex Process indicates, on the basis of the limited data available, that continuous dissolving of A-12 irradiated uranium is not economically attractive.
- c) A study has been completed evaluating the incentive of substituting uranium oxide for uranium metal in the Revised Base Case MTA lattice (350 Mev, 1/2 amp., 700 g/T). Based on a calculated production figure of merit of 85 percent for oxide as compared to an all-metal lattice computations indicate a negative incentive of \$25,000,000 over a 6-2/3 year period, assuming the cost of metal to be \$2.50 per pound more than the cost of oxide. If lattice efficiency can be optimized to 95 percent a positive incentive of \$20,000,000 is indicated. The break-even efficiency is 91 percent. With a price differential of \$5.00 per pound the break-even point occurs at 87 percent. Intangible advantages of the oxide lattice for an MTA installation appear to be virtual self-sufficiency as regards lattice fuel and avoidance of the uranium growth problem.
- d) A preliminary study was made to determine the optimum product to fuel ratio (g/T level) for an A-12 thorium lattice assuming a constant

2043-143

production rate. Based on unit product costs as calculated by Dr. Mason Benedict's method, the optimum level for U-233 production was found to be about 500 (al00) grams per ton. In general, the minimum unit product cost represents a balance between product inventory charge, fuel cost, and capital investment in fabrication and processing plants.

- e) An economic comparison between the Chelate - TBP and Purex processes as they apply to A-12 chemical separations was completed. A Chelate - TBP plant designed according to conditions most favorable to the process was compared to a conservatively designed Purex plant. The small marginal saving in construction and operating costs of Chelate-TBP plant approximate the estimated cost of a Chelate-TBP process development program. Consequently, at this time there appears to be little economic incentive for further investigation of the Chelate-TBP process.

#### Livermore Unit Operations Laboratory

Equipment schematic flow diagrams have been completed for the cells containing dissolver, column extraction, mixer-settler, and feed preparation equipment. A revised schedule of waste streams from the Unit Operations Laboratory has been prepared.

The Process Design Group's representatives assigned to Oak Ridge have continued to assist in Purex and Thorex design work carried on at ORNL and to maintain contact with process development at that site.

2043-144



## 16. ELECTRON MODEL CLOVERLEAF CYCLOTRON STUDIES

### Electron Model II

Robert V. Pyle  
UCRL

Experiments on extracting the beam with a magnetic channel were continued. The cut-away region of the poles started at 15 in. radius at the center-line of a hill (see Fig. 1). The electrons entered the cut-away portion with a clockwise rotation. In principle, the frequency of radial oscillation of the full energy electrons was such that they had a large radial component of velocity after a few revolutions through the rapidly decreasing magnetic field, and left the cyclotron.

Experimentally, the electrons emerged from the cyclotron over a region  $110^\circ$  in azimuth, with trajectories between the dashed lines at A and B in Fig. 1. Attempts to concentrate the spillout beam by adjusting the angle at which the circulating beam struck the channel were only slightly successful.

By empirically increasing the magnetic field in the region C, those electrons which otherwise would have emerged near B were kept inside of the cyclotron for another revolution and brought through the channel once more. The circulating orbits were not disturbed. That part of the spill beam which was flying out with a very large radial velocity was bent inward by the strong field at the outside edge of the channel (D).

Ninety percent of the electrons circulating at 14 in. radius spilled out through the channel. By increasing the magnetic field at C, 80 percent of the spill beam was concentrated in a patch 1 in. high and 6 in. wide (E) located 22 in. along a line perpendicular to the center line of the channel hill at a radius of 15 in. The remaining 20 percent of the electrons were spread between B and E. This rather crude attempt produced a large improvement in the spatial distribution of the spill beam and the result was independent of the amplitude of the rf voltage on the accelerating electrodes.

Further concentration of the spill beam appeared possible but time consuming, and as the electronic and vacuum components were needed elsewhere the cyclotron was torn down on August 15.

### Electron Model III

E. L. Kelly  
UCRL

The magnetic field has been measured, shimmed, and remeasured. Reduction of the data of the shimmed field measurement is still in progress. Preliminary checking indicates that at no point does the field between radii of 7 in. and 18 in. differ from the desired theoretical values by more than 100 milligauss. Between 18 in. and 19 in. parts of the field at the hills are low by as much as

2043-145

150 to 200 milligauss. Inside a radius of 7 in. the field is high, increasing to an error of as much as 200 to 300 milligauss at 3 in. (The design value of the field at the center is 19.3 gauss).

The vacuum pumping system has been completed and tested with the vacuum analyzer and is now ready to turn on. Dees and magnetic field trimming coil assemblies are complete and ready for installation. The design of probes and probe locks is under way. In short, the machine is now ready for final assembly and testing. It will certainly be in operation by October.

Some mention should probably be made of the problems that were met and overcome in measuring and shimming the magnetic field. In order to measure the field to 25 milligauss or better, Minard Leavitt and his group have devised and built a special magnetometer. This in essence is a very small transformer consisting of a permalloy wire surrounded by two coaxial coils. One coil, the primary, carries an a. c. signal (160 Kc) and a d. c. bucking current. The secondary coil picks up the a. c. and its harmonics, and the second harmonic is selected by a band pass filter. This second harmonic controls the d. c. bucking current in such a manner as to null out the second harmonic which occurs only when the permalloy wire is in a zero magnetic field. Thus the bucking current is a measure of the external magnetic field. This instrument has proven to be extremely satisfactory and can be recommended for magnetic fields of 50 gauss or less. This instrument will be discussed in detail in a separate report.

Another problem was the difficulty of maintaining a field that was constant in time. The magnet current supply, devised and built by Minard Leavitt and his group, was constant to one part in 50,000. Stray external fields, unfortunately, were not. To reduce the effects of these fields, the magnet current supply was modified so as to be controlled by a magnetometer of the type mentioned above. In this way the field at the monitor probe location was held constant to about 10 milligauss. Even so, the external field gradients were too high to ignore, so all accurate measurements were made on the owl shift when most of the stray field sources were not operating. At this point still another problem became evident. The armco iron poles have a magnetic memory in spite of the most careful annealing and degaussing. To overcome this, a standard degaussing cycle was set up starting at a magnet current five times the operating current and cycling slowly down to zero. In addition it was found necessary to have a motor driven magnet turn-on device for coming up to operating current and also for turning off the magnet current. Otherwise, even after degaussing, the field was not reproducible.

In making the field measurements of course a carefully controlled motor driven mechanism was required to position the magnetometer search probe. The searching coil drive used required approximately 12 min. to cover 360° azimuth. During this time field information was fed continuously from the magnetometers into a Leeds and Northrup Speedomax two-pen recorder. One pen recorded the monitor magnetometer signal and the search magnetometer signal alternately, switching every five seconds. The other pen recorded the search magnetometer signal continuously on a scale magnified 20 times. It

should be noted here that much of the difficulty encountered was due to the rapid change of field; at the largest radius the field changed from a minimum of 7 gauss to a maximum of 38 gauss every  $60^\circ$  of azimuth.

Rf System (Bob H. Smith)

The rf and servo control equipment for the 36 in. Model III electron machine has been completed and is now being installed. The dees have been installed and tuned to resonance at 54 mc.

2043-147

**SECRET**

-149-

UCAL-2043



Fig. 1 Section 16  
Electron Model II  
Pole with Magnetic Channel

**SECRET**

**END**

2043-148